UNIVERSITA' VITA-SALUTE SAN RAFFAELE

CORSO DI DOTTORATO DI RICERCA INTERNAZIONALE
IN MEDICINA MOLECOLARE

Curriculum in Basic and Applied Immunology and Oncology

AQP11 mediates H_2O_2 fluxes to regulate cellular redox homeostasis and signalling

DoS: Prof. Roberto Sitia
Second Supervisor: Prof. Vsevolod Belousov

Tesi di DOTTORATO DI RICERCA di Ilaria Sorrentino
Matr. 014376
Ciclo di Dottorato: XXXIV
SSD BIO11/BIO13

Anno Accademico 2020/2021

RELEASE OF PHD THESIS

Il/la sottoscritto/a / *I, the undersigned* ……*Ilaria Sorrentino*……
Matricola / *registration number*……..*014376*…….
nat_ a/ *born in* ……*Milano (MI)*……
il/*on*……*01/06/1993*……..

autore della tesi di Dottorato di ricerca dal titolo / *author of the PhD Thesis titled*

AQP11 mediates H_2O_2 fluxes to maintain cellular redox homeostasis and signalling

- □ AUTORIZZA la Consultazione della tesi / AUTHORIZE *the public release of the thesis*

- ▪ NON AUTORIZZA la Consultazione della tesi per ..12.... mesi /DO NOT AUTHORIZE *the public release of the thesis for* ...12... *months*

a partire dalla data di conseguimento del titolo e precisamente */ from the PhD thesis date, specifically*

Dal / *from* 15/12/2021 Al / *to* 15/12/2022

Poiché /*because*:

- □ l'intera ricerca o parti di essa sono potenzialmente soggette a brevettabilità/ *The whole project or parts of it may be the subject of a patent application;*

- ▪ ci sono parti di tesi che sono già state sottoposte a un editore o sono in attesa di pubblicazione/ *Parts of the thesis have been or are being submitted to a publisher or are in the press;*

- □ la tesi è finanziata da enti esterni che vantano dei diritti su di esse e sulla loro pubblicazione/ *the thesis project is financed by external bodies that have rights over it and its publication.*

Data /Date .....15/11/2021..... Firma /Signature 

Declaration

This thesis has been composed by myself and has not been used in any previous application for a degree. Throughout the text I use both 'I' and 'We' interchangeably.

All the results presented here were obtained by myself, except for:

1) The Subcellular Fractionation showed in Fig. 22B, was performed in collaboration with Dr. A Rimessi and Dr. P. pinton, Department of Morphology, Surgery and Experimental Medicine, Section of Pathology, Oncology and Experimental Biology, Laboratory for Technologies of Advanced Therapies (LTTA), University of Ferrara, 44121, Ferrara, Italy.
2) The experiment for determining the topology of AQP11 showed in Fig. 23A was performed by Dr. S. Bestetti and Dr. M. Galli Protein transport and secretion unit, Division of genetics and cell biology, San Raffaele Scientific Institute, Milan, Italy.
3) The immunoprecipitations showed in Fig. 24A and Fig 28A and B were performed by Dr. Medraño-Fernandez, Redox signalling in regenerative medicine, Department of Bioengineering and aerospatial engineering, Carlo III De Madrid University, Madrid, Spain.
4) The Electron-microscopy images was produced by Dr. A. Raimondi, Alembic, Experimental Imaging Centre, San Raffaele Scientific Institute, Milan, Italy.
5) The data described in the section 3.1 have been already published in a research paper appeared in 2020 (Bestetti et al., "Human aquaporin-11 guarantees efficient transport of H_2O_2 across the endoplasmic reticulum membrane" Redox Biology) of which I am co-first author

All sources of information are acknowledged by means of reference.

Acknowledgment

First of all, I would like to thank my Director of Studies, Professor Roberto Sitia. He always gave me useful suggestions and helps during my PhD student adventure.

I gratefully acknowledge my second supervisor, Professor Vsevolod Belousov, for his understanding, personal attention and scientific advice, which have helped me through all the steps of my work and moreover for the useful exchange of reagents., ideas and exciting scientific discussion.

I am really grateful to Dr. Iria Medraño-Fernandez for welcoming me and becoming a second mother to me.

My deep appreciation goes also to my irreplaceable labmates, former and present. They were able to lighten my hard times and I always learn a lot from our discussions.

And last but not least I want to thank my family and friends for having always been present on this long journey.

THE

DEDICATION

OF THIS THESIS

IS SPLIT

SEVEN WAYS:

TO ALESSIA,

TO ALBERTO,

TO ROSY,

TO DANIELE,

TO ORSOLA & CAROLINA,

TO ANTONIO & FILIPPO,

AND TO YOU,

IF YOU HAVE

STUCK

WITH ME

UNTIL THE

VERY

END.

Adapted from Harry Potter and the deathly hallows, JK Rowling.

Abstract

Like many reactive oxygen species (ROS), H_2O_2 is an essential second messenger at low levels, but toxic at high concentrations. For this reason, sophisticated mechanisms evolved to channel useful redox signals limiting unwanted effects. Thus, proteinaceous channels are needed to regulate H_2O_2 transport across lipid bilayers. In principle, therefore, there should be an H_2O_2 conduit (hence endowed with peroxiporin activity) in all organelles that produce it (plasma membrane., ER and mitochondria). Members of the aquaporin family have been shown to transport H_2O_2, in addition to water. Of these, AQP3, 8, 9 are present in the plasma membrane. We investigated whether additional family member(s) reside(s) primarily in the ER. This compartment hosts oxidative folding: as such it is a source of H_2O_2. Using imaging and biochemical techniques, we demonstrated that AQP11 is an ER resident protein, partly accumulating in mitochondrial associated membranes (MAM). Its silencing inhibits the entry of exogenous H_2O_2 into the ER, confirming that AQP11 acts as a peroxiporin. It also favors the accumulation of H_2O_2 in the ER lumen, suggesting that AQP11 mediates a constitutive ER-to-cytosol flux. To investigate the source(s) and significance of this flux, I knocked-down Ero1α and NADPH oxidase 4, two ER-resident enzymes known to produce H_2O_2. Unexpectedly, however, even higher concentrations of H_2O_2 accumulated in the ER of Ero1α^{KD} cells. The simultaneous silencing of AQP11 prevented H_2O_2 accumulation, suggesting that AQP11 channels can internalize H_2O_2 originating from a different compartment. By using a combination of techniques, I identified complex III in the inner mitochondrial membrane as an external source capable of insufflating H_2O_2 into the ER through AQP11. These results identify a novel pathway regulating interorganellar redox homeostasis and pave the way for the identification of the underlying signals and functional role.

Table of contents

Acronyms and Abbreviations

$-S^-$	Thiolate
-SH	Thiol
$-SO_2H$	Sulfinic Acid
$-SO_3H$	Sulfonic Acid
-SOH	Sulfenic Acid
-SS-	Disulfide
AQP	Aquaporin
Cys	Cysteine
DMSO	Dimethyl Sulfoxide
DTT	Dithiothreitol
ER	Endoplasmic Reticulum
Ero1α	ER oxidoreductin-1α
ETC	Electron Transport Chain
GOE	Great Oxidation Event
GPX	Glutathione Peroxidase
H_2O_2	Hydrogen Peroxide
IMM	Inner Mitochondrial Membrane
IMS	Mitochondrial Intermembrane Space
KD	Knock Down
KDEL	ER retention sequence Lys-Asp-Glu-Leu
KO	Knock Out
LCS-1	4,5-dichloro-2-(3-methylphenyl)-3(2H)-pyridazinone
MAM	Mitochondrial associated Membrane
MM	Mitochondrial Matrix
NOX	NADPH Oxidase
O_2	Molecular Oxygen
$O_2^{\cdot -}$	Superoxide Anion
$OH^{\cdot}$	Hydroxyl Radical
OMM	Outer Mitochondrial Membrane

OXPHOS	Oxidative phosphorylation
PDI	Protein Disulfide Isomerase
PM	Plasma Membrane
PP1	Protein Phosphatase 1
PRX	Peroxiredoxin
PTP	Protein Tyrosine Phosphatase
ROS	Reactive Oxygen Species
S1QEL1.1	N^1-(3-acetamidophenyl)-N^2-(2-(4-methyl-2-(*p*-tolyl) thiazol-5-yl)ethyl)oxalamide
S3QEL 2	1-(3,4-Dimethylphenyl)-N,N-dipropyl-1H-pyrazolo[3,4-d] pyrimidin-4-amine
SOD	Superoxide Dismutase
TKR	Tyrosine Kinase Receptor
UPR	Unfolded Protein Response
VDAC	Voltage dependent anion-selective channel

List of Figures and Tables

1. Introduction

1.1 Oxygen and life: the importance of redox reactions

Life began in very different conditions compared to those of today. Indeed, carbon, nitrogen, and sulfur were the most predominant elements in the primordial atmosphere. In this context, primordial bacteria lived in an oxygen-free milieu (Kasting, 1993) thus evolving their metabolism in a reducing environment. In this context, Oxygen started to appear around 3 billion years ago due to development of oxygenic photosynthesis by Cyanobacteria. Then, about 2.5 billion years ago the Great Oxidation Event (GOE) occurred, causing the appearance and accumulation of oxygen (O_2) on the planet (Fig. 1). The result was a revolution for most living organisms (Lyons *et al*, 2014). They had to suddenly switch from a mild reducing habitat to an oxidizing one.

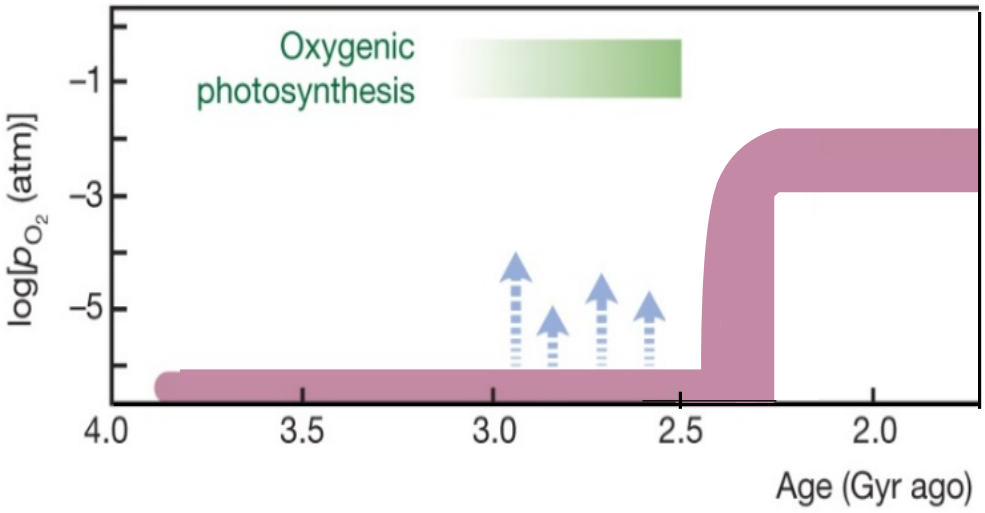

Figure 1: ***Appearance of Oxygen in the early atmosphere.*** *The pink line shows a simplified two-step mechanism, before oxygen and after oxygen. The blue arrows represent the initial putative "whiffs" of O_2. The green upper part denotes the appearance of cyanobacteria and therefore the beginning of O_2 production. Adapted from Lyons et al. Nature 2014*

After the GOE, one of the most important advantages acquired by organisms was the increase in complexity derived from the availability of new energy sources and facilitated by metabolic reprogramming. On the other hand, there was a fee for this benefit: cells needed to arm themselves against harmful oxidative events (Fridovich, 1998; Lyons *et al*, 2014). This was the context in which steep redox gradients were formed and redox reactions were adopted as signaling devices. Redox reactions are chemical events where the oxidation state of prone atoms is modified. They consist of an electron transfer from an oxidizing species, that becomes reduced, to a reduced one that now becomes oxidized (Fig. 2). Redox reactions intervene almost in all cellular processes, but despite their central consequences for health, aging, and disease, we have only unveiled a little part of the multitude of the circuits that can be redox-coordinated in biological systems.

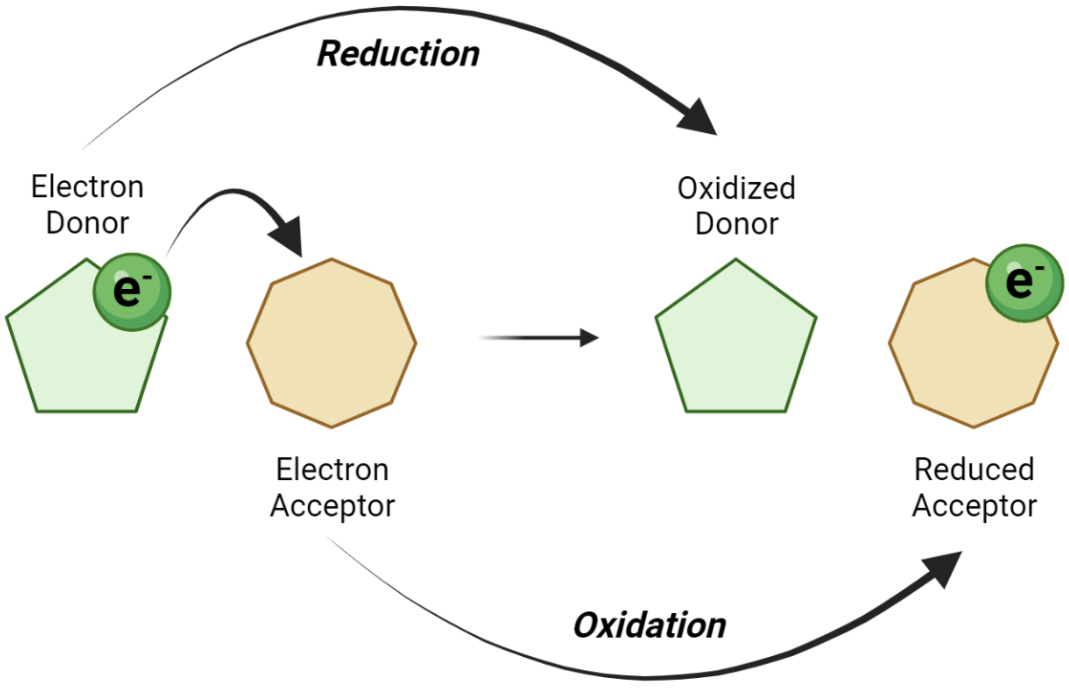

Figure 2: Principles of oxidation-reduction reactions or redox reactions.

1.1.1 Redox homeostasis

Cells continuously receive endogenous and exogenous stimuli that they have to interpret to maintain homeostasis. This is true also for redox inputs. Indeed, due to oxygen's features, essential yet toxic depending on its concentration, cells have evolved different systems to guarantee redox homeostasis (redoxstasis). The "oxidative eustress" represents the basal redox tone, or in other words, the set of reactions that maintain redoxstasis at physiological levels (Sies & Jones, 2020) (Fig. 3).

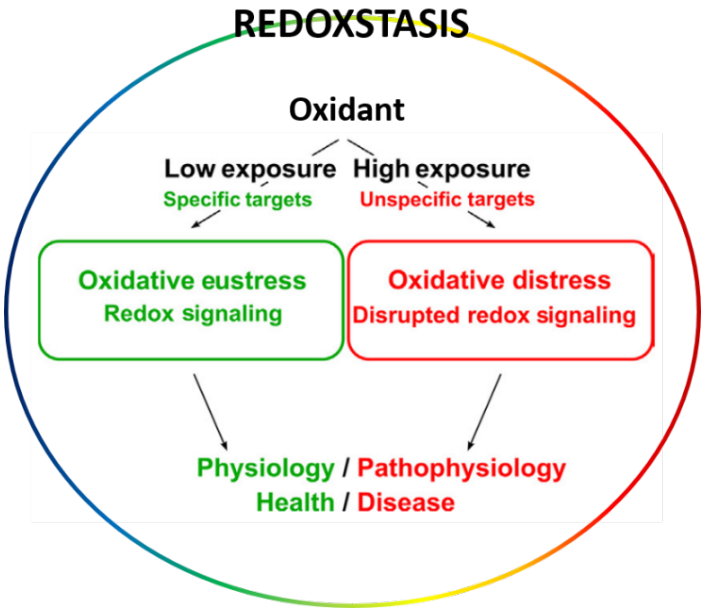

Figure 3: Redoxstasis and specificity of redox signalling. *Redox signalling is regulated by low oxidant levels acting on specific residues. On the other hand, high oxidant levels lead to the oxidation of unspecific targets. Thus, the dysregulation of redoxstasis is involved in many different pathological conditions. Adapted from Sies H. Antioxidants 2020.*

This concept suggests that low levels of oxidants act as signalling molecules. Indeed, nowadays is well accepted that redox signalling rules many processes, such as proliferation (Geiszt & Leto, 2004; Foreman *et al*, 2003), differentiation (Sauer *et al*, 2000), migration (Ushio-Fukai, 2006), apoptosis (Cai, 2005; Gechev & Hille, 2005), and many others (Sies & Jones, 2020; Finkel, 2000; Chiarugi *et al*, 2003)(Fig. 3).

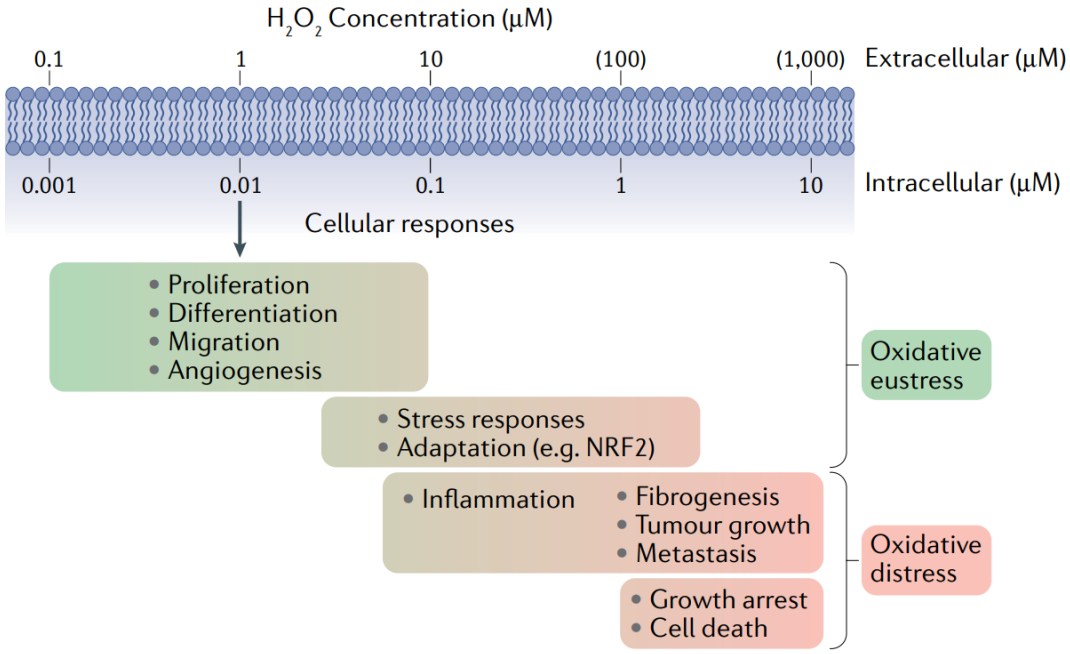

Figure 4: Relationship between H_2O_2 concentration and cellular outcomes. *Low concentration guarantees the transmission of intracellular signals related to different processes (Oxidative eustress). High concentration disrupts intracellular transmission and activates stress responses and cell death. From Sies H. & Jones DP, Nature reviews 2020 (License number 5191911043957)*

The maintenance of redoxstasis is vital for cells. When it is lost, a process called "Oxidative Stress" is triggered. Oxidative stress is then defined as "an imbalance between oxidants and antioxidants in favor of the oxidants, leading to a disruption of redox signalling and/or molecular damage" (Sies & Jones, 2007; Sies *et al*, 2017). This concept has been developed since 1985 (SIES, 1985; Sies, 2018), and implies the well-known oxidative damage of nucleic acids, proteins, and lipids. Thus, dysregulation in redoxstasis has been suggested as one of the main contributors to cellular aging and death (see both Fig. 3 and Fig. 4).

1.1.2 Reactive Oxygen Species (ROS)

Among the whole collection of chemical species that can act as oxidants, reactive oxygen species (ROS) are probably the best characterized. These are molecules generated by the sequential univalent reduction of O_2 (Dickinson & Chang, 2011). The most relevant ROS are hydrogen peroxide (H_2O_2), superoxide anion ($O_2^{\cdot-}$), and hydroxyl radical ($OH^{\cdot}$). They are different in their reactivity, stability, and specificity of action (Fig 5).

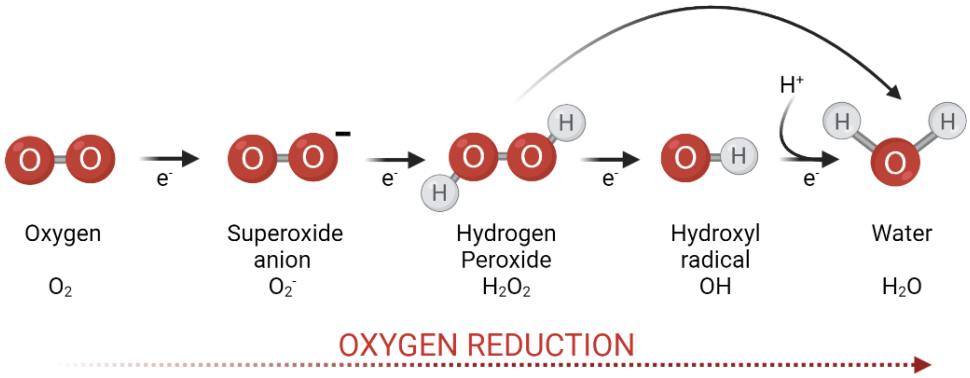

Figure 5: Sequential univalent reduction of molecular oxygen. *Adapted from Nordzieke DE and Medraño-Fernandez I, Antioxidants 2018.*

Among all ROS, H_2O_2 emerges as of paramount interest. Compared to the other species, it is selectively reactive, abundant, and stable in cells. Moreover, due to its long half-life, H_2O_2 is supposed to have enhanced diffusion capabilities being better equipped to reach its specific biological targets (Meng *et al*, 2002). All these features ensure that H_2O_2 is an ideal candidate for a role as a second messenger. In fact, it is well established that it modulates important signalling elements, such as phosphatases and kinases, allowing them to fluctuate between an on and an off position, thus amplifying intracellular cascades (Chiarugi *et al*, 2003). Therefore, the consequences derived from its action activating or inhibiting target proteins has pivotal importance in the pathophysiology of cells and organisms (Reth, 2002; Bae *et al*, 1997; Lee *et al*, 1998; Sundaresan *et al*, 1995).

1.1.3 A key molecule of redox signalling: H_2O_2

H_2O_2 was discovered by Luis Jaques Thenard in 1818 (Lindström & Pettersson, 2003; Thénard, 1818; Thenard, 1818). Biochemically, it is a two-electron oxidant that needs a high activation energy to release its oxidizing power (Winterbourn, 2013) a fact that results in a slow impact on the majority of the biological molecules. Thus, H_2O_2 does not release its redox potential indiscriminately like other oxidants, but its action is specific on particular prone proteins and likely spatiotemporal-dependent. The best characterized H_2O_2-dependent modification is the oxidation of the thiol side-chain of cysteines leading to the formation of different moieties depending on concentration: sulfenic (-SOH), sulfinic ($-SO_2H$) or sulfonic ($-SO_3H$) derivatives (Fig. 6).

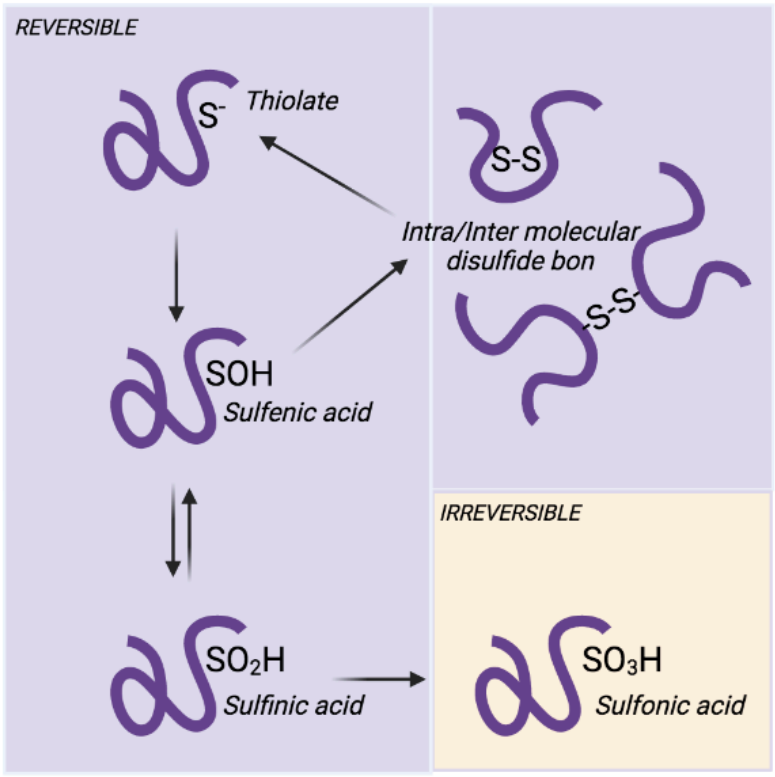

Figure 6: Cysteine residues fate upon H_2O_2 oxidation. *All the reactions that are illustrated with purple background are reversible (-S⁻, -SOH, - SO_2H, and -SS-) and associated with different outcomes (stability, localization). Instead, the -SO_3H formation is an irreversible reaction usually related to the degradation of the proteins.*

Regarding the H_2O_2-sensitive proteins, the cysteine must be in its deprotonated form (S^-, thiolate). As thiol protonation is dependent on the local pKa environment, not all cysteines in the cell are sensitive to ROS oxidation. Cysteines must be situated in a low pKa ambient (pKa=6.4-7)(Wall *et al*, 2012) and yet accessible to react with H_2O_2. These modifications can be reversible or irreversible, and for this reason, they have different biological outcomes (Holmström & Finkel, 2014)(Fig. 6 and Fig. 7). The mild oxidation of specific thiol groups of reactive cysteines usually leads to a change in protein function.

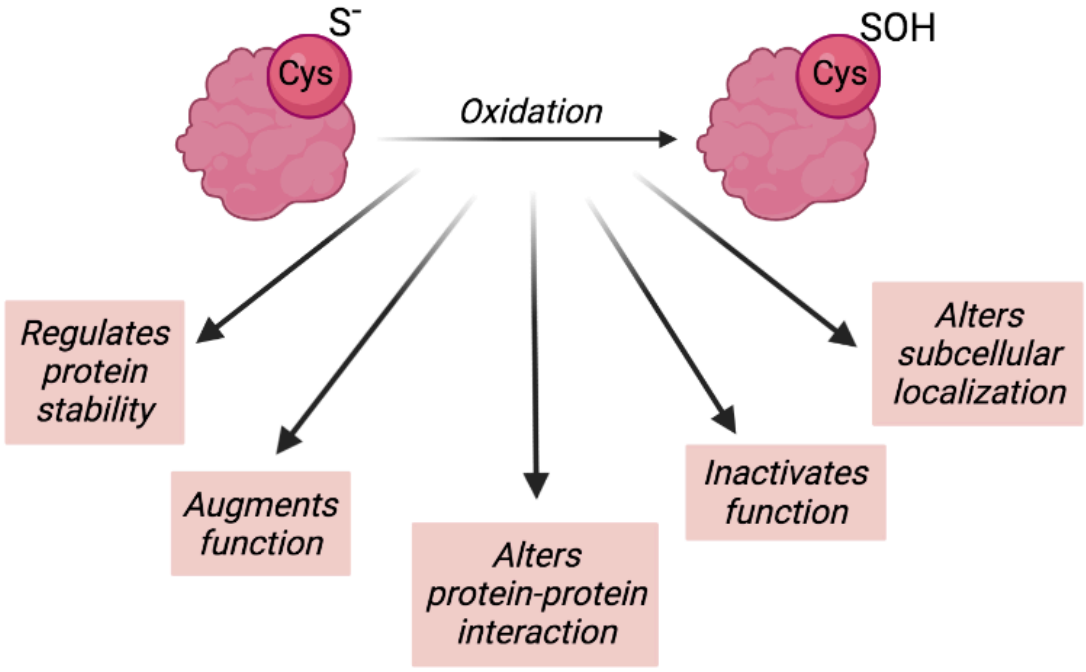

Figure 7: Biological readout of redox modified cysteines. *Afterward, the redox modification of a target cysteine in proteins changes their behaviors. For example, they can alter their subcellular localization, or change interactors. Adapted from Holmstrom & Finkel, Nature reviews 2014.*

Moreover, to efficiently tune H_2O_2-driven pathways while protecting themselves against the harmful effects of high concentrations, cells have evolved many regulatory mechanisms based on the versatility of cysteine oxidation:

1. Different pathways are sensitive to changing levels of H_2O_2: as a relevant example, the multifunctional protein p53 has been shown to activate the transcription of different subsets of genes depending on H_2O_2 levels (Sablina *et al*, 2005) (Fig. 8).
2. H_2O_2 cannot freely diffuse across membranes and cells modulate the quantity of H_2O_2 distributed depending on cellular needs (Bertolotti *et al*, 2013; Bienert *et al*, 2007; Miller *et al*, 2010). This step is regulated by switching the opening/closure state of H_2O_2 specific-channels belonging to the aquaporin (AQP) protein family (Fig. 8).
3. It has been suggested that cells have a sophisticated architecture dedicated to redox signalling (Nordzieke & Medraño-Fernandez, 2018). This hypothesis means that they may be able to virtually regulate the initiation, duration, and intensity of signals localizing or de-localizing H_2O_2 targets, sources, and scavengers (Nordzieke & Medraño-Fernandez, 2018) (Fig. 8).

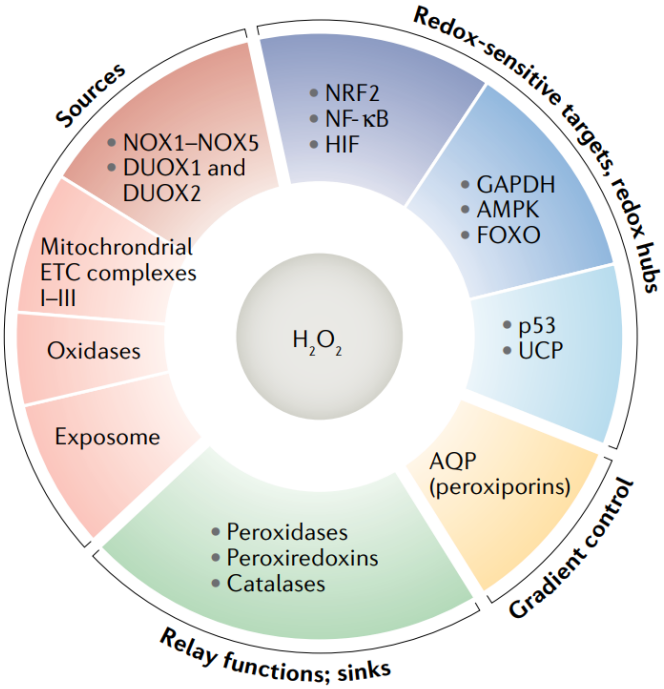

Figure 8: Mediators of Redox signalling. *Here are listed the most important proteins that specifically contribute to the metabolism of H_2O_2 (red and green). H_2O_2 targets (blue), and the H_2O_2 Gradient controllers (yellow). From Sies H. & Jones DP, Nature reviews 2020 (License number 5191911043957)*

Though the necessity for precisely controlling redox signals is well accepted, how the signal is propagated within the cell is still without a clear answer. The constant rate of reaction of peroxiredoxins (PRX) and glutathione peroxidases (GPX) is around 10^7-10^8 $M^{-1}s^{-1}$ (Winterbourn & Metodiewa, 1999; Peskin *et al*, 2007; Winterbourn & Hampton, 2008). These values deeply contrast with the rate of reactivity of the major part of the cysteinome, that is calculated to be around 20 $M^{-1}s^{-1}$ (Poole, 2015). Currently, the hypotheses in the field for the transmission of redox signals are:

1. Direct cysteine oxidation: Some target cysteines may have a reaction rate equal to or higher than the ones of scavenger proteins (Fig. 9A).
2. Binding/Vicinity: sources and targets are close to each other excluding antioxidant reactions (Fig. 9B).
3. Floodgate model: PRX/GPX can be inactivated under over-oxidative conditions opening the possibility for H_2O_2 to react with slower targets (Fig. 9C).
4. Relay model: Highly reactive thiols of specific proteins, particularly in antioxidant enzymes, can acquire first the redox equivalents and then release them to other substrates (Fig. 9D).

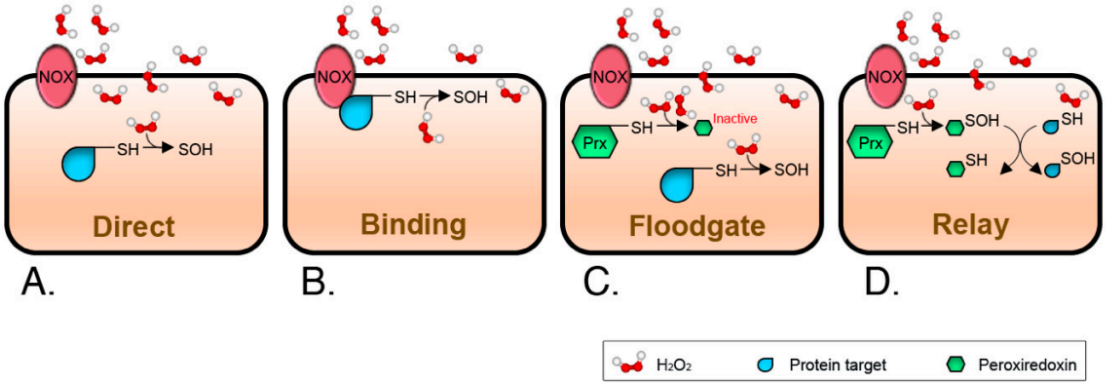

Figure 9: Main hypotheses of ROS signal transmission to cysteines.
From Nordzieke DE and Medraño-Fernandez I, Antioxidants 2018.

1.1.4 ROS sources

As stated above, ROS must be tightly regulated to maintain redoxstasis and avoid unwanted toxic effects. One fact that demonstrate that is not produced as a by-product of some reactions, is that different proteinaceous systems dedicated to distribute this molecule (Winterbourn, 2013, 2018). A peculiar feature of H_2O_2 production in cells is that its main sources, NADPH oxidases (NOX), Mitochondria and, ER, are always compartmentalized behind a lipid bilayer (Nordzieke & Medraño-Fernandez, 2018; Sies & Jones, 2020) that separates them from the cytosol where almost all H_2O_2 targets are localized. Indeed, membranes are essential to establish gradients that permit the transmission of redox signalling. For practical reasons, the most traditionally studied isolating/signal propagating barrier in redox biology has been the plasma membrane. In fact, the outer lipid bilayer not only protects the cytosol from exogenous oxidative insults but also accommodates many proteins involved in ROS homeostasis. NOXes are the main ROS producers in the plasma membrane, pouring superoxide (Bedard & Krause, 2007; Rada *et al*, 2008) in the extracellular space. Extracellular superoxide dismutases (SOD) metabolize this species to H_2O_2 while AQPs mediate their internalization into the cell to carry out its signalling role. The system offers several points of damage control such as timed production in response to activation of tyrosine kinase receptors (TKR), modulation of superoxide/ H_2O_2 conversion, and regulated uptake by the channels, the membrane itself guaranteeing the safety of the process (Fig.10). Notable intracellular pathways take advantage of these events including angiogenesis, insulin signalling and, many others (Geiszt & Leto, 2004).

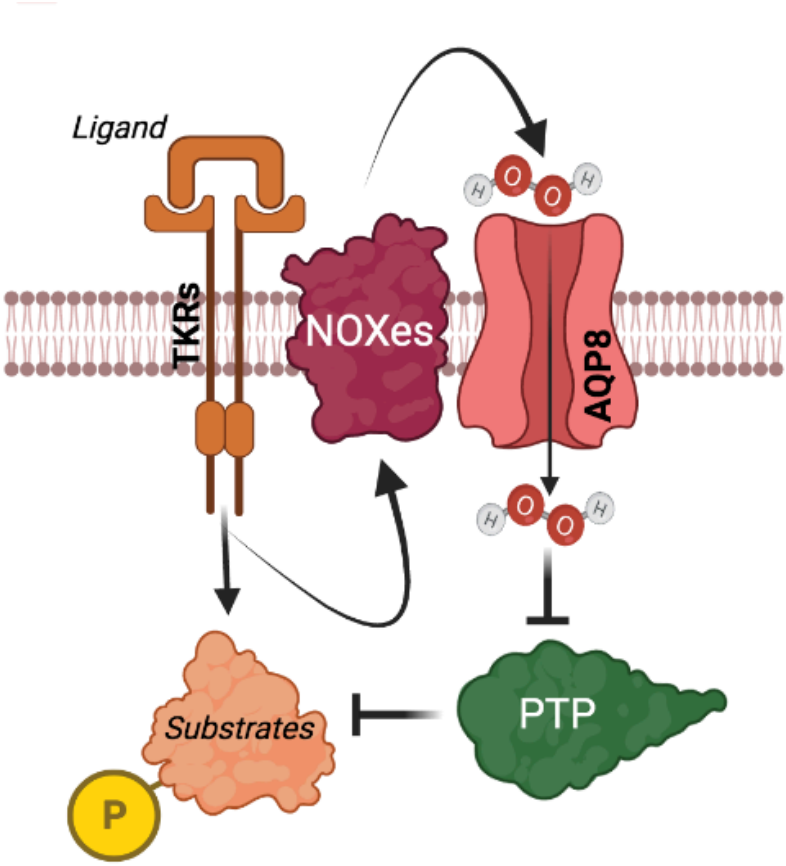

Figure 10: Redox signalling hubs at the plasma membrane. *TKRs, after the binding of their ligand, activate both specific phosphorylation cascades and NOX enzymes to produce H_2O_2 into the extracellular space. H_2O_2 uses an AQP as proteinaceous transporter to cross the plasma membrane. In the cytosol, H_2O_2 inhibits protein tyrosine phosphatases (PTP) enhancing the intensity and duration of the signal. Adapted from Medraño-Fernandez & Sitia, 2020*

However, also mitochondria and the endoplasmic reticulum (ER) have been categorized as vigorous ROS producers, in rates comparable to stimuli-activated NOXes. Remarkably, the putative signals that may arise from these organelles have been often disregarded, as ROS generation in these organelles has been classically considered a mere consequence of essential house-keeping processes. Nonetheless, if we contemplate that other signalling pathways are not only restricted to acute induction but depend on the tonicity of the signals, the fact that a constitutive production of ROS is constantly emanating from internal sources is well worth more careful analysis.

1.1.4.1 Mitochondria

Mitochondria are, probably, the first organelles that come to mind talking about ROS production. Interestingly, the localization of the different redox-generating centers on their structure -divided in two different compartments the mitochondrial matrix (MM) and the intermembrane space (IMS), an architecture essential for ATP production that suggests that organelle compartmentalization could also house spatially-controlled redox functions. Oxidative phosphorylation (OXPHOS) consists of an electron flow derived from electron donors, that runs along with several protein complexes that constitute the electron transport chain (ETC). The result is the accumulation of protons in the IMS that creates a positive electrochemical gradient across the mitochondrial inner membrane that drives ATP formation via an ATP synthase. The flow through OXPHOS causes the reduction of oxygen to water, but not all electrons arrive to the end reaction. Indeed some of them constantly leak from the ETC resulting in $O_2^{\cdot -}$ generation (Orrenius, 2007). Remarkably, mitochondrial activity is very susceptible to oxidative damage triggered by dysregulation in metabolism or by other stressful conditions, increasing the production of superoxide. The final outcome of mitochondrial stress is linked to a decrease in ATP production, a change in Ca^{2+} handling, to an increased mitochondrial membrane permeability. All these alterations, when sustained, lead to the activation of cellular apoptosis (James & Murphy, 2002). While other ROS producing sites not related to OXPHOS exist in mitochondria, two of the ETC complexes stand out in terms of ROS production: the NADH dehydrogenase or Complex I and the Cytochrome c reductase or complex III (Koopman *et al*, 2010; Orrenius, 2007; Orrenius *et al*, 2007).

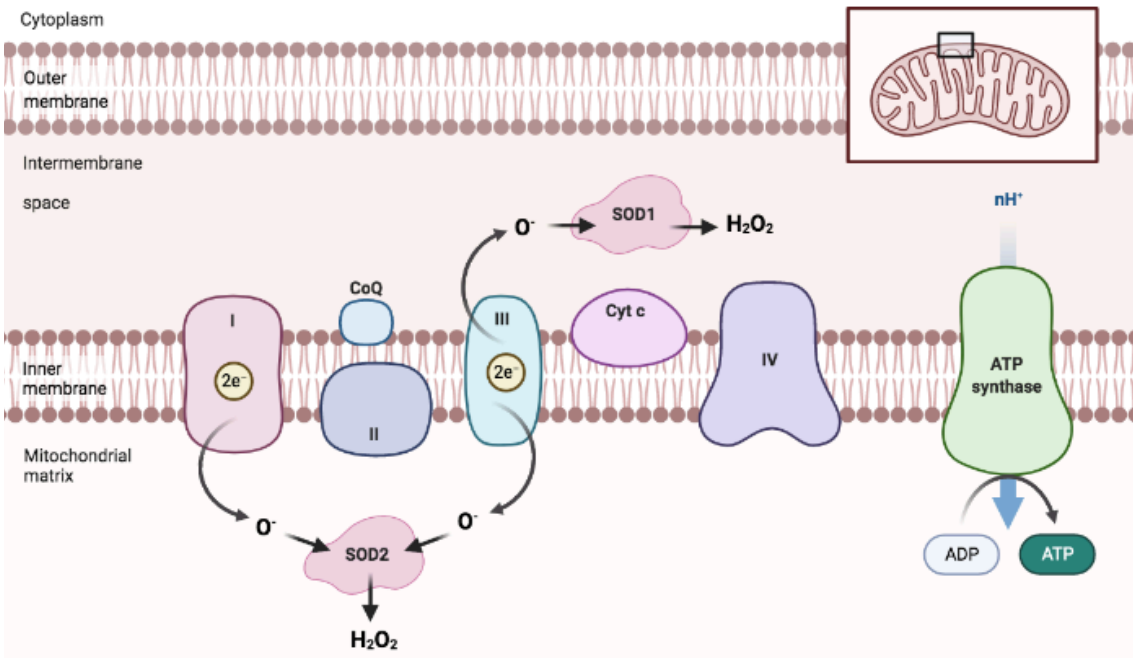

Figure 11: Mitochondrial Electron Transport Chain (ETC). *Schematic representation of ETC complexes. The site of production of superoxide in complex I and III is highlighted as well as the place in which the two different mitochondrial superoxide dismutases (SOD1 and SOD2) are localized. This architecture may reflect that ROS produced at either side of the IMM have different functions or usages. Adapted from Biorender templates.*

Complex I relies on the NADH/NAD^+ isopotential to work and release superoxide directly into the MM. Complex III, instead, takes advantage of the equal redox potential of the ubiquinol/ubiquinone (QH_2/Q) couple and produces superoxide on either side of the inner mitochondrial membrane (IMM) (Brand, 2010, 2016). As early mentioned above, maintenance of redoxstasis is critical for mitochondria and consequently, detoxification ROS enzymes are also compartmentalized. The superoxide produced by Complex I and III is rapidly quenched by dismutation using two distinct SOD enzymes. SOD1 in the IMS and SOD2 in the MM. Both enzymes have as reaction product H_2O_2 (Han *et al*, 2003). The IMM is highly impermeant to these molecules. This characteristic, which is essential to maintain the electrochemical gradient needed for cellular respiration, practically results in a sharp physical separation of the ROS produced in the MM from those generated at the IMS (Fig. 11). Thus, ROS of MM is confined while the ROS of the IMS have been suggested to more freely diffuse across the outer mitochondrial membrane

(OMM), using voltage dependent anion-selective channels (VDAC) (Yang *et al*, 2006; Bertolotti *et al*, 2013). Resembling the plasma membrane situation, all these strictly regulated mechanisms of producing, transporting, and scavenging suggest that mitochondrial ROS may well play a role in organelle-to-cytosol redox signalling. As a matter of fact, there is some evidence that points to the possible roles of mitochondrial ROS in regulating intracellular pathways even if this is still debated in the redox field. As an example, it has been shown that insulin secretion by pancreatic β cells not only depends on ATP synthesis. Actually, the increase in glucose metabolism first generates a boost of NADH and FADH2, with consequent production of superoxide rapidly converted into H_2O_2. that finally stimulates insulin secretion (Leloup *et al*, 2009).

1.1.4.2 Endoplasmic Reticulum

The endoplasmic reticulum (ER) has lately arisen as a central player in redox physiology and pathophysiology; indeed, it is the organelle that harbors the greatest H_2O_2 concentration inside cells (Gao *et al*, 2017). Here, the extremely regulated H_2O_2 metabolism is managed by different producing/scavenging enzymes that guarantee the redox homeodynamics of the organelle (Lloyd *et al*, 2001). All these systems are important to preserve the major function of the ER: to generate and maintain the correct oxidative milieu for proteins synthesis and the formation of disulfide bonds, a process known as oxidative folding (Frand *et al*, 2000). The best characterized H_2O_2 source in the ER is the ER oxidoreductin-1 (Ero1) flavoprotein that was identified in the '90s in yeast (Frand & Kaiser, 1998). Ero1α partners with the oxidoreductase protein disulfide isomerase (PDI) to insert disulfides in proteins during their folding. In addition, PDI also ensures the isomerization of non-native disulfides or reduction of some in terminally misfolded proteins to facilitate their degradation.

The establishment of disulfide bonds is a dynamic process that consists in the oxidation of target cysteines (-SS-) and the reduction (-SH) of others in a partner-based redox

reaction. The process can be described starting from PDI. PDI, in its oxidized, form reacts with cysteines donating a disulfide bond and acquiring electrons. To ensure the continuous formation of disulfide bonds, PDI must be re-oxidized by Ero1α exchanging a disulfide for electrons (Fig. 12).

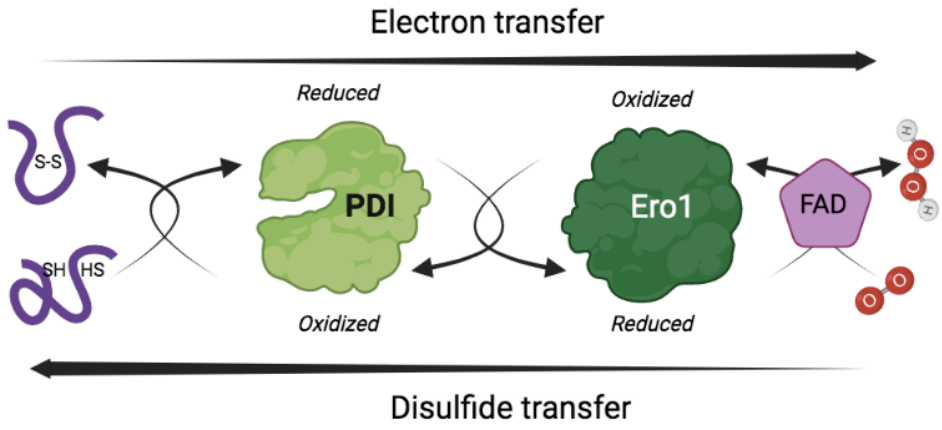

Figure 12: Schematic representation of ER oxidative protein folding*. Ero1α due to its ability to produce de novo disulfides continuously recycles PDI. Oxidized PDI transfers disulfide bonds directly to substrates. Adapted from Van Anken & Braakman, critical reviews in biochemistry and molecular biology*

These reactions are sustained by Ero1α specific features. Being a flavoprotein, it contains a FAD moiety that can directly transfer electrons to molecular oxygen allowing its reduction to H_2O_2. This relay is activated to maintain Ero1α in its oxidized status ready for reduced PDI. Ero1α itself is continuously re-oxidized by a sophisticated mechanism using two different couples of redox cysteines. The first couple (outer active site) donates a disulfide and acquires electrons from PDI. Then, the second couple (inner active site) re-oxidizes the outer active site accepting its electrons. In the end, the oxidation of the inner active site is restored due to interaction with FAD. Thus, Ero1α forms *de novo* disulfides that are essential for the ER redox potential. Indeed, it was determined that for each disulfide bond established, one H_2O_2 molecule is formed (Tu *et al*, 2000; Tu & Weissman, 2004). The large amount of H_2O_2 produced by Ero1α has been shown to be

consumed at least in part by glutathione peroxidase 8 (GPX8) and peroxiredoxin 4 (prx4) (Ramming *et al*, 2014). For many years, the ability to supply oxidizing equivalents was attributed to glutathione. Glutathione is a tripeptide, which exists in two different forms: a reduced thiol (reduced glutathione [GSH]) and an oxidized disulfide (oxidized glutathione [GSSG]). The ratio GSH/GSSG represents the redox state of an intracellular compartment. It corresponds to a ratio of 30:1-100:1 in the cytosol (Hwang *et al*, 1992) while it is 5:1 in the ER (Dixon *et al*, 2008). But, nowadays, Ero1α is considered the "major" producer of oxidizing potential in the ER. Rather, the role of glutathione seems to be a source of reducing equivalents for the isomerization of non-native disulfide bonds (Chakravarthi & Bulleid, 2004; Molteni *et al*, 2004). All these considerations may indicate that Ero1α is an essential protein for the cells. Indeed, it is ubiquitously expressed in all human tissues. Another isoform, Ero1β, is only expressed in a few secretory cell types such as spermatocytes and pancreatic β cells (Cabibbo *et al*, 2000; Pagani *et al*, 2000) and its expression can be upregulated during the unfolded protein response (UPR), probably to enhance the possibility of forming disulfide bonds. Surprisingly, knock-out (KO) mice lacking Ero1α or Ero1β show only a minor folding defect. Ero1β KO mice evolve a mild nonprogressive pancreatic β cell dysfunction with glucose intolerance; Ero1α KO mice have an abnormal cardiac response to adrenergic stimulation (Chin *et al*, 2011; Zito *et al*, 2010a). On the contrary, the lack of the homolog Ero1p is lethal in yeast and simple metazoans such as worms and flies (Frand & Kaiser, 1998; Pollard *et al*, 1998; Tien *et al*, 2008; Zito *et al*, 2010b; Tavender & Bulleid, 2010), suggesting that at some point of the evolutionary road mammalian cells have developed a strong compensatory mechanism to overcome mutations in Ero1. Remarkably, both the mammalian proteins are not anchored to the ER membrane as the yeast one is. They have lost the C-terminal tail that mediates membrane association in Ero1p (Pagani *et al*, 2001). Moreover, differently from other metazoan soluble proteins that reside in the ER, they lack the classical ER retention sequence Lys-Asp-Glu-Leu (KDEL). Instead, they have been reported to be retained in the ER by ERp44, a KDEL-bearing chaperon (Anelli *et al*, 2003). Ero1α could be the perfect candidate to be a master regulator protein in maintaining redox homeostasis in the ER. Actually, its capacity to emit signalling molecules such as H_2O_2 in amounts that are proportional to oxidative folding could be used to communicate the robustness of the processes underlying disulfide bond formation,

not only within the ER itself but also in other compartments. Interestingly, there are many reported connections between ER oxidative stress and the activation of unfolded protein response (UPR) caused by protein overload or aggregation (Cao & Kaufman, 2014; Eletto *et al*, 2014). Specifically, deregulation of the levels of both oxidizing or reducing equivalents during leads to ER stress and hence UPR (Sies & Jones, 2020). In addition, other seemingly non-related-to-folding ROS sources have been described in the ER. Because of its rate of production NOX4, a NADPH oxidase can also be a candidate for emanating redox signals from the ER (von Löhneysen *et al*, 2012; Ushio-Fukai, 2006; Laurindo *et al*, 2014; Nordzieke & Medraño-Fernandez, 2018)(Fig. 13).

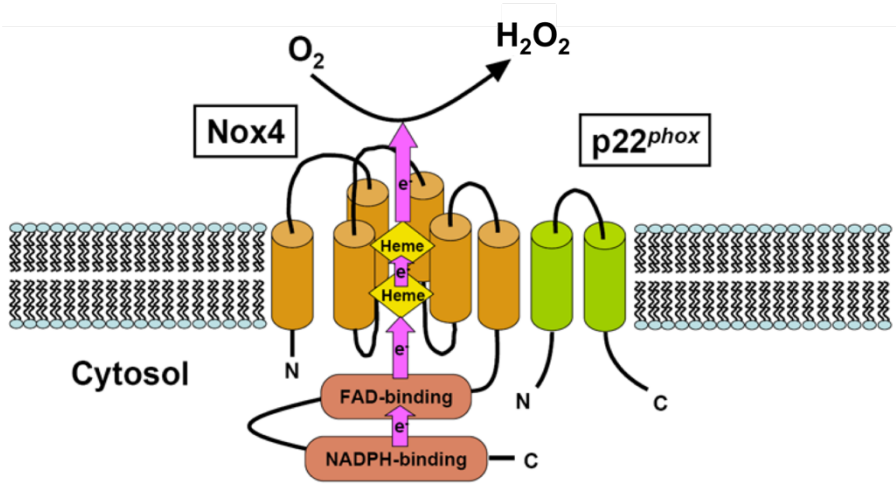

Figure 13: Structure of NADPH Oxidase 4 (NOX4). *From Kuroda, J., Sadoshima, J., Journal of Cardiovasc. 2010*

NOX4 has, at least, two main differences compared to all other NOXes. First, it directly produces H_2O_2 instead of O^- (Laurindo *et al*, 2014). Second, NOX4 seems to be constitutively active, as no regulator of its activity has been found yet (Nisimoto *et al*, 2010). Thus, also, in this case, it can be hypothesized that H_2O_2 produced by NOX4 can putatively participate in signalling pathways at the interface between the ER and the cytosol. For example, it has been demonstrated that it modulates the redox activation of Protein phosphatase 1 (PP1) and thus the regulation of the α-subunit of the eukaryotic

initiation factor 2 (eIF2α) with consequent impact on protein synthesis (Santos *et al*, 2016).

Other sources of H_2O_2, like cytochromes belonging to the P450 family, are less well categorized by their signalling potential capacity, but for the same very reason, a role on redox homeostasis cannot be discarded (Sies, 2020; Konno *et al*, 2021)(Fig. 14).

In summary, the highly dynamic redox environment of the ER presents many opportunities for signalling. This immediately suggests that redox-driven communications may exist among ER and other organelles. The consequences theoretically will imply that the ER compartment is not a redox island but an integrated system that sustains cellular life.

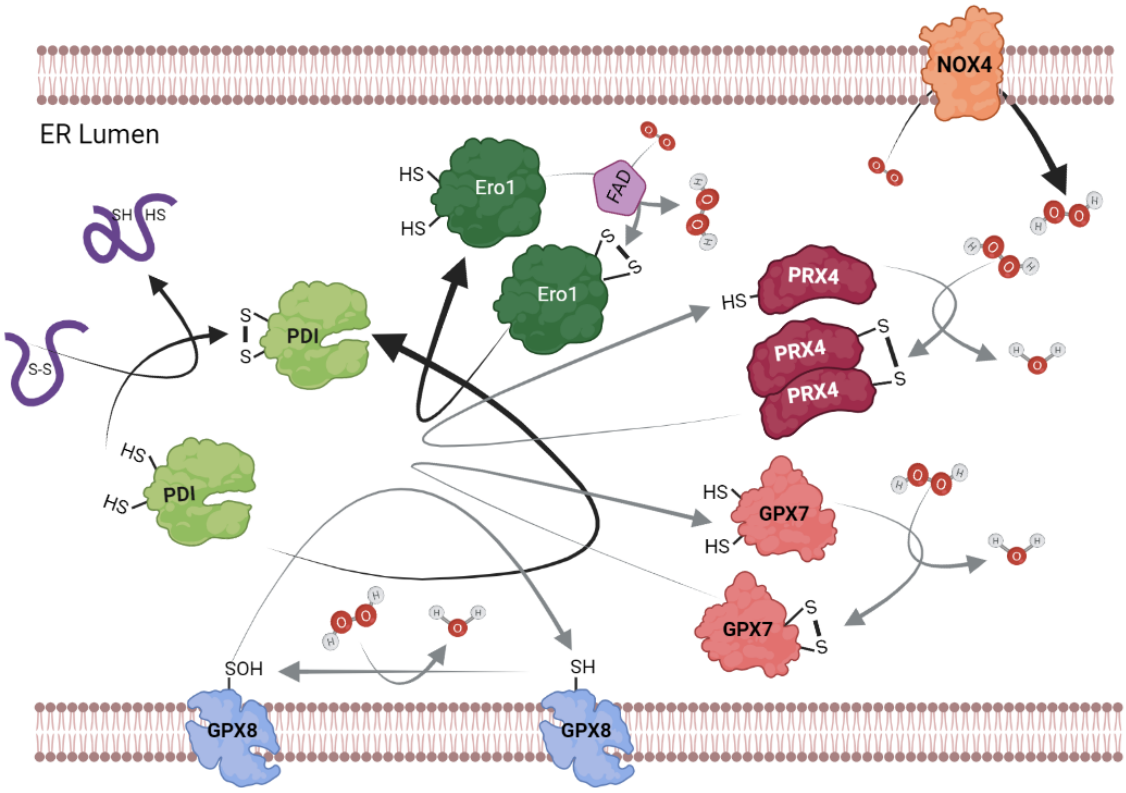

Figure 14: Representation of the major sources and scavengers of H_2O_2 in the ER. *The arrows indicate the direction of the transferred disulfide bonds. Adapted from Konno T et al., Cells 2021*

1.1.4.3 Mitochondrial-Associated Membranes (MAM)

For both the ER or the mitochondria is crucial to maintain a coordinated homeostasis. Not surprisingly, they share a particular sub-region called "mitochondria-associated membranes" (MAMs) dedicated to inter-organellar communications (Fig. 15). MAMs are the sites in which mitochondria and the ER physically interact one with each other, communicating themselves using the exchanging of solutes and second messengers, like Ca^{2+} (Bravo-Sagua *et al*, 2013).

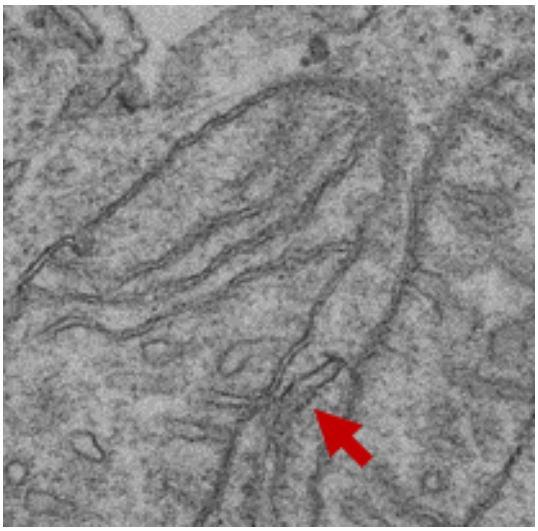

Figure 15: Electron microscopy image of MAM. *(the red arrow highlights MAMs) Sorrentino et al, unpublished*

The distance among the two organelles is a crucial parameter for guarantying their correct functionality. Some researchers restrict the maximal "gap" to <30 nm, while others enlarge this measurement to even up to 80 nm (Giacomello & Pellegrini, 2016). As both connected organelles are involved in constitutive H_2O_2 production and maintain a tight regulation on their redox homeostasis, it has been proposed that a regulatory link exists between ER oxidative protein folding and OXPHOS electron leakage (Simmen *et al*, 2010). Interestingly, the ER lumen side of MAMs is highly enriched in redox enzymes related to oxidative folding, like, Ero1α, and many others (Gilady *et al*, 2010)**.** If this reveals to be true, the existence of a redox crosstalk in MAMs would substantially enhance the possibility of adding another level of complexity in the regulation of H_2O_2 by establishing an interorganellar redox communication axis potentiated by the vicinity of the organelles.

1.2 Controlling H_2O_2 distribution: the importance of Aquaporins (AQPs)

The plasma membrane has not only the role of enclosing the cytoplasm and the cellular organelles. Due to its capacity of isolation, it creates electric and chemical gradients essential for living cells. As a matter of fact, between the extracellular milieu and the cytosol, there is a constant exchange of molecules, one of them being H_2O_2. Specific AQPs called peroxiporin (Bienert *et al*, 2017; Nordzieke & Medraño-Fernandez, 2018) have been shown to transport H_2O_2 in a regulated manner to impact cytosolic targets (Bertolotti *et al*, 2013; Medraño-Fernandez *et al*, 2016). Using a channel H_2O_2 is transported at a rate compatible with effective signalling. Thus, peroxiporins have arisen as of vital importance in the transmission of redox signals (Fig. 16).

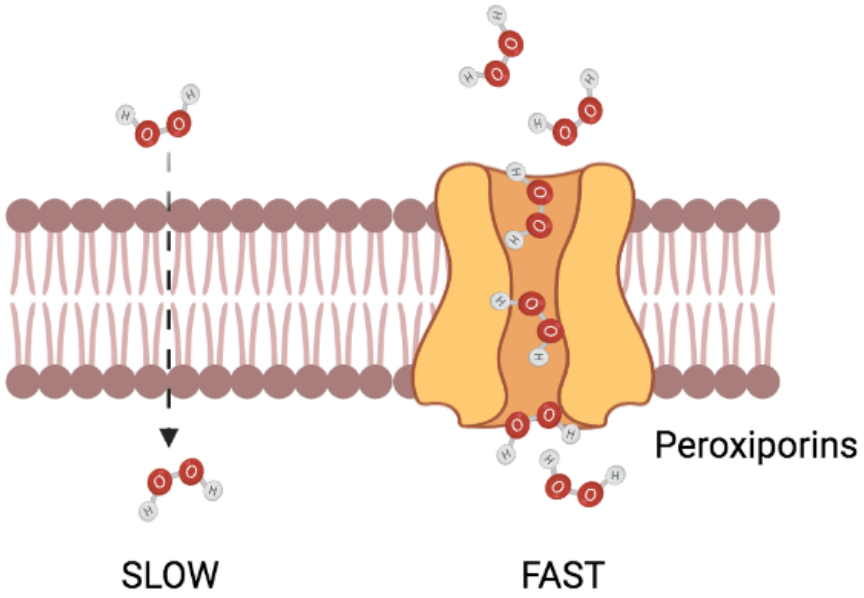

Figure 16: Rate of transport of H_2O_2 across membranes. *H_2O_2 slowly traverses lipid bilayers (left side). Instead, high rate H_2O_2 fluxes through peroxiporins allow efficient internalization (right side), a fact that is essential for signal transmission.*

1.2.1 AQPs family: an historic perspective

In 2003 the Nobel prize for Chemistry was awarded to Peter Agre for the discovery of a protein that enhanced membrane water permeability (Fig. 17) (Preston *et al*, 1992).

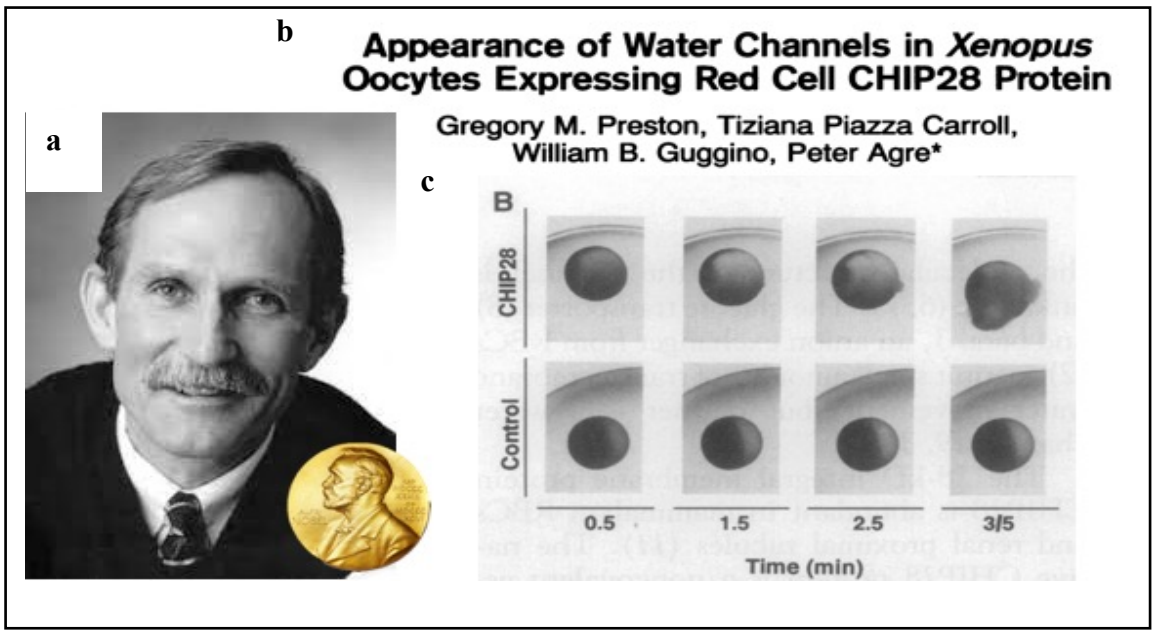

Figure 17: Discovery of Aquaporins*. A) Peter Agre, Nobel prize for Chemistry 2003. B) Heading of the report where Aquaporin-1 (AQP1) was described for the first time C) Central figure of this paper showing that CHIP28 (then AQP1) is a water channel. Adapted from Preston et al., Science, 1992.*

Before Agre's studies, the notion that water can freely pass biological membranes was a totally accepted hypothesis that was completely puzzled by the identification of the first member (AQP1) of a family, of water-transporting channels by his team. Aquaporins (AQPs) are a class of proteins encoded in almost all organisms (Finn & Cerdà, 2015; Gazzarrini *et al*, 2006). In fact, during the last decades, it has been shown that AQPs assure the flux not only of water but also of other small uncharged molecules such as glycerol, urea, and H_2O_2.

The human genome contains 13 different AQPs isoforms (AQP0-12). They have been encountered differently distributed in diverse tissues, suggesting that both solute permeability and means of regulation may have been selected to express one particular isoform preferentially depending on tissue functions (Tab. 1).

Aquaporins	Tissue expression	Other solutes transported
AQP0	Highly expressed in the lens	-
AQP1	Renal tubules, exocrine pancreas, bile ducts, subsets of cells in the intestine, myoepithelial cells of breast and endothelial cells	-
AQP2	Renal tubules	-
AQP3	Epithelial and glandular cells, including renal collecting ducts	Hydrogen peroxide, urea, glycerol
AQP4	CNS, lung, thyroid gland and stomach	-
AQP5	Salivary gland and testis	-
AQP6	Renal tubules	-
AQP7	Adipose and soft tissue	Glycerol, urea
AQP8	Colon, rectum and pancreas	Hydrogen peroxide, ammonia
AQP9	Liver and gallbladder	Hydrogen peroxide, urea, glycerol
AQP10	Small intestine- and duodenum glands	Urea, glycerol
AQP11	Ubiquitous, most abundant in gastrointestinal tract and adrenal gland	-
AQP12	Pancreas and epididymis	-

Table1. Patterns of expression and solutes transported (different than water) of the 13 mammalian AQPs (The Human Protein Atlas).

One of the first attempts of classification was based on the dual transporting specificity early described for their members: orthodox AQPs were only water permeable (AQP0, AQP1, AQP2, AQP4, AQP5, AQP6, and AQP8) while aquaglyceroporins transport water but also glycerol (AQP3, AQP7, AQP9, and AQP10) (Verkman, 2011). To this, a new class called unorthodox or superaquaporins (AQP11 and AQP12) which are intracellular and with little homology to the other members were lately added (Verkman, 2011; Ishibashi *et al*, 2014). In more recent years, new studies have identified other proteins belonging to the family of unknown solute preference: AQP13 and -14 in Metatheria and Prototheria and non-mammalian vertebrates, AQP15 and AQP16 (Finn & Cerdà, 2011; Finn *et al*, 2014). However, in our days, the initial classification seems to be overcome since many AQPs belonging to both main groups share substrates different from water and glycerol. This is the case of H_2O_2-transporting AQPs, as this molecule can flux through the orthodox AQP8 (Bertolotti *et al*, 2013), and be a substrate for the aquaglyceroporins AQP3 (Miller *et al*, 2010) and AQP9 (Watanabe *et al*, 2016), defining a functional group known as peroxiporins (Bienert *et al*, 2017).

All AQPs, independently from their preferred transported molecule, share a common homotetrameric core structure: each monomer is made by six transmembrane α-helix linked by five loops forming a single functional pore (Törnroth-Horsefield *et al*, 2010). In addition, to this basal common structure, some AQPs have been shown to undergo posttranslational modifications like phosphorylation or N-glycosylation among others that impact on the regulation of their opening/closed state or in their localization (Li & Wang, 2017). The differences in solute permeability depend on two very conserved selectivity filters. The first one generates an electrostatic barrier for charged ions and is formed by two asparagine–proline–alanine (NPA) motifs (Murata *et al*, 2000). The second, known as the aromatic/arginine (ar/R) constriction site, determines the size of the solutes that can cross the channel (Törnroth-Horsefield *et al*, 2010)(Fig. 18).

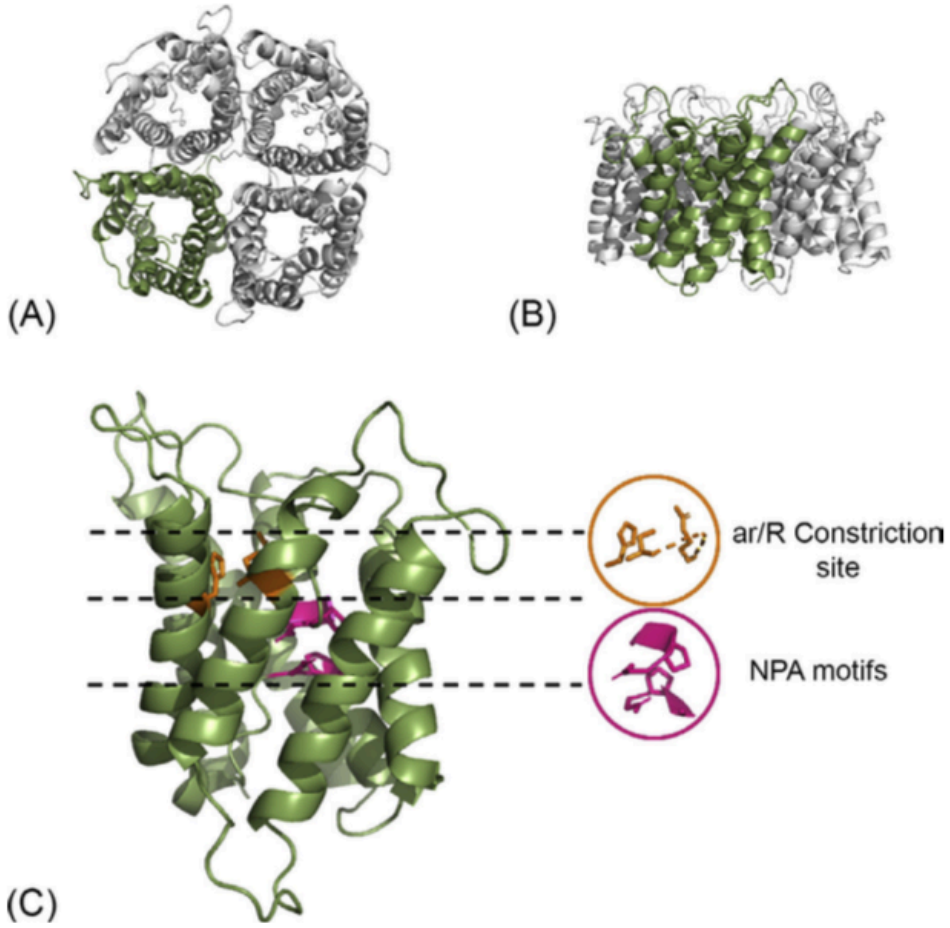

Figure 18: Structure of AQPs channel. *A) Aquaporin homotetramers seen from top. B) and from the side. C) Single monomer of an aquaporin. In green the six transmembrane helices; in purple the NPA motifs important for the exclusion of charged molecules; in orange the ar/R constriction site that acts as a size exclusion filter. From Medraño-Fernandez & Sitia, 2020 (License number 5191930505655)*

1.2.2 AQP-mediated H_2O_2 transport

The physical and biochemical properties of H_2O_2 -extensively described above- together with the involvement of extracellularly produced molecules on cytosolic redox modifications, early suggested the idea of using a membrane transporter. The first researchers that hypothesized that H_2O_2-specific channels may exist were Henzler and Steudle (Henzler & Steudle, 2000). They showed that mercury chloride, a broad AQP inhibitor, can decreases H_2O_2 membrane permeability of isolated internodes of the algae *Chara corallina* (49). In 2007 arrived the first proof of the identity of these peroxiporin channels. Bienert and coworkers showed that some members of the AQP family facilitated the entry of H_2O_2 in yeast cells. They engineered yeast cells with different AQPs of different species and correlate the yeast survival to increasing concentrations of H_2O_2 (Bienert *et al*, 2007) (Fig. 19).

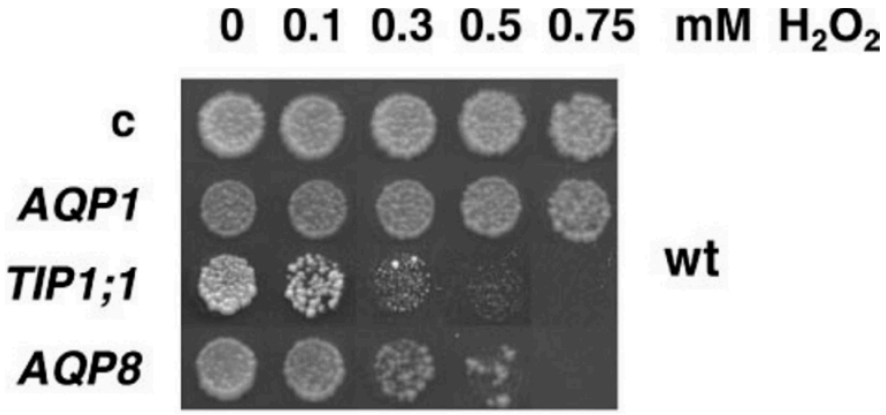

Figure 19: Yeast survival and growth assays. A wt *yeast strain (WT) transfected with either an empty vector (c), hAQP1, yTIP1;1, or hAQP8 and cultured in media containing different concentrations of H_2O_2. Yeast transfected with yTIP1;1, and hAQP8 survived and grew less because they are able to transport H_2O_2, increasing its intracellular content and hence leading to cell death. AQP1 was used as control as it transports only water. From Bienert GP et al., The Journal of biological chemistry 2007.*

1.2.3 Mammalian peroxiporins

1.2.3.1 The aquaglyceroporins AQP3 and AQP9 as H_2O_2 transporters

AQP3 was the first functional peroxiporin identified in mammalian cells (Miller *et al*, 2010) when Miller and coworkers reported that both chemical and genetically-encoded H_2O_2-sensitive probes showed higher activation rates in response to exogenous H_2O_2 when HEK cells were transfected with human AQP3 (Fig. 20).

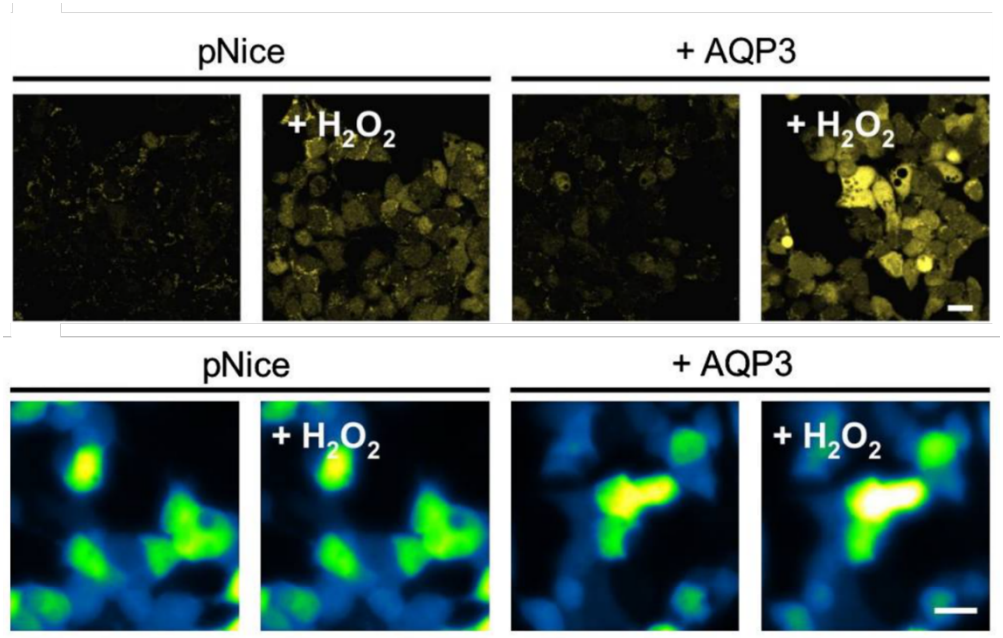

Figure 20: AQP3 is a peroxiporin. *Overexpression of control vector (pNice) or a plasmid codifying for AQP3 in a cell line loaded with boronate-based fluorescent dyes (upper panels) or co-expressing the genetically-encoded sensor HyPer (lower panels). AQP3-overexpressing cells have higher probe activation rates in both cases. From Miller et al., Proc Natl Acad Sci U S A, 2010.*

Moreover, they showed that down-regulation of AQP3, using a specific shRNA, causes both a reduction in H_2O_2 permeability and in downstream H_2O_2-mediated signalling.
Since then, AQP3 has been linked to many different processes involving redox signalling, from chemokine-dependent T lymphocyte migration during immune responses in mice (Hara-Chikuma *et al*, 2012), and regulation of migration of breast cancer lines (Satooka

& Hara-Chikuma, 2016), psoriasis (Hara-Chikuma *et al*, 2012), and scleroderma pathogenesis (Luo *et al*, 2016).

Following a similar approach using an encoded sensor, also AQP9 has been revealed as an H_2O_2 transporter. Thus, downregulation or over-expression of this isoform accordingly impacts H_2O_2 permeability (Watanabe *et al*, 2016).

1.2.3.2 AQP8 as an H_2O_2 channel

In 2007, AQP8 was the first human AQP to be identified as a peroxiporin using an overexpression set up in a yeast cells model (Bienert *et al*, 2007). Later on, the finding was further confirmed by our lab in human lineages by showing that silencing of AQP8 using specific siRNAs completely inhibits H_2O_2 transport across the membrane of HeLa and B cells (Bertolotti *et al*, 2013, 2016). Furthermore, we were also able to show that the channel is endowed with a peculiar two-step gating mechanism that controls H_2O_2 permeability following cellular needs. The mechanism depends on a redox sensitive cysteine (Cys53) localized inside the AQP8 pore. As H_2O_2 enters cells using AQP8 it sulphenylates Cys53 (-SOH), priming the cysteine to a second reaction. As the flux of H_2O_2 enters the cytosol, it activates an H2S-producing enzyme Cystathionine-β-synthase (CBS) that triggers the formation of a persulfide on Cys53 (-SSH). The result is the movement of the modified side chain of Cys53 that blocks the further entry of H_2O_2 (Fig. 21). The closure mechanism of AQP8 adds the possibility to allow cells to precisely regulate the intracellular levels of H_2O_2. Indeed, mutations in this residue make cells more resistant to different stressors allowing their survival and proliferation even the harsh conditions (Medraño-Fernandez *et al*, 2016; Bestetti *et al*, 2018; Medraño-Fernandez & Sitia, 2020).

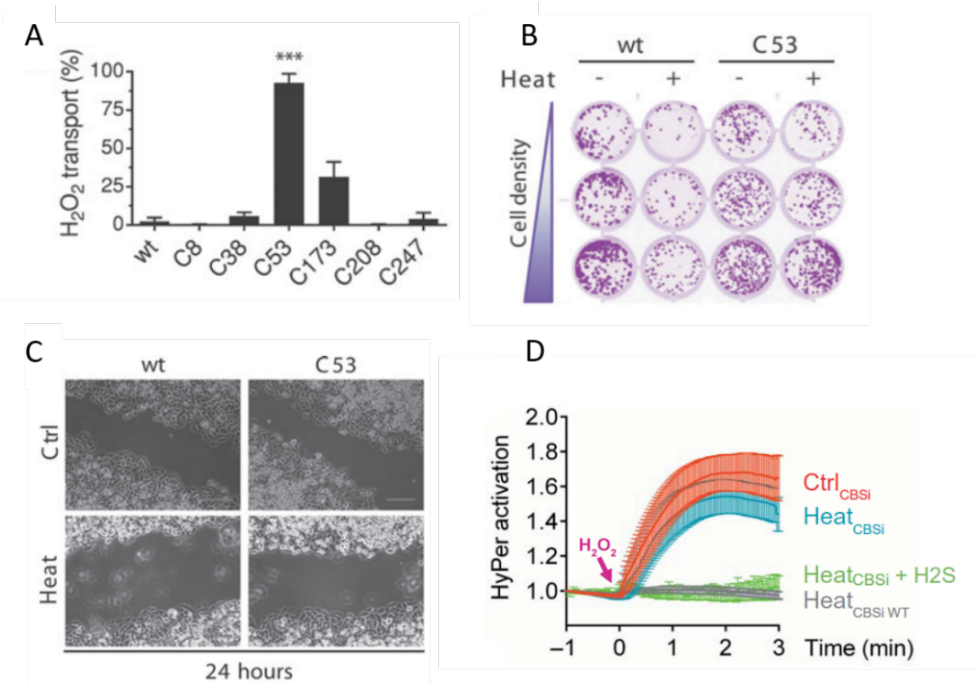

Figure 21: The cysteine 53 on AQP8 is key to inhibit AQP8. *A) Hela cells co-expressing HyPer sensors and wt AQP8 or different cysteine-mutant versions. After a heat-shock that will induce closure, only C53S can transport H_2O_2 across the plasma membrane. B&C) Hela cells expressing AQP8C53S mutants survive and proliferate more than their wt counterpart after stress. D) Time-course of exogenous H_2O_2 internalization showing that H_2S is fundamental to the mechanism of AQP8 closure. Red trace corresponds to basal control conditions (ctrl, open) and grey trace are heat-shocked cells (Heat, closed). Cyan trace shows the uptake under CBS silencing that is comparable to control cells even if they are stressed Green trace results from the addition of exogenous H_2S to cells whose expression of CBS is downregulated. From Medraño-Fernandez et al., ARS, 2016 and Bestetti et al., Science Advances, 2018.*

The existence of this sophisticated mechanism to control H_2O_2 permeability, undoubtedly suggests that we have only a small piece of information regarding the influence of peroxiporins on redox signalling. As oxidative stress is the starting point for many pathologies, knowing whether regulation of H_2O_2 transport is redox-induced and impacts other redox-driven pathways when using other isoforms to traverse membranes results in central biomedical interest. Curiously, all the above-reported peroxiporins are housed in the PM. However, as mentioned above, there are other organelles that result relevant contributors to cell redoxstasis. Thus, it arises the idea that intracellular peroxiporins could exist and could be implicated in regulating redox communications among different compartments. Thus, my PhD project aims at the identification of the ER resident peroxiporin.

2 Aims

The final goal of my Ph.D. was to characterize the ER-resident peroxiporin AQP11. Despite the long experience of the "Redox team" of Sitia's laboratory on the study of the plasma membrane-localized AQP8, when I joined this project many questions were still open. In particular, the lab had just started to address the possible involvement of AQP11 in redox homeostasis. Thus, my work is focused to solve the following questions:

- Does AQP11 allow H_2O_2 fluxes across the ER membrane?
- Do these fluxes control signals emanating during ER stress?
- Does its enrichment in MAM imply redox exchanges between ER and mitochondria?

To assess these questions, I took advantage of HyPer probe expressed in different subcellular compartments to examine H_2O_2 fluctuation in and between ER, mitochondria, and cytosol.
In the three years of my PhD program, I found at least partial answers to these questions. My studies uncovered an unforeseen mechanism of communication between mitochondria and the ER, in which the two organelles interact to maintain redoxstasis. Altogether, the knowledge gathered sheds further light onto the complex mechanism that allow redox signals to propagate in crowded cells and limit oxidative stress.

3 Results

3.1 Human aquaporin-11 guarantees efficient transport of H_2O_2 across the endoplasmic reticulum membrane

The data described in this section have been already published in a paper appeared in 2020 (Bestetti et al., "Human aquaporin-11 guarantees efficient transport of H_2O_2 across the endoplasmic reticulum membrane" Redox Biology) of which I am co-first author.

The ER is a highly dynamic organelle that only begins to be characterized now also from a redox signalling point of view. It is a major ROS producer in living cells, and tight are the relationships between disulfide bond formation and H_2O_2 (Tu & Weissman, 2004). Starting from these viewpoints and considering the potential role of the ER as a source of redox signals, we surmised that ER may also house a functional peroxiporin. Importantly, mice lacking an intracellular AQP, AQP11, showed signs of oxidative stress and died two weeks after birth having developed a Polycystic Kidney-like disease (Morishita *et al*, 2005). This phenotype suggested that AQP11 could be a good candidate and prompted us to analyze the localization, topology, and function of this protein.

3.1.1 AQP11 resides in the ER

To determine whether the intracellular localization of AQP11 corresponds with the ER, tagged versions of AQP11 were engineered. When expressed in different cell lines, the chimeric AQP11 accumulated in the ER, largely co-localizing with the ER marker calnexin (CNX, Fig. 22A, upper panels). Little if any was present at the plasma membrane (stained with ConA before cell permeabilization, middle panels) and only slightly in mitochondria (stained with antibodies to peroxiredoxin-3, PRX3, bottom panels). Analyses of the coincidence of the AQP11 fluorescent signal for the entire cell volume with each organelle marker by the Pearson correlation coefficient (Dunn *et al*, 2011), confirmed a high degree of co-distribution (> 0.7) for the CNX-AQP11 pair and a low value (discretely over the > 0.3 positive limits) for Prx3-AQP11 (Fig. S1B). The localization of AQP11 was further evident in cells co-expressing Flag-tagged AQP11 and HaloAQP8 proteins (Fig. S2A): a strong signal was observed for AQP8 at the cell perimeter where this channel normally concentrates, while AQP11 has the typical reticular staining of ER-resident molecules. Pixel intensity profiles of both AQPs concurred with this observation (Fig. S2B), ConA profile highlighting plasma membrane areas. That is, the vast majority of AQP11 occupied zones corresponding to the cytoplasm, whereas the AQP8 profile showed strong overlap with ConA profile and a less prominent signal at the cytoplasmic area, probably corresponding to the fraction of AQP8 that is travelling from the ER to the plasma membrane. Importantly, the position and nature of the attached tags did not alter the distribution of chimeric proteins (Fig. 22A and Fig. S1A), confirming that the features of the internal sequence of AQP11 determine its localization. Even though AQP11 is highly co-distributed with CNX, their respective localization pattern did not perfectly converge, suggesting that the two proteins might reside in different subregions of the ER. In eukaryotic cells, particular subregions of the ER membrane that are tethered to mitochondria are key signalling platforms that allow the exchange of redox signals between the two organelles (Yoboue *et al*, 2018). These are known as mitochondrial-associated membranes (MAM)(van Vliet *et al*, 2014). As we surmised that AQP11 may function as an ER-resident peroxiporin, we sought evidence to establish whether the channel is present at those sites. Following a validated protocol

(Wieckowski *et al*, 2009), we obtained fractions enriched for Sigma1 receptor (Hayashi & Su, 2007), a MAM marker, but devoid of protein markers of the cytosol, mitochondria, Golgi, and ER (tubulin, Tom20, GM130 or GRP94, respectively. Fig. 22B). Accordingly, this fraction contained also IP3 receptors and VDAC also reported to reside in these sub-regions (Yoboue *et al*, 2017; Anelli *et al*, 2012), and hence likely corresponded to MAMs. These biochemical data were in line with the results of the Pearson coefficient described above (Fig. S1B), in which a modest degree of co-distribution was observed between AQP11 and the mitochondrial marker Prx3. Thus, at least in part, AQP11 resides in MAMs.

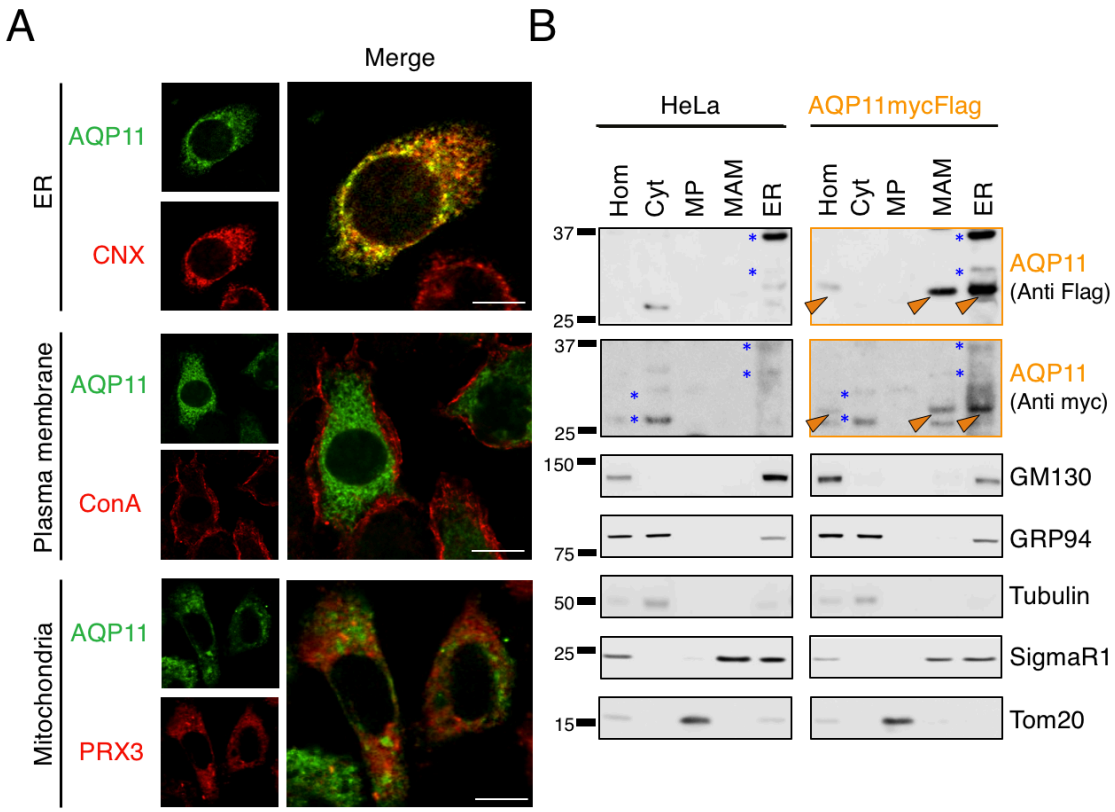

Figure 22: AQP11 resides in the ER.

A) HeLa cells transfected with HaloAQP11 were co-stained with fluorescent Halo ligands, and with antibodies against calnexin (CNX) or peroxiredoxin-3 (PRX3), to visualize AQP11, ER, and mitochondria, respectively. To label the plasma membrane, cells were incubated with concanavalin A (ConA)-FITC that recognizes glycoproteins, in absence of cell permeabilization, and then fixed (middle panels). Scale bar=10µm.

*B) HeLa cells transiently expressing AQP11mycFlag were fractionated as previously described (Yoboue et al, 2017; Wieckowski et al, 2009) and see material and methods section. Aliquots were resolved electrophoretically and blots decorated with the indicated antibodies. Hom, total post-nuclear homogenates. Cyt, cytosol. MP, pure mitochondrial fraction. MAM, mitochondria- associated membranes. ER, endoplasmic reticulum (Blue * indicates background).*

(Bestetti et al, 2020)

3.1.2 AQP11 topology

To describe whether AQP11 has the typical AQP membrane-orientation in which both end-termini facing the cytosol, we produced a recombinant AQP11 protein fused with a Halo tag at its N-terminal and a Flag tag at its C-terminal (HaloAQP11-Flag). If both its N- and C-termini share the topology of the rest of AQP isoforms, the tags should be accessible to antibodies or membrane-impermeant Halo ligands upon incubation with digitonin (Fig. S3), a detergent that permeabilizes the plasma membrane but not the membrane of the ER (Molteni *et al*, 2004). Clearly, both the non-permeant Halo ligand and an anti-Flag antibody showed a positive signal on digitonin-treated cells (Fig. 23A), indicating that AQP11 follows the regular AQP structural scheme, with both ends oriented to the cytosol. Calreticulin (CRT), an ER luminal protein, was not detected in digitonized cells unless they were additionally treated with the stronger Triton X100 detergent to permeabilize the ER (Fig. S3), confirming the integrity of the ER membrane during our experiments. Analyzing protein glycosylation further confirmed that the C-terminus of AQP11 lies in the cytosol. Despite the presence of a potentially accessible N-glycosylation site in human AQP11 (NHT, residues 264–266, see scheme on Fig. 23B), neither endoglycosidase-H (Endo-H) nor peptide N-glycosidase F (PNGaseF) caused mobility shifts to the protein (Fig. 23B, lower panels and, Fig. S4A), and a sharp band was present regardless of the enzyme used. In contrast, human AQP8 yielded three bands, serving as a positive control of glycosidase activities in this assay: the slower-migrating band contains AQP8 glycoforms that are resistant to Endo-H and hence had traversed the Golgi complex; the slower of the two sharper bands is sensitive to both Endo-H and PNGaseF, and most likely corresponds to N-glycosylated molecules in route to the Golgi; the third band carries instead no N-glycans. Altogether, the above data suggest that whilst most AQP8 molecules travel through the secretory pathway and are processed before reaching the plasma membrane, AQP11 resides in the ER with both its N- and C-termini facing the cytosol.

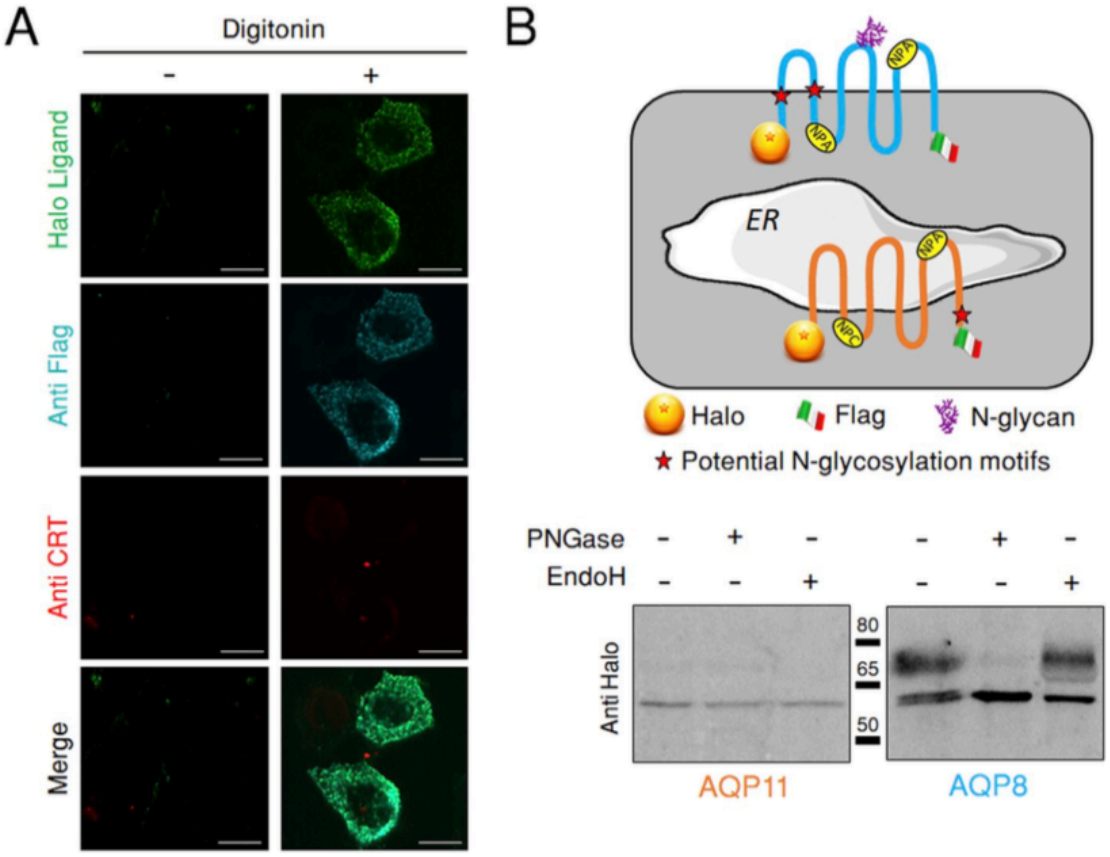

Figure 23: Both the N- and C- termini of AQP11 protrude into the cytosol.

A) HeLa cells expressing HaloAQP11-Flag were treated or not with digitonin to selectively permeabilize the plasma membrane, and then incubated with a membrane-impermeant Halo ligand (green) or with antibodies specific for Flag (cyan) or calreticulin (CRT, red), an ER lumenal protein. See Supplementary Fig. S2 for further details on the protocol. Note that both the N- and C-termini of HaloAQP11-Flag face the cytosol, as schematized in panel B (top scheme). Scale bar = 10 µm.

B) The top panel shows the topology of AQP11 and AQP8 (orange and blue, respectively) as determined by immunofluorescence (Fig. 22A) and biochemical analyses (bottom panel). The absence of N-glycosylated AQP11 species in HeLa transfectants contrasts with the easily detectable Endo-H resistant AQP8 glycoforms.

(Bestetti et al, 2020)

Next, we assessed if also AQP11 forms tetramers, as other members of the AQP family do. To address this question, AQP11mycFlag was transiently co-expressed in HeLa cells with HaloAQP11 or, as specificity controls, with either Halo proteins preceded by a signal sequence and extended at its C-terminus with an ER localization motif (-RDEL) or fused to the transmembrane domain of the ER protein Gpx8 (HaloGpx8 TM, see (Yoboue *et al*, 2017). Clearly, anti-Flag antibodies precipitated HaloAQP11 (Fig. 24A). Neither Halo nor HaloGpx8 TM were instead coprecipitated, even if they were more abundant than HaloAQP11 in the cell lysates (compare the anti-Halo signals in the 3 left lanes, labeled as Input), indicating that mixed assemblies can be formed by differently tagged AQP11. To confirm and expand this notion, we fractionated lysates of HeLa cells expressing either HaloAQP11-Flag or HaloAQP8-Flag on discontinuous sucrose gradients. In Fig. 24B, the two red arrows indicate the migration of 7S and 19S purified immunoglobulins, and their respective molecular weights used as controls. Based on those settings, both AQP11 and AQP8 co-fractionated with marker molecules of around 200 kDa (Fig. 24B and Fig. S4C), a size compatible with a tetrameric conformation. However, the gel distribution profile suggests that AQP11 tends to form higher molecular weight complexes than AQP8.

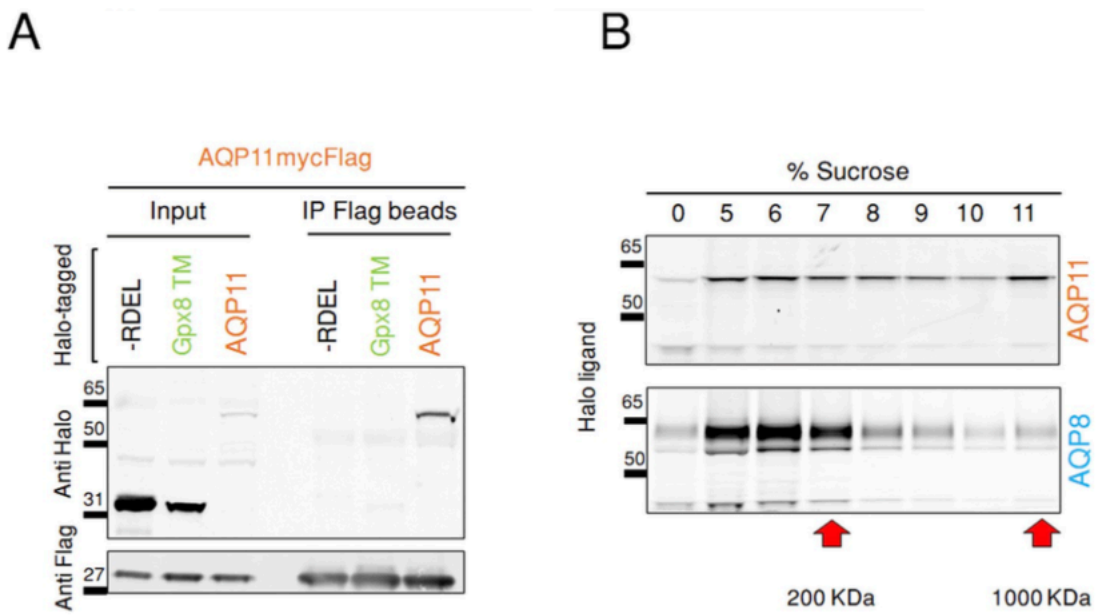

Figure 24: AQP11 forms tetramers.

A) Aliquots of the lysates of HeLa cells transfected with AQP11mycFlag and either Halo-RDEL, HaloGpx8 TM, or HaloAQP11 proteins were immunoprecipitated using immobilized anti-Flag antibodies and analyzed by western blotting using anti- Halo or anti-Flag specific antibodies. IP, immunoprecipitation.

B) Lysates of HeLa cells expressing either HaloAQP11-Flag or HaloAQP8-Flag were separated through a discontinuous 5–11% sucrose density gradient, and aliquots of each fraction were subjected to reducing SDS-PAGE. The presence of the recombinant proteins was assessed by direct detection of bound fluorescent Halo ligands on the gels using a laser scanner imager.

(Bestetti et al, 2020)

3.1.3 AQP11 is a peroxiporin facilitating the transport of H_2O_2 across the ER membrane

To analyze whether AQP11 could work as a peroxiporin, we engineered HeLa cells to stably express HyPer sensors (Belousov *et al*, 2006) in the ER lumen (*HyPerERLum*), cytosol (*HyPerCyto*) or, the mitochondrial matrix (*HyPerMito*). The *HyPerERLum* probe had a higher level of activation at a steady state (Fig. S5A), as reported previously (Malinouski *et al*, 2011). Nonetheless, its oxidation upon exposure of cells to exogenous H_2O_2 was clearly detectable (Fig. 25). Lowering the basal oxidation state of *HyPerERLum* by pretreating cells with 5 mM DTT for 5 min allowed to better visualize the entry of H_2O_2 into the ER (green trace in Fig. S5A). However, as the results could be easily quantified also in the absence of DTT pretreatment, we performed our experiments without the addition of reducing agents. Consistent with AQP11 being an ER-resident protein, silencing its expression (Fig. S5B) had different effects on the three organelle-targeted HyPer sensors: while oxidation of *HyPerERLum* was severely inhibited (Fig. 25A, AQP11low left graph), AQP11 silencing had no significant effects on *HyPerCyto* (see Fig. 25A, right graph) or *HyPerMito* (see Fig. S5C) activation. As expected, silencing of AQP4 -a protein devoid of peroxiporin activity (Bertolotti *et al*, 2013)- did not impair significantly *HyPerERLum* oxidation (Fig. S5D). Thus, in agreement with its subcellular distribution, knockdown of AQP11 yielded functional consequences only on the permeability of the ER membrane to H_2O_2.

Importantly, $AQP11_{low}$ cells consistently revealed a higher basal oxidation state of *HyPerERLum* when compared to mock cells (Fig. 25B, left graph). Therefore, a possible explanation of the failure to detect *HyPerERLum* changes upon challenge with exogenous H_2O_2 could be that basal activation of the sensor is maximum in the more oxidizing environment of the ER. However, reproducible changes in the 488/405 ratio can be constantly recorded after the addition of H_2O_2 also in $AQP11_{low}$ cells (Fig. S6A). These results suggest that a continuous efflux of the ER-produced H_2O_2 reaches the cytosol through the channel. Accordingly, *HyPerCyto* sensors were significantly less oxidized at a steady state in $AQP11_{low}$ cells (Fig. 25B, right graph), whereas the *HyPerMito* probe showed minimal changes (Fig. S6B).

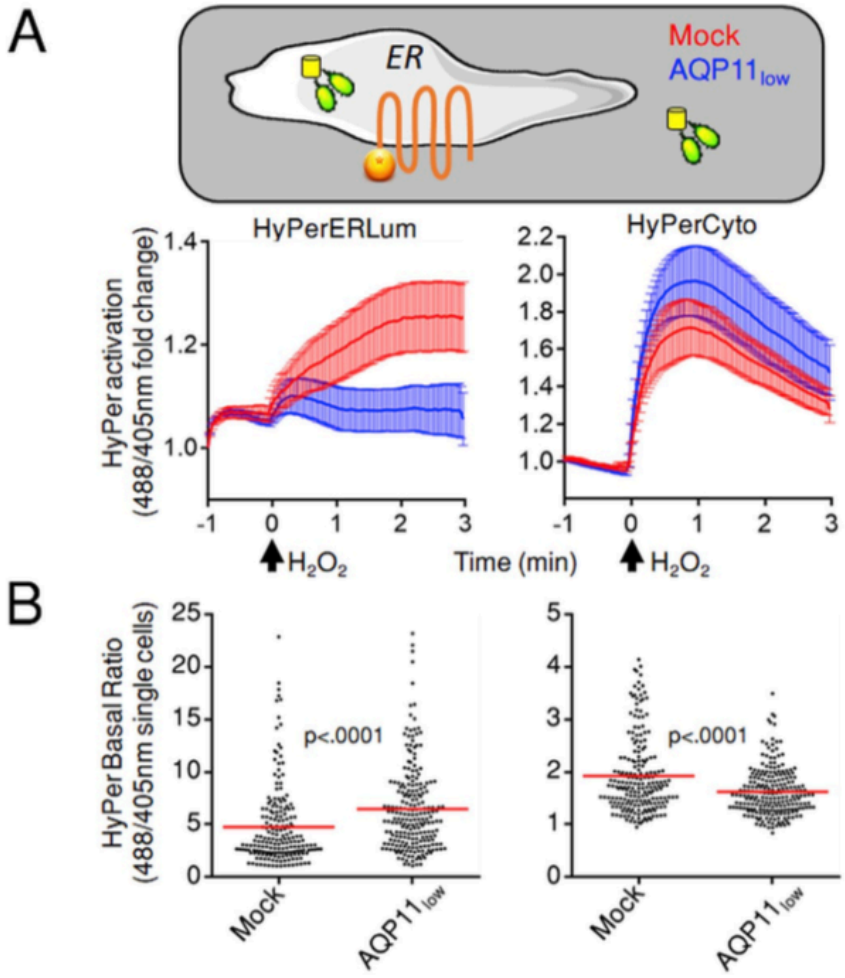

Figure 25: AQP11 is a peroxiporin.

A) HeLa cells stably expressing HyPer in the ER lumen (HyPerERLum) or in the cytosol (HyPerCyto) were treated with AQP11-specific or control small interfering RNAs (siRNAs) and the kinetics of probe activation upon exposure to 50 µM H_2O_2 plotted against time. The black arrow indicates the time of H_2O_2 addition. Data are shown as mean fold changes of the 488/ 405 nm ratio and corresponds to ≥5 experiments ± standard error of the mean (SEM). Note that AQP11 silencing inhibits HyPerERLum activation without interfering with the cytosolic sensor.

B) Measurement of the basal oxidation state of HyPerERLum and HyPerCyto. Each dot represents a single cell distributed in the graph according to its 488/ 405 nm ratio. Comparing the panels highlights that AQP11 silencing impacts in opposite ways the ER lumenal and cytosolic HyPer sensors.

(Bestetti et al, 2020)

Differently from silencing efficiency, which impacts the majority of cells (Figs. S5B and S6A, lower panel), plasmid-driven transfection induces overexpression in half or less of the cells. This limitation was quite useful, as it allowed to perform imaging experiments with internal controls, in which the responses of $AQP11_{low}$ cells with those that were reconstituted with a Halo-tagged version of AQP11 engineered to be silencing-resistant could be compared (Fig. 26A). Clearly, expression of the transgene rescued H_2O_2 transport across the ER membrane, allowing the oxidation of the *HyPerERLum* probe (Fig. 26A, left panels, and 26B, upper graph). The higher basal ratio level of *HyPerERLum* in non-rescued $AQP11_{low}$ cells was evident also in this experiment (Fig. 26B, lower graph). Importantly, it did not increase significantly upon exposure to exogenous H_2O_2, confirming that the ER membrane was impermeant to H_2O_2 in the absence of AQP11 (Fig. 26A). Consistently with our previous results, in cells whose ER peroxiporin capacity had been rescued by HaloAQP11 expression, the *HyPerERLum* basal ratio returned to the levels seen in mock controls (Fig. 26B, lower panel). Cells expressing both transfected HaloAQP11 and the endogenous protein displayed the lowest basal ratios, suggesting that ER permeability to H_2O_2 is related to the number of channels expressed at its membrane.

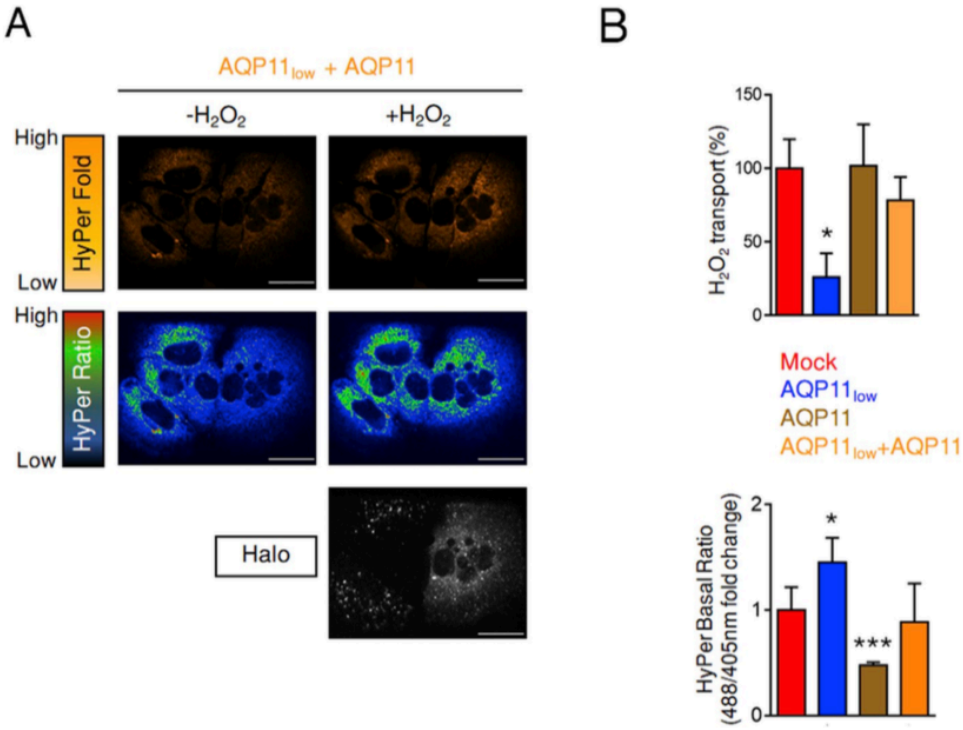

Figure 26: AQP11 restores H_2O_2 fluxes in silenced cells. *HyPerERLum HeLa transfectants were silenced for AQP11 expression and then transfected with a silencing-resistant HaloAQP11.* ***Note the higher basal ratio of silenced cells when compared with mock counterparts and that rescue efficiently restores both permeability and compartment oxidation.***

A) Representative immunofluorescence analyses of one of the experiments averaged in panel B confirm the lower response to exogenous H_2O_2 (top panels, HyPerERLum fold changes, in orange) and higher basal oxidation of HyPer ER lumen (middle panels, basal ratio, in the rainbow) in AQP11-silenced cells. Both features are rescued by re-expression of HaloAQP11, as monitored using fluorescent Halo ligands as shown in the lower panel (in white).

B) The efficiency of the entry of exogenous H_2O_2 (50 µM, top graph) and the basal oxidation state of the HyPer ER lumenal probe (bottom panel) were measured as in Fig. 25, in control or $AQP11_{low}$ cells, before or after rescuing. Results are represented as the percentage of H_2O_2 transported 1.5 min after H_2O_2 addition relative to controls (Mock), and as the fold change in the basal 488/405nm ratio (bottom). Average on ≥3 experiments ± SEM.

(Bestetti et al, 2020)

3.2 An interorganellar redox communication sustains the ER oxidative environment

The data reported in this section will be soon submitted as an original research manuscript in which I will be sole first author.

In our previous paper (Bestetti *et al*, 2020), we observed that the absence of AQP11 causes an increase in the basal oxidative level of the ER and a decrease in the cytosol. These results suggested that a continuous flux of H_2O_2 exists between these two organelles. To dissect the phenomenon, we hypothesized that identification of the source would serve to unveil its function. To shed light on the putative source(s) of this flux it was reasoned that, among all ROS producers residing in the ER, two proteins, Ero1α and NOX4 were the ideal candidates, as both are constitutive H_2O_2 producers. Hence Ero1α or NOX4 were silenced alone or in combination with AQP11 and the ER basal oxidative levels were measured. NOX4 silencing slightly decreased *HyPerERlum* oxidation, but most surprisingly, silencing of Ero1α caused a significant increase in the basal ER H_2O_2 levels. The unexpected observation took all our attention to the mechanism behind this result. Pursuing this aim, we defined that a redox interorganellar communication was established between ER and mitochondria in the absence of the ER major oxidase.

3.2.1 H_2O_2 increases inside the ER upon Ero1α silencing

The ER is the organelle with the highest concentration of H_2O_2 inside the cell, harboring an enormous potential for emitting redox signals following a gradient concentration (Gao *et al*, 2017). Our last work (Bestetti *et al*, 2020) showed that AQP11, a functional peroxiporin is housed in the ER, and guarantees a constitutive redox flux directed to the cytosol. Hence, we wanted to characterize this flow. We used our established model consisting of HeLa cells stably expressing HyPer (Belousov *et al*, 2006) in the ER lumen (*HyPerERLum*) to identify the putative source(s). As reported before (Bestetti *et al*, 2020), these cells were suitable to measure oscillations in the ER oxidative basal levels, even the high oxidation environment of this organelle. Among the many ROS-producing enzymes localized in the ER, we selected two, Ero1α and NOX4, because of their high activity rate (Zito *et al*, 2010b; Nguyen *et al*, 2011). Ero1α collaborates with PDI in the formation of disulfide bonds producing as byproduct H_2O_2 (Tu & Weissman, 2004). NOX4 constitutively produces H_2O_2 in the absence of a known activation signal (Nisimoto *et al*, 2014). To understand whether one of those can be the culprit, we knocked-down their expression either individually or in combination with AQP11. Single-silenced AQP11 knock-down cells revealed a higher basal oxidation state of *HyPerERLum* when compared to mock cells (Fig. 27A unboxed columns, 27B and S7A) in line with our previous observations (Bestetti *et al*, 2020). Down-regulation of NOX4 induced a slight decrease of *HyPerERLum* basal ratio, in agreement with its oxidizing functions and suggesting a modest contribution on ER basal oxidative state (Fig. 27A unboxed columns, 27B and S7A). In contrast and rather surprisingly, the knock-down of Ero1α strongly increased the basal oxidative level of the ER seemingly in contradiction with the absence of an oxidase inside the ER (Fig. 27A unboxed columns, 27B and S7A). As HyPer activation relies on the formation of a disulfide bond, and due to the involvement of Ero1α in mediating the introduction of disulfides, we expressed an ER-targeted catalase (ER-CAT (Konno *et al*, 2015)) at the same time than we silenced the expression of the oxidases. In all the conditions tested, a reduction of the HyPer basal state (Fig. 27A pink boxed columns, 27B and S7C) was recorded, indicating that the increases sensed in the absence of both Ero1α and AQP11 were caused by an increase in H_2O_2 concentration levels. Parallel experiments using a HyPer probe insensitive to pH

fluctuations (SHyPer), to further confirm that the pH of the organelle was not altered (Fig. S7B).

Analyses of the single-cell ER oxidation state of *HyPerERLum* cells upon individual silencing (either AQP11, NOX4, or Ero1α) yielded similar results. However, double silencing of AQP11 in combination with Ero1α knock-down completely abrogated the increase, suggesting that an extra-ER H_2O_2 source can fuel the ER when the oxidase is absent. Instead, silencing both AQP11 and NOX4 expression induced an increase in HyPer basal oxidation state compared to the single silencing of NOX4 comparable to the one observed when silencing AQP11 alone, which may reflect Ero1α activity in the absence of an escaping channel (Fig. 27C). This latter result points to Ero1α as the origin of the source, though we cannot exclude that the NOX4 silencing induces a compensatory oxidative mechanism inside the ER that compensates for its absence.

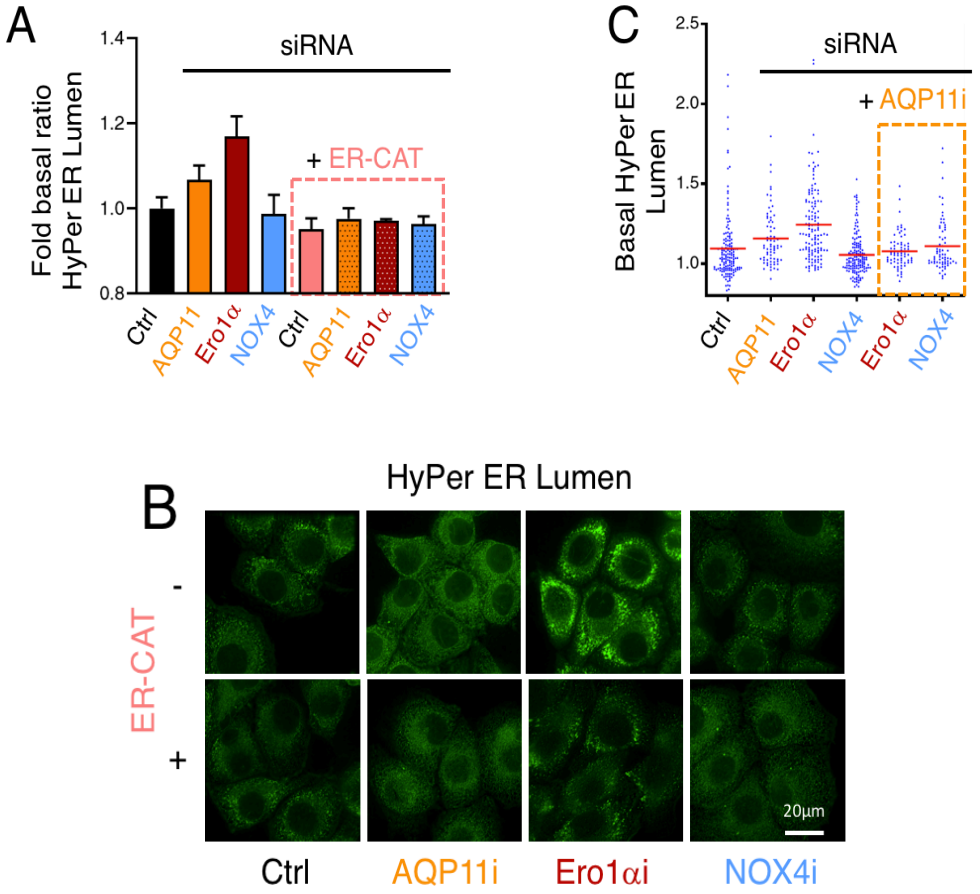

Figure 27: The absence of Ero1α increases the basal oxidative level of the ER.

A) The graph represents the changes in the basal ratio (488/405) of HyPerERlum, expressed in fold change with respect to untreated cells, upon AQP11, Ero1α, or NOX4 down-regulation. The silencing of AQP11(orange column) caused an increase in probe oxidation, as previously reported (section 3.1 (Bestetti *et al*, 2020)*). Silencing of NOX4 (Blue column) had minor effects, whilst Ero1α downregulation caused a higher increase in basal HyPerERlum oxidation than AQP11 silencing alone. Noteworthy expression of ER-Catalase abolished the differences, confirming that the observed results reflected rises in the luminal concentration of H_2O_2. Average of ≥5 independent experiments ± SEM*

B) Single time frames of HeLa cells expressing HyperERLum under silencing conditions with or without (lower and upper panels, respectively) the co-expression of an ER-targeted catalase.

C) The plot shows the trend of distribution of the basal ratio (488/405) of single HeLa cells. The data presented in the orange box (silencing of Ero1α+ AQP11 and NOX4+AQP11) reflects the contribution of each possible source. Note that the cell profile is similar in all conditions except for the one corresponding to the Ero1α siRNA treatment. Mean of the ratio of single cells of ≥5 paired experiments.

To further investigate the relationship between AQP11 and either NOX4 or Ero1α and due to the limited diffusion of H_2O_2 in environments equipped with antioxidant enzymatic systems, we checked whether the channel interacted with the oxidases. To this aim, HeLa cells were co-transfected with NOX4-Flag and either Halo-AQP11, Halo-AQP8, Halo-GPX8, or Halo-RDEL proteins and aliquots of lysates immunoprecipitated using beads crosslinked with an anti-Flag antibody. The experiment showed that Halo-AQP11 and a small fraction of Halo-AQP8 (ER retained, Blue arrow) were coprecipitated by NOX4-Flag, while both the soluble control and the ER transmembrane control were not (Fig. 28A). Since the boundary was detected by overexpressing both proteins as not good antibodies are available, physical interaction is assured, but no direct assessment of a constitutive association can be guaranteed. Instead, for testing the interaction with Ero1α we relied on a specific antibody that recognizes Ero1α endogenous proteins. In this case, HeLa cells were transfected with Halo-AQP11 alone and precipitated using anti- Ero1α conjugated beads. Clearly, also in this case endogenous Ero1α pulled down the

transfected HaloAQP11 (Fig. 28B). The nature and sequence of this interaction are still without an answer as we have not deepened on whether they form part of tripartite complexes or the channel pairs with specific ROS-producers following redox signalling needs. For sure the matter would need further investigation.

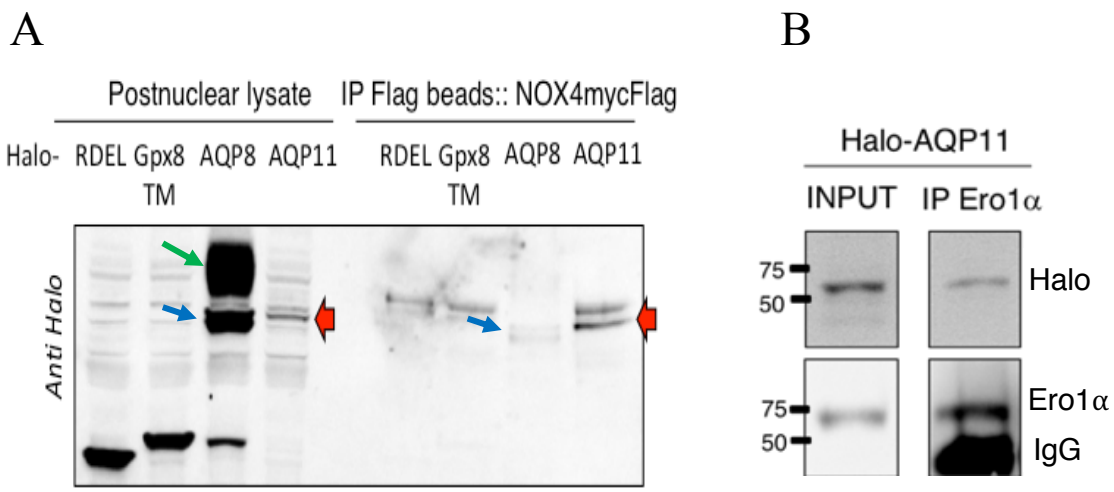

Figure 28: AQP11associates with NOX4 as well as Ero1α

A) Lysates from HeLa transfectants co-expressing NOX4-Flag with Halo-AQP11(Red arrows), Halo-AQP8 (Green arrow: mature form located in the PM; Blue arrow: immature form processed in the ER), Halo-GPX8, or Halo-RDEL were immunoprecipitated with commercial anti-Flag beads. Bands were detected using rabbit anti-Halo antibodies (Promega). This experiment was done five times.

B) Lysates from HeLa transfectants expressing HaloAQP11 were immunoprecipitated with anti-Ero1α 2G4 monoclonal antibodies immobilized onto Protein A/G sepharose beads (Ronzoni *et al*, 2010)*) and decorated with either anti-Halo or anti-Ero1α. Note that HaloAQP11 is coprecipitated by anti-Ero1α antibodies. The figure shows a representative western blot. Similar results were obtained in 3 independent experiments. (Note: the whole image is also shown below in Fig.33)*

3.2.2 Mitochondria are the main source of H_2O_2 that reaches the ER of cells with low Ero1α level

The behavior of the basal oxidative state of *HyPerERLum* when Ero1α or the couple Ero1α/AQP11 were downregulated suggested the presence of an external source of H_2O_2. Looking at the ROS producers within the cells we first thought that mitochondria could be a valid candidate. Actually, in mitochondria are characterized at least 11 different ROS sources (Brand, 2016) and both the ER and these organelles can be co-regulated by exchanging second messengers such as calcium (Anelli *et al*, 2012; Booth *et al*, 2016). Moreover, both AQP11 (Bestetti *et al*, 2020) and Ero1α (Benham *et al*, 2013) have been reported to be partially localized in the MAMs, a hub for signalling. To assess this point, we turned to our cell model stably expressing HyPer in the MM (*HyPerMito*). Therefore, the basal level of *HyPerMito* was measured both in Ero1α or Ero1α/AQP11 downregulated cells. Remarkably, the results showed that in the absence of the ER soluble oxidase, that is Ero1α, we were also able to measure an increase of the basal oxidative state of the MM (Fig 29A and 29B). The rise in the oxidative state of mitochondria was also detectable when the Ero1α/AQP11 pair was silenced (Fig 29A red column in the orange box and 29B), indicating that even if the channel was depleted the absence of Ero1α impacted an external-to-the-ER organelle. Furthermore, the result can be interpreted as that no H_2O_2 molecules exiting the ER via AQP11 are implied in the process.

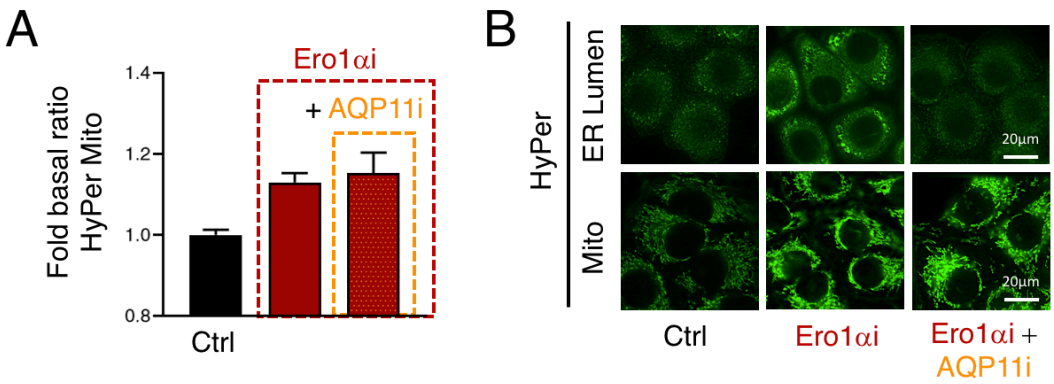

Figure 29: Mitochondria as the source of H_2O_2 that fuels ER

A) Variations in the basal oxidative level of HyPerMito are expressed in fold change relative to control cells. Silencing of Ero1α favors the oxidation of the MM sensor (red column), irrespective of AQP11 activity (red column in the orange box). Average of ≥5 independent experiments ± SEM.

B) Representative images of HyPerERlum and HyPerMito fluorescence after the knock-down of Ero1α or of Ero1α/AQP11 simultaneously.

3.2.3 Complex III is the main source of H_2O_2 molecules that replenish the ER of cells with low Ero1α levels

To identify the mitochondrial player involved, they were taken first into consideration the complexes belonging to the electron transport (ETC) chain since a link between OXPHOS and the rate of protein synthesis has been known for many years (FIALA & FIALA, 1959). In the ETC, complex I and complex III are the most vigorous ROS producers by leaking electrons to molecular oxygen during their activity. Complex I produce superoxide only in the MM whereas complex III generates it both in the IMS and in the MM (St-Pierre *et al*, 2002; Brand, 2016). We initially sought to evaluate whether complex III was the key element of the mechanism considering that it produces directly in the IMS. Hence the H_2O_2 molecules have to cross only the OMM that is less selective than IMM (Kühlbrandt, 2015). To inhibit this protein complex a new compound named S3QEL was selected. S3QEL, differently from other ETC inhibitors traditionally used to block mitochondrial functions, blocks only the leakage of the electron responsible for superoxide formation but not the flow responsible for ATP formation (Orr *et al*, 2015). Thus, *HyPerERLum* cells were silenced for Ero1α expression and a time-course experiment treating cells with S3QEL was performed. As surmised, a time-dependent decrease in the basal state of *HyPerERLum* Ero1α-silenced cells was recorded, sensors reaching control levels after a period of 2h (Fig. 30 and Fig. S8A). Repeating the assay on *HyPerMito* Ero1α-silenced cells yielded similar results (Fig S8B). Even if recovery was complete and for this reason completely attributed to Complex III ROS production, we also tested whether blocking the leakage from Complex I would show the same effect. In that case, the drug used was another compound that also inhibited the leakage of electrons to oxygen while not blocking the whole ETC, S1QEL (Brand *et al*, 2016). S1QEL similarly to S3QEL induced a decrease in the redox ambient of mitochondria, as detected with the *HyPerMito* sensors (Fig. 30, Fig. S8A and S8B). However, the increase in basal the basal ratio of the ER induced by the absence of Ero1α and sensed with *HyPerERLum* probes remained unaffected. To further confirm the involvement of complex III, we intervened in a different step of the putative pathway. The biophysical features of AQP pores do not allow charged molecules to traverse the channel. Thus, peroxiporins are only able to transport redox equivalents once that a cellular SOD has

converted the superoxide produced into H_2O_2. In the IMS of mitochondria, SOD1 is the enzyme that metabolizes the superoxide produced by complex III, while the confined to the MM SOD2 does the same job for Complex I. Hence, we decided to block the dismutation of superoxide produced by SOD1 using a specific drug called LCS-1 (Somwar *et al*, 2011). As shown in Fig. 30, *HyPerERLum* cells silenced for Ero1α expression showed a time-dependent decrease of the basal oxidative state of ER after treatment with LCS1 that paralleled the direct block of the electron leakage of Complex III (Fig. 30 and Fig. S8A). Thus, we concluded that complex III in Ero1α-silenced cells was activated to produce superoxide that was rapidly converted into H_2O_2 that, at this point, reached the ER via AQP11.

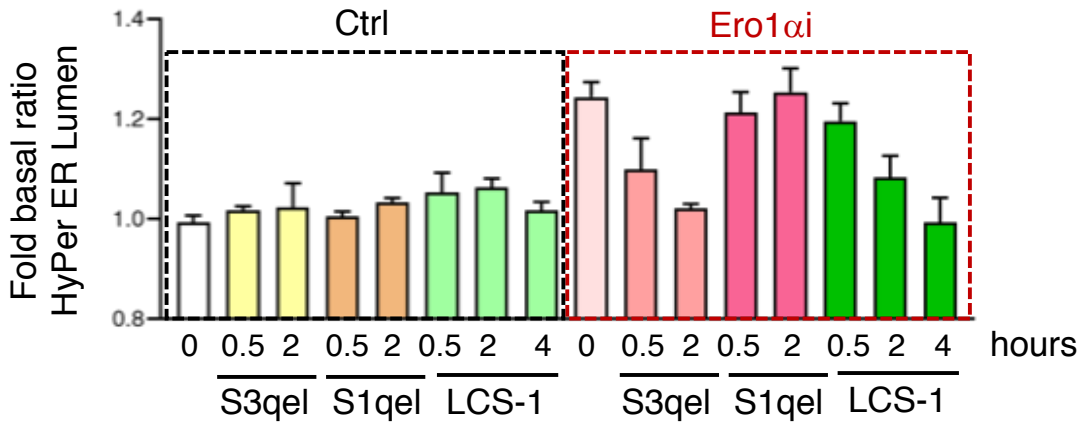

Figure 30: ETC Complex III is the mitochondrial source that fuels the ER in Ero1α-silenced cells

Effects of the indicated drugs on the basal oxidative level of HyPerERLum before (black box) or after (red box) Ero1α silencing. The "0" column represents control cells treated with the drug vehicle (DMSO). S3QEL and S1QEL hit Complex III and Complex I, respectively; LCS-1 inhibits specifically SOD1. Average of ≥3 independent experiments ± SEM.

3.2.4 Ero1α-silencing induces MAM formation

The transfer of redox equivalents shown by the above experiments immediately suggested that the contact sites between mitochondria and the ER determined as MAMs could be preferential areas to mediate the ER refilling (Booth *et al*, 2016). Remarkably, not only many oxidative folding-related enzymes are located in MAMs, but also we have recently demonstrated that AQP11 is partially situated on that ER sub-regions (Bestetti *et al*, 2020). Therefore, we used transmission electron microscopy (TEM) on HeLa cells in which we have selectively knock-down Ero1α or double silenced Ero1α/AQP11 expression to address whether the different conditions impacted MAM formation. To this end, each mitochondrion appearing on TEM images was examined and the number and length of each contact were measured using ImageJ. As the gap between the ER and the mitochondria that can be considered a MAM is still a matter of debate, we selected the most stringent accepted cut-off (<30nm) (Giacomello & Pellegrini, 2016) for our considerations. When analysing the quantity of contacts established between the ER and the mitochondria it resulted that both the single and the double silencing led to an increase of at least 3-fold in the number of MAMs (Fig. 31A, 31B, Fig. S9A, and Fig. S9B). Thus, not only mitochondria produce H_2O_2 to replenish the ER, but they also rearranged more MAM contact points between both organelles to improve signal transmission.

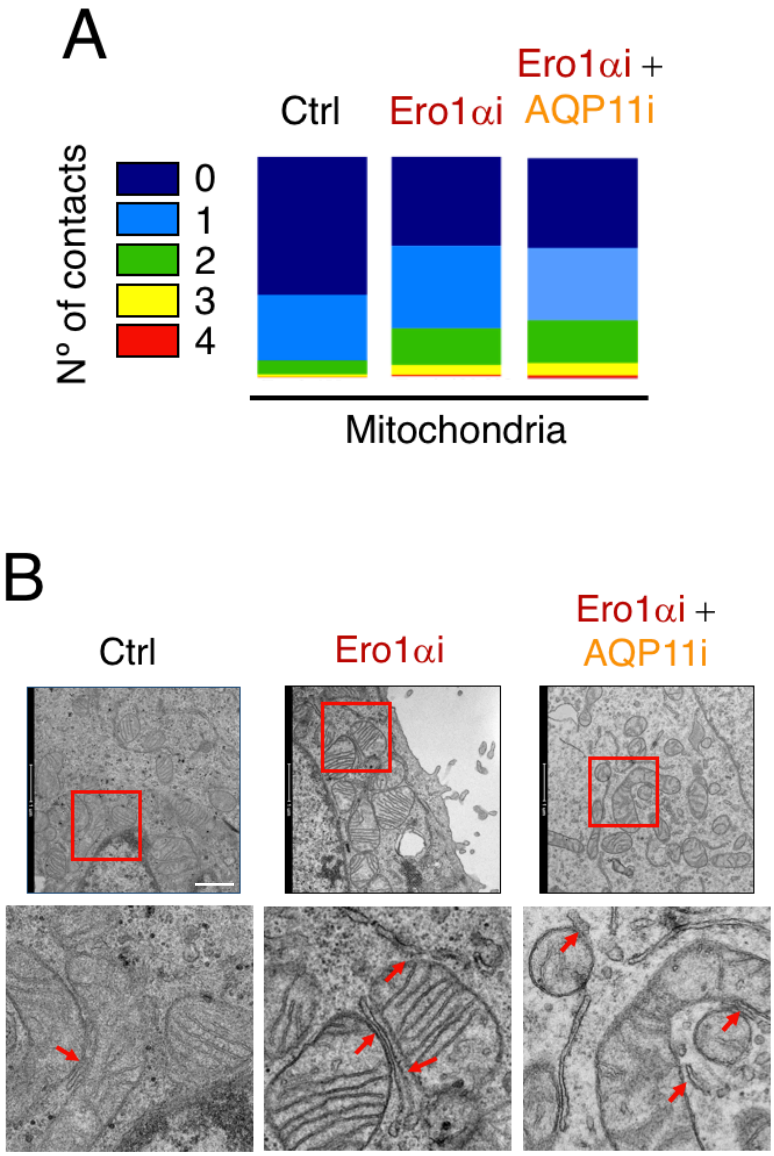

Figure 31: Ero1α-silencing induces MAM formation.

A) Representation of the number of contacts between the ER and the mitochondria. Each mitochondrion revealed by TEM imaging was drawn using the freehand selection of ImageJ. The cut-off to consider a contact as a MAM is <30nm. Mean of two independent experiments.

B) Representative TEM image frames of MAMs for each condition assayed. Scale Bar = 1μm.

3.2.5 Mitochondrial flux maintains the correct redox environment in absence of Ero1α

One of the major functions of Ero1α is to recycle PDI into its oxidized form to sustain oxidative folding. Importantly, cells lacking Ero1α are still able to introduce disulfide bonds by using the activity of Prx-4 (Konno *et al*, 2015). However, still, Prx-4 needs an oxidative source for redox equivalents, yet to be identified. Thus, we sought to analyze whether Complex III-mediated flux would have a role as a backup mechanism for the maintenance of oxidative folding. To test this possibility, HeLa cells were silenced either for AQP11, Ero1α, or both expression and disulfide formation was assessed using a radioactive J-Chain folding assay (Bertoli *et al*, 2004). This protocol measures the velocity of re-oxidation of the J-chain, a proteinaceous component of antibodies rich in disulfides, and that further forms oxidation-dependent oligomers. Thus, in control conditions and after a pulse with DTT, the J-chain is completely converted into its monomeric reduced form, which rapidly disappears when retiring the reducing agent simultaneously with the appearance of a lower molecular weight form corresponding with the protein acquiring its native oxidized fold that is more compact. Furthermore, if chased for enough time, the oxidated monomeric J-chain oligomerizes, increasing its electrophoretic mobility (Bertoli *et al*, 2004). Interestingly, when performing the assay, we observed no differences between control cells and each single silencing on the ratio of monomeric oxidized/reduced forms. Notwithstanding, the oxidized form predominated over the reduced one when both AQP11 and Ero1α were silenced as if the monomeric oxidized form accumulated without oligomerizing (Fig. 32A and Fig. 32B). Unfortunately, our method assay did not allow us to observe oligomers. However, a plausible explanation for this result would still be that H_2O_2 is not involved in introducing disulfide bonds on proteins but more likely in the isomerization of incorrect ones by PDI, thus preventing the appearance of complex associations. While the oxidative activity of PDI on introducing disulfide bonds relies directly on Ero1α, its isomerizing activity depends on an appropriate redox environment. The GSH/GSSG ratio is the major buffer preserving the oxidative poise inside the ER required for accurate folding (Chakravarthi & Bulleid, 2004). Remarkably, maintenance of the ratio favorable for GSSG is also promoted by Ero1α (Delaunay-Moisan *et al*, 2017). To evaluate the redox state of the

ER inferred from the GSH/GSSG ratio, we measured these species using a luminescence-based assay after silencing either Ero1α, AQP11, or both in HeLa cells. The results obtained showed that in absence of only the oxidase the GSH/GSSG ratio is equal to control conditions, thus supporting the hypothesis that a compensatory mechanism allows for the formation of GSSG in the absence of Ero1α. On the contrary, GSH aberrantly predominates over GSSG both when cells were single silenced for AQP11 and when the channel is silenced together with the oxidase (Fig. 32C). While this result can be interpreted as if the peroxiporin absence somehow promotes ER reduction, it can be also conceivable that due to the interaction observed before between both proteins (Fig. 28B), single silencing of AQP11 may be analogous to combined silencing, as both conditions may impact similarly in terms of situating Ero1α at a particular ER location.

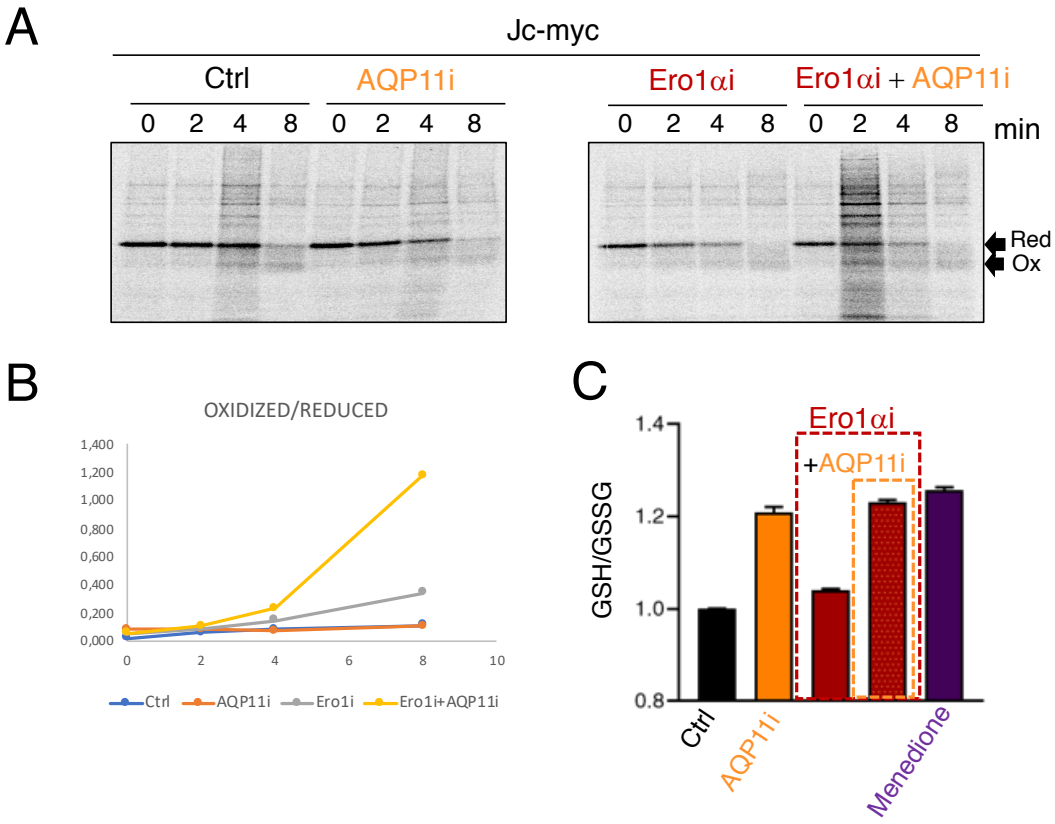

Figure 32: Mitochondrial complex III mediated flux sustains ER redox environment.

A) radioactive J chain folding assay. Cells were silenced for AQP11, Ero1α, or both and transfected with J-chain Myc tagged. After 48h cells were subjected to a DTT 5mM pulse for 5 min. Then, cells were washed and collected at different times adding NEM to block free cysteines. Anti-Myc Ip was performed.

B) Graph of the values obtained in panel A. Mean of 3 different experiments ± SEM.

C) GSH/GSSG experiment. The Promega GSH-Glo™ ***Assay*** *was performed based on manufacturer instructions. Only one experiment with at least three technical replicates. Mean ± SEM.*

3.3 Is the ER-mitochondria redox communication used physiologically?

The data presented in this section are preliminary.

We have shown during the work that constitutes the basis of the present thesis, that the absence of Ero1α increases mitochondrial ETC complex III electron leakage to produce superoxide. This molecule is converted rapidly into H_2O_2 and reaches the ER via AQP11. One of the limitations of the model is that our results were obtained after Ero1α siRNA-mediated silencing. However, we surmised that the complete absence of the oxidase may not be the unique trigger of this mechanism. Notably, it has been reported that during several stresses or under high protein secretion demanding conditions, Ero1α leaves the ER to become phosphorylated in the Golgi (Zhang *et al*, 2018). Therefore, we decided to explore whether inducing ER stress would be a manner to activate the interorganellar redox flux we have described. To this end, we incubated the ER stressor tunicamycin, which blocks N-linked glycosylation promoting the accumulation of unfolded proteins inside the ER (Surani, 1979), with our HeLa cells stably expressing *HyPerERLum*, and measure the basal state of the compartment at different time-points (Fig. 33). As prompt as 15min after adding the drug, the oxidation of HyPerERLum started to increase, reaching a maximum at 30 min and then decreasing. Curiously the effect seemed to be an early event preceding full triggering of the unfolded protein response as measured by activation of two of its branches, PERK phosphorylation and xbp1 splicing (Fig. S10A). To correlate the result to a putative change in Ero1α localization, cells overexpressing Halo-AQP11 were immunoprecipitated with anti- Ero1α conjugated beads during tunicamycin treatment. Remarkably, the highest oxidation rate of HyPer after inducing ER stress matches with the lack of the oxidase linked to AQP11, while recuperation of the oxidative tone in the ER paralleled the return of the oxidase to the channel (Fig. 33A and Fig. 33B). As Ero1α silencing induced MAM reshaping, we sought to determine whether this was also the case during ER stress. Again, and as we predicted, TEM images revealed that the number of contacts between the mitochondria and the ER was higher after 30min of incubation with tunicamycin than under control conditions and that this number returned to normal following the HyPer decrease in fluorescence (Fig. 33C). All

these data together may indicate that mitochondria-ER communication substitutes the temporary absence of the redox couple Ero1α-AQP11 during cell stress.

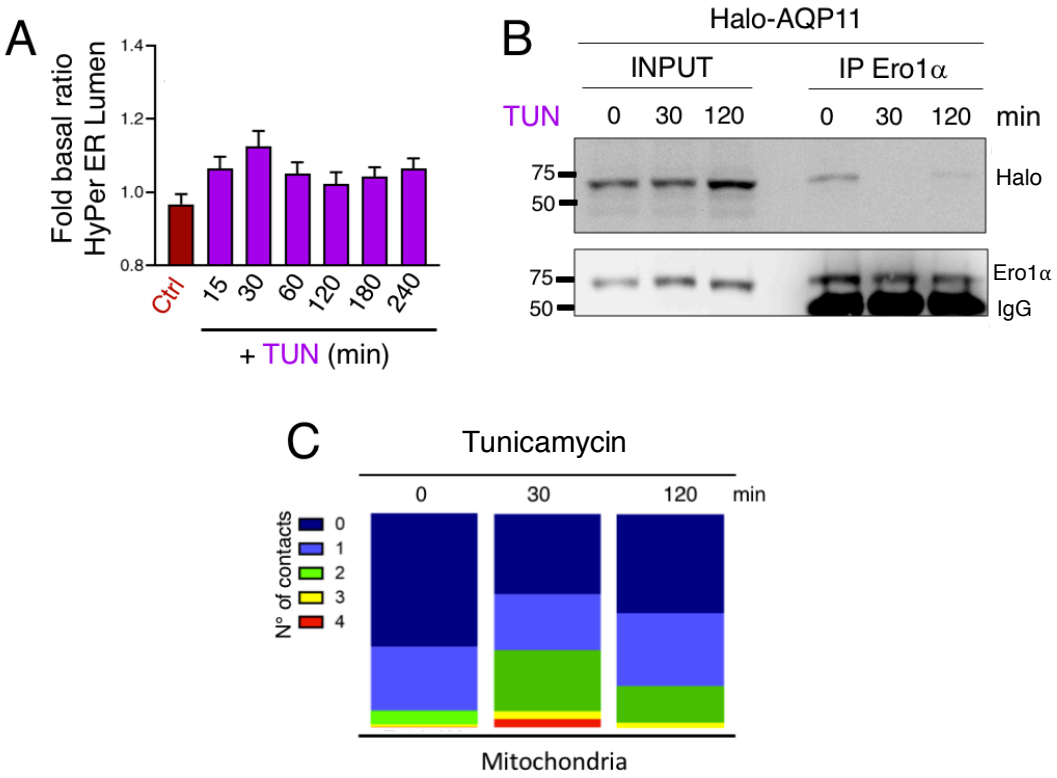

Figure 33: Tunicamycin treatment activates a transitory increase in ER oxidant content.

A) The graph represents the fold change with respect to control of the HyperERLum basal level in samples treated with tunicamycin at different time points. The cell impermeant reducing agent MESNA was added at the whole setup to bypass the gating of the plasma membrane peroxiporin AQP8 triggered by cell stress, without altering the intracellular milieu. Average on ≥7 independent experiments ± SEM.

B) Immunoprecipitation of Halo-AQP11 with Ero1α linked beads. Cells were treated with tunicamycin and collected at different time points before lysis.

C) Representation of ER-Mitochondria contact sites after tunicamycin treatment. At least 5 independent images for each condition were analyzed.

4 Discussion

The dual role of H_2O_2, an essential second messenger while cytotoxic depending on its concentration (Meng *et al*, 2002) implies the existence of accurate systems regulating its production, clearance and, transport. Membrane impermeability becomes hence essential for establishing the gradients that allow transmission of redox signals. It is now clear that the efficient transport of H_2O_2 across membranes requires proteinaceous channels, some of which belong to the aquaporin (AQP) family. A few members of this family can conduit not only H_2O but also H_2O_2. For this important property, AQP3 (Miller *et al*, 2010), AQP8 (Bienert *et al*, 2007; Bertolotti *et al*, 2013), AQP9 (Watanabe *et al*, 2016) are now defined peroxiporins (Bienert *et al*, 2017; Nordzieke & Medraño-Fernandez, 2018). The existence of several isoforms immediately implies different functions and/or regulation modes. Let us consider the signalling role of H_2O_2, via inhibition of protein tyrosine phosphatases in the cytosol. As the task implies competition with abundant peroxidases, topological considerations become paramount. In this scenario, the presence of AQP8 on the plasma membrane and AQP11 in the ER suggest that a cartography of redox signals could exist. In different cell lines, plasma membrane NOXes produce H_2O_2 upon TKR activation. The presence of peroxiporins on the cell surface allows entry of H_2O_2 into the cytosol, boosting downstream signalling pathways (Bertolotti *et al*, 2013, 2016). Furthermore, an elegant redoxstat mechanisms gates AQP8, limiting overoxidation (Medraño-Fernandez *et al*, 2016; Bestetti *et al*, 2018). Mitochondria and the ER are instead constitutive H_2O_2 producers. Yet, it is hard to see them as passive watchers in the redox circuitry of the cell. Thus, my PhD project started in this challenging scenario.

The first question was to identify whether a resident peroxiporin could be used to establish a redox signalling axis emanating from the ER. The results summarized in the first part of my thesis show that AQP11 is a functional ER-resident peroxiporin and suggest that a continuous flux of H_2O_2 exists between ER and cytosol.

The second aim was the identification of the main sources of this H_2O_2-mediated intracellular flux. And here I had a really unexpected result. Opposite to our predictions,

the selective down-regulation of Ero1α, a flavoprotein that generates H_2O_2 to promote disulfide bond formation, increased the basal level of H_2O_2 inside the ER lumen. This surprising finding attracted my attention inducing me to get more insight into the mechanism. These results are described in the last part of my thesis, the central part of which describes an interorganellar communication between the ER and the mitochondria upon perturbation of luminal redoxstasis, entailing H_2O_2 exchange.

I) AQP11 is an ER resident peroxiporin

There is a general agreement that the ER is more oxidizing than the cytosol. However, redoxstasis in the ER is as fascinating as complicated as a phenomenon. A cohort of resident enzymes catalyze the targeted formation, isomerization, and reduction of disulfide bonds, acting coordinately with a set of oxidant/antioxidant non-protein systems to maintain secretory proteostasis and redoxstasis. Thus, a single plasma cell can produce up to 10^5 disulfides per second to sustain Ig production. This entails the production of as many molecules of H_2O_2 (Tu & Weissman, 2004) that can possibly also act as intra- or inter-cellular signals. The ER also houses NOX4, an enzyme that differently from most other NOX family members, directly produces H_2O_2 inside the ER and is constitutively active. So, due to its high oxidative environment and functions, it can be surmised that a resident peroxiporin may be used to transport redox molecules from the ER. Previous work on AQP11 reported a strong impact of the lack of this channel on renal development. Indeed, KO mice die soon two weeks after birth due to a polycystic Kidney-like disease associated with aberrant glycosylation of Polycystin-1(Morishita *et al*, 2005; Inoue *et al*, 2014) and evident signs of oxidative stress. Remarkably, polycystin-1 is a protein that is folded, processed, and early modified in the ER and that resulting from this process can have varied cell localization, including an ER-resident form (Boletta, 2009). In light of this evidence, it may not be surprising that the results presented in Fig. 22 confirm that, in contrast with other AQP isoforms equally synthetized in the ER but with the plasma membrane as the final destination, AQP11 resides exclusively in the ER in all the cell models that we have exploited (Fig. 22A and 22B and Fig S1A, (Bestetti *et al*, 2020); Speranza et al, unpublished). Unfortunately, due to the lack of specific and reliable

antibodies, we must rely so far on silencing and overexpression experiments. The latter might lead to mis-targeting or overflow, yielding artefactual results. Yet, ER localization was observed with numerous chimeric AQP11 constructs, which differed for the type and location of the tags, and irrespective of their expression levels. In addition, other AQPs have been reported to reside in the ER of plant cells. These putative ER-AQPs concur with AQP11 on presenting variations in the highly conserved NPA-NPA motif that normally define AQP channels (NPA-NPC for AQP11).

How is AQP11 retained in the ER? A feature common to AQP11 and plant ER-resident AQPs is the presence of a classical C-terminal di-lysine (-KK) retention motif (Gao *et al*, 2014). In our hands, however, neither KK deletion nor the extension of AQP11 C-terminus led to its re-localization to the plasma membrane (not shown). It seems therefore that other features contribute to ER retention. In this connection, most of the hydrophobic segments of AQP11 are shorter than in AQP8, an isoform that reaches the plasma membrane. The length of the transmembrane regions is an important determinant of the subcellular localization of membrane proteins (Sharpe *et al*, 2010). However, others have reported the presence of AQP11 in the plasma membrane (Gorelick *et al*, 2006; Ikeda *et al*, 2011). Although we could not detect this outermost localization, I do not discard the possibility that cell-specific mechanisms exist to determine the extent of AQP11 transport along the exocytic route. Indeed, some cellular lineages secrete PDI, ERp44 , other proteins with C-terminal KDEL motifs that are instead efficiently retained by most other tissues (Sannino *et al*, 2014). It thus appears that cells have the means to target the same protein to more than one compartment, likely to fulfill different physiological tasks. For example, oxidoreductases that normally reside in the early secretory pathway are found in extracellular space where they contribute to regulating coagulation (Holbrook *et al*, 2010).

Remarkably, our cell fractionation experiments not only confirmed a main ER localization of the AQP11 but revealed also its presence in MAM, an important signalling hub where also redox (Ero1α, Gpx8) and calcium (IP3R) regulators accumulate (Fig. 22B). Unfortunately for us, using a non-dosable overexpression system hampers the

possibility of determining whether most of the protein actually resides only in MAMs or is only re-localized there after a particular event.

Whatever its precise localization inside living cells, no doubts remain instead that AQP11 is a functional peroxiporin. This conclusion was achieved using specific H_2O_2-sensitive HyPer probes targeted to different intracellular compartments, kindly provided by the Belousov and Geitz labs. Thus, the downregulation of AQP11 but not of AQP4 – a "pure" water channel devoid of peroxiporin activity- prevents the internalization of H_2O_2 inside the ER without perturbing the passage across the plasma or mitochondrial membranes (Fig. 25A and Fig S5D). Expression of a silencing-resistant version of AQP11 restores H_2O_2 ER permeability. These experiments together imply that AQP11 is in an ideal position to be a critical actor for interorganellar redoxstasis and signalling.

II) Why should the ER compartment need a resident peroxiporin?

To do these studies we selected an HeLa cells line that had an ER oxidant state that permits to measure H_2O_2 fluctuations. For sure HeLa cells have many experimental limits but we are interested to characterize these phenomena from the biochemical point of view that should not change in relation with the cell types. In the future will be interesting test if these could also occur in primary cell lines. As already mentioned above, the ER homes multitude of redox reactions that are essential for cells. An obvious role for specific peroxiporin(s) in this organelle would be that of a regulated valve to release excess oxidation. Such a role would place AQP11 (and possibly other H_2O_2 conducing channels) in the position to mediate interorganellar signalling. Hence, So far, my results downregulating AQP11 clearly point to the existence of a continuous flux of H_2O_2 from the ER to the cytosol. Thus, a possibility would be that, independently from its source, H_2O_2 molecules accumulating in the ER and flowing through AQP11 activate a specific subset of targets, particularly those located in the cytosolic mouth of the channel. As the scavenging systems of the antioxidant defense are abundant and rapid it cannot be assumed that the redox systems residing at the plasma membrane take out all the redox signals that a cell must decode. Hence to transmit specific signals coming from

information generated in the ER, the best option would be to locate the targets in the vicinity of specific ER-resident H_2O_2 channels (Nordzieke & Medraño-Fernandez, 2018).

Putative signals from specific sources/for specific target/ interorganellar communication

The Ero1α -PDI pathway is thought to produce H_2O_2 in stoichiometric amounts to the disulfide bonds formed (Tu & Weissman, 2004). Much has been discussed whether and how these molecules are used or quenched to avoid unwanted damage. However, in light of the presence of a peroxiporin able to conduit H_2O_2 towards sensitive targets in the cytosol, it is conceivable that Ero1α-produced H_2O_2 be a way to transmit information about the efficiency and rate of oxidative folding to the signalling networks that govern cell fate.

Also, NOX4 produces H_2O_2 in the ER lumen. The available evidence indicates that unlike other members of the NOX family, this isoform is constitutively active, its levels being increased by stress (Laurindo *et al*, 2014). Hence, H_2O_2 molecules reaching the cytosol could derive from the activity of this protein. In respect to this, it is already reported that AQP3, AQP8 and, AQP9, all located in the plasma membrane, are the conduits used to uptake the H_2O_2 extracellularly produced by NOXes upon activation of different receptors. This panorama leads to an intriguing possibility: are there specialized organelle-localized redox couples formed by a NOX H_2O_2-source and a peroxiporin? In this connection, H_2O_2 produced by cell surface NOXes has been widely reported to affect plasma membrane vicinal targets, while NOX4 can regulate the phosphorylation status of eIF2α inhibiting only the ER proximal pool of PP1 (Santos *et al*, 2016).

AQP11 could potentially transport the H_2O_2 produced by either Ero1α, NOX4, or other sources, depending on concentration, timing, places, or stimuli. This could be correlated

with the results obtained in the sucrose experiment presented in the results section of this thesis (Fig. 24B), which showed a plethora of high molecular weight complexes for AQP11 that could represent several platforms composed of different proteins in which the peroxiporin is taking part.

Since AQP11 acts as a bidirectional channel following concentration gradients, a redox unbalance that increases the presence of H_2O_2 molecules in the cytosol or any other proximal organelles such as mitochondria or peroxisomes, could potentially be transformed in a flux inside the ER. Abundant ROS are produced by mitochondria under stress conditions. Moreover, a considerable fraction of HaloAQP11 is present in MAMs (see fig. 22B), signalling hubs of continuous interorganellar exchange, particularly from Ca^{2+}-mediated signalling. Previous work from our and other labs has already documented redox-dependent modifications of this signalling circuitry.

A redox ER-mitochondria crosstalk is activated in absence of Ero1α

From a physiological point of view, I reckoned that the most immediate suspects for mediating the constitutive flux pouring out from the ER via AQP11 were Ero1α and NOX4 as both are constant producers of H_2O_2. So, I silenced them singly or in combination. Obviously, I expected the basal levels of H_2O_2 detected by *HyPerERLum* to decrease. Whilst this was the case upon silencing NOX4, knocking-down Ero1α increased *HyPerERLum* oxidation even more than AQP11 silencing did. Considering that Ero1α is thought to fuel oxidative folding, and the shift in *HyPerERLum* emission depends on the formation of a disulfide bond, this result was indeed paradoxical. Removing an oxidase increased the oxidation state of a sensitive probe. The first explanation that came to mind was that Ero1α somehow inhibits NOX4. However, the simultaneous silencing of AQP11 counteracted the effects of Ero1α. Either AQP11 is needed to mediate fluxes between different ER subregions, or an external source is activated that replenishes the ER lumen of H_2O_2 via AQP11 when Ero1α is missing. Since peroxiporins are channels, H_2O_2 concentration must be higher in such a source than that we can measure in the ER, suggesting that indeed organellar compartmentalization is more likely the answer.

Thus, the results I obtained have several implications. First, the increase of the ER basal oxidative level indicates that Ero1α silencing activates a potent source of redox molecules. Second, the requirement for AQP11 implies an external-to-the-ER producer. Third, the source uses AQP11 to replenish the ER. Fourth, Ero1α silencing abrogates the H_2O_2 increase detected in $AQP11^{KD}$ cells.

Mitochondria sustain ER oxidative environment

Compelling evidence demonstrates that ER and mitochondria are intimately interconnected physical protein-protein interactions. The two organelles exchange lipids and second messengers. This dynamic cooperation is presumably clustered in the sub-regions of the external face of the two organelles that establish tight contacts: The MAMs. These structures can be rapidly assembled and disassembled in response to different situations, including ER stress and hypoxia (Kumar & Maity, 2021). My work shows that also lowering Ero1α levels triggers a tightening of the contacts that are presumably correlated to H_2O_2 transfer from mitochondria to the ER. Efficient transfer implies that a reversed H_2O_2 gradient is generated. Accordingly, Ero1α silencing causes a dramatic increase in the concentration of H_2O_2 in the mitochondrial matrix. My data indicate that the mitochondria ETC complex III is the main culprit of this increase. Its involvement was assessed using a panel of drugs known to specifically inhibit the electron leakage to molecular oxygen while permitting the flow along the chain. Remarkably, the inhibition of Complex III, but not of Complex I suppressed the refilling of H_2O_2 sensed in the ER. These findings depict a scenario in which H_2O_2 produced by Complex III in the IMS and reaches the ER via AQP11. Tighter physical connections between ER and mitochondria are likely important to target H_2O_2 toward the ER lumen and limit its diffusion into the cytosol. This model is supported by the results I obtained inhibiting SOD1. This enzyme is crucial in the scheme as it is needed to transform the superoxide produced by complex III into H_2O_2. Since charged superoxide molecules are either unable to cross lipid membranes and use AQP channels, we reasoned that inhibiting SOD1 in the IMS would prevent the rise of H_2O_2 in the ER lumen upon Ero1α silencing. The results demonstrate that this was the case, leading to two conclusions. First, it is H_2O_2 that arrives in the ER;

Second, neither AQP11 nor other unknown channels can favor the transport of superoxide across the ER membrane.

The interorganellar exchange of H_2O_2 via MAMs highlights the overall importance of an accurate regulation of redox signalling and homeostasis for the fitness of the whole cell. These observations raise obvious mechanistic and functional questions: how and why? To answer the first, we must explain how a soluble ER oxidase could impact events occurring in the IMS. Neither Ero1α nor Ero1β have hydrophobic stretches to mediate membrane insertion and both are secreted by cells when overexpressed. However, a fraction of them was shown to be associated with membranes (Cabibbo *et al*, 2000). In this connection, the finding that HaloAQP11 coprecipitates endogenous Ero1α molecules (Fig. 28B) is of particular relevance: on the one hand, it provides a shortcut for the constitutive flux and supports the idea of H_2O_2 being a convenient indicator for oxidative folding in the lumen. The association does not seem to be relevant in providing the signal that emanates from the ER and activates Complex III in the IMS. In fact, the concomitant silencing of AQP11 did not prevent the accumulation of H_2O_2 in the mitochondrial matrix of Ero1α^{KD} cells. The nature of the signal(s) induced by lowering Ero1α, remains therefore a mystery. No more than educated guesses include calcium ions or oxygen tensions. Considering the Ca^{2+} hypothesis: it is described that Ero1α is partially localized at the MAM (ref) and its levels -both upregulation and downregulation- regulate Ca^{2+} fluxes between ER and mitochondria (Anelli *et al*, 2012). Regarding the oxygen hypothesis: it is reported that both Ero1α and ETC complex III are regulated by oxygen levels. Indeed, under hypoxia condition Ero1α leaves MAMs and it goes to Golgi compartment, where it is phosphorylated (Gilady *et al*, 2010; Zhang *et al*, 2018). Moreover, also complex III is oxygen-sensitive and it starts to produce even more ROS under hypoxia condition. This suggests that the absence of the redox couple Ero1α-AQP11 could cause the redistribution of the oxygen intracellular content that activates complex III. Dissecting this fundamental pathway is clearly a challenge worth being pursued.

Why is mitochondrial ROS production activated when Ero1α levels fall?

An answer that immediately comes to mind for this mitochondrial-to-ER flux is a compensatory mechanism aimed to sustain ER functions in the absence of the major oxidative folding oxidase. Two possibilities stand out immediately following the known Ero1α functions: a direct impact of these H_2O_2 molecules in protein folding or an indirect one in which the redox equivalents are used to maintain the redox environment necessary for the folding machinery.

Being an essential process for cell survival, more than one backup mechanisms guarantee the efficiency of disulfide bonds formation. Interestingly, while Ero1α knock-out is lethal in yeast, KO mice lacking this protein survive and show surprisingly only minor phenotypes (Chin *et al*, 2011; Zito *et al*, 2010a). Similarly, cells can adapt to the absence of Ero1α. In this case, formation of disulfide bonds is supported by peroxiredoxin 4 and glutathione peroxidases 7 and 8, enzymes that reside in the ER and can cause H_2O_2 to promote oxidative folding (Konno *et al*, 2015, 2021). However, my experiments with the J-chain folding assay show only small differences in the double knockdown of Ero1α-AQP11. Instead, the GSH/GSSG ratio increases in the ER upon double but not the single Ero1α-AQP11 knockdowns. This finding suggests that the GSSG levels in the ER are related to H_2O_2 levels (Delaunay-Moisan *et al*, 2017).

The minor differences observed in protein oxidation rates highlight once more the strength of compensatory mechanisms, as well as the complexity of the regulatory networks that control ER redoxstasis.

In this complicated scenario, my results suggest that AQP11 and Ero1α can form a complex that may link oxidative folding, redox homeostasis, and redox signalling. Extreme caution must be taken since our results were obtained with overexpressed HaloAQP11. However, we were able to detect its strong association also with a flag-NOX4 in the ER membrane (Fig. 28A). It seems therefore that AQP11 sits close to either one of the two main H_2O_2 sources.

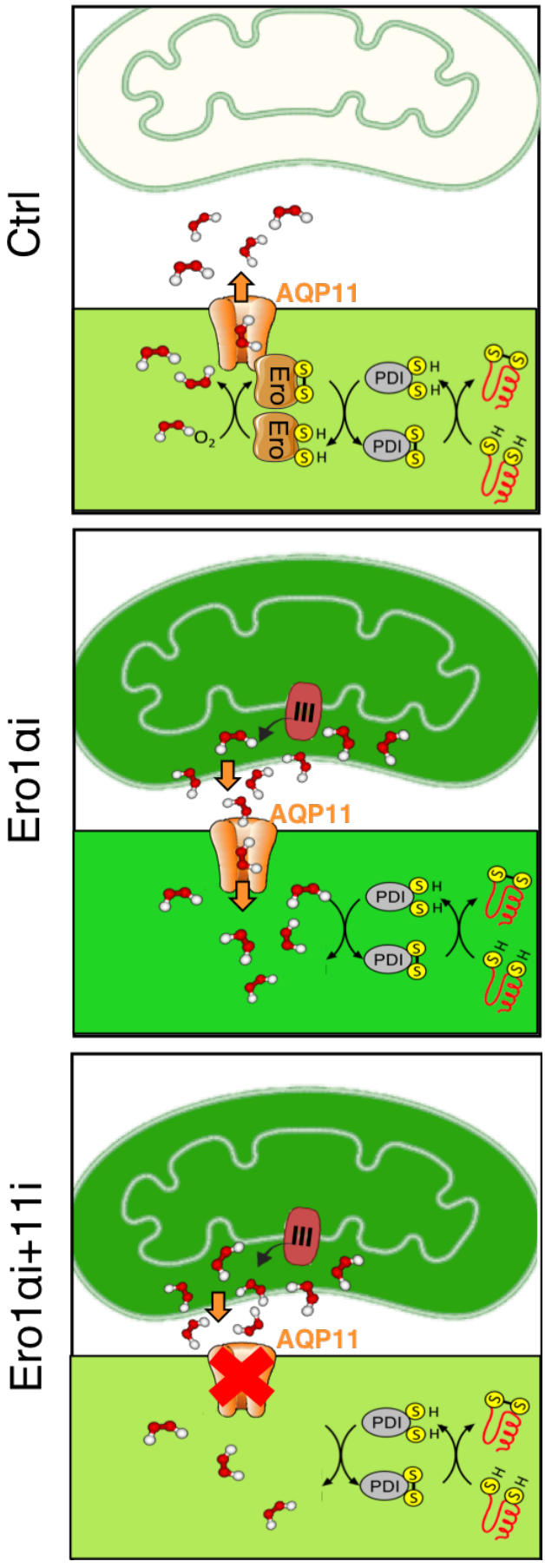

***Figure 34: Model of Ero1α-AQP11 signalling pathway**. In the control condition, Ero1α and AQP11 are bound together. H_2O_2 passes through AQP11 and reaches cytosol (upper pannel). When Ero1α is silenced, ETC complex III is activated and produces ROS that inflates ER and, together there is the reshaping of MAMs (middle pannel). When also AQP11 is downregulated complex III continuous to produce ROS but now they cannot reach the ER (Lower pannel). The green intensity of the organelles represents the HyPer basal state of that compartment.*

III. The stress connection

Having shown this mechanism, one of the first questions that comes to light is "can this occur also in a more physiological situation?". As the ER is the cradle for about one-third of the proteome, a disfunction of this compartment would be a catastrophe for cells. To avoid this possibility, cells have developed a tripartite response to adapt the folding capacity of the ER to new challenges. The UPR can have two opposite outcomes. Either the restoration of homeostasis or cell death by apoptosis. My preliminary results reveal an increase of the *HyPerERLum* oxidation already after 30 minutes of tunicamycin treatment, before detectable activation of Ire1 or PERK. This correlates both with the disruption of the Ero1α-AQP11 complex and with the reshaping of MAMs (Fig 33A, Fig. 33B, Fig., and Fig S10). What is not expected is that all this system is activated before the initiation of the "canonical" UPR. This would mean that either it is a different signal or a UPR early event. After two hours there is an initial reformation of the complex, a restoration of the ER basal level and the fewer MAMs. These data may be interpreted as that Ero1α movement inside the ER promotes a prompt attempt to adapt to overload and the mitochondria substitutes in part its canonical function. Once the situation worsens, Ero1α may come back and classical signals of UPR are detected. In the end, if the situation is not resolved Ero1α may also have a further role in MAMs controlling Ca^{2+} signalling that ultimately will lead to apoptosis. This third part presents preliminary data on the relevance of the interorganellar redox communication described here during cellular stress, a pathophysiological condition frequently occurring in cells. A clear example of this would be aging. Indeed, the link between the decline in chaperon fitness and ROS-related diseases has been known for many years (Soti & Csermely, 2003). Actually, the hallmarks of aging, like mitochondrial dysfunction protein denaturation and others, will fit perfectly with the data presented here. The decrease on the expression of chaperones, including Ero1α, may promote a mitochondrial-derived flux of ROS. When sustained in time and even increased as the organism ages it is conceivable that mitochondria will be affected. Indeed it has been constantly suggested that oxidants contribute to lifespan (Sies & Jones, 2020). Thus, the relation between ROS and diseases need more studies to understand the role of redoxstasis in maintaining cellular processes and how it is possible to use as potential treatment.

5 Materials and methods *

* Part of this section comes from Bestetti S. et al. *Redox Biol*. 2020, in which I am Co-first author.

5.1 The HyPer probe as a tool to study H_2O_2 fluctuations

Many of the findings described in the previous section could have never been done without the flourishment of sensitive and efficient H_2O_2 probes. H_2O_2 sensors can be either chemical, like the boronate-based fluorescent dyes used by Miller et al, or genetically encoded like the family of HyPer probes (Fig. 20) (Bilan & Belousov, 2018). Over the chemical ones, genetically engineered probes have widely shown their advantages on the spatial localization of signals, and thus will be further introduced here.

HyPer technology takes advantage of a bacterial transcription factor that senses H_2O_2 levels. In bacteria, the increase in intracellular H_2O_2 levels triggers the formation of a disulfide bond between two redox-sensitive cysteines in the OxyR promoting the activation of the transcription factor and the upregulation of antioxidant genes. In HyPer, the two cysteines have been separated by a modified YFP. Thus, when the probe is exposed to H_2O_2 the formation of the disulfide is induced, and as consequence, the rearrangement of the 3D structure changes the emission spectra of the linked YFP. The modified fluorescent domain has two different excitation wavelengths (420nm and 480nm), and both emit at 520nm. The ratio between the modifications of the emission spectra correlates with H_2O_2 levels.

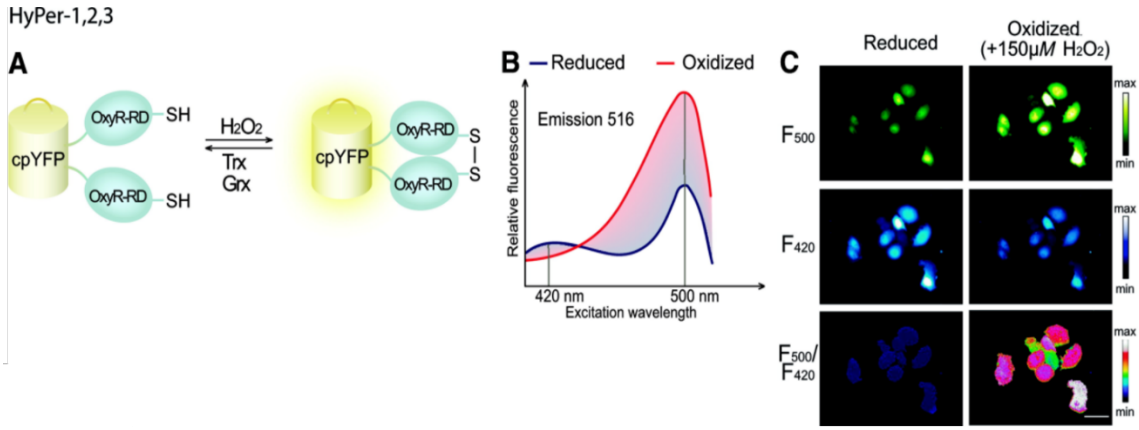

Figure 35: Graphical scheme of HyPer Probe. *A) Structure and functioning. B) Excitation spectra of HyPer. In blue is the reduced form and in red is the oxidized form. C) Images of HyPer before and after the addition of H_2O_2. The lower panel represents the ratio between the two spectra. From Bilan & Belousov, ARS, 2018.*

The advantages of HyPer probes are:

1. High sensitivity: specifically sensitive to H_2O_2 and not to other ROS.
2. Reversibility: the oxidation state of the two cysteines can be reversed under more reducing conditions.
3. Being encoded, it can be fused either to organelle targeting sequences or particular proteins.
4. The two fluorescences assure ratiometricity that allow measurements to be independent of HyPer expression levels.

For these reasons, these probes help to map all the pathways related to H_2O_2 and, in the end, to understand how redox-regulated systems interact with each other and regulate intracellular processes.

5.2 Cell culture and generation of HeLa polyclonal stable cell lines

HeLa, CHO, COS-7 and HEK293 cells were grown in Dulbecco's modified Eagle's medium (DMEM) + GlutaMAXTM-I medium (Gibco, ThermoFisher) complemented with 10% fetal bovine serum (FBS; EuroClone) and 5 mg/ml penicillin-streptomycin (Lonza). HeLa transfectants stably expressing HyPer in the ER (*HyPerERLum*), in the cytosol (*HyPerCyto*), or in the mitochondrial matrix (*HyPerMito*) were generated by transfecting the cells using the PEI method (ThermoFisher) and then selected with 0.5 mg/ml of G418 (Sigma).

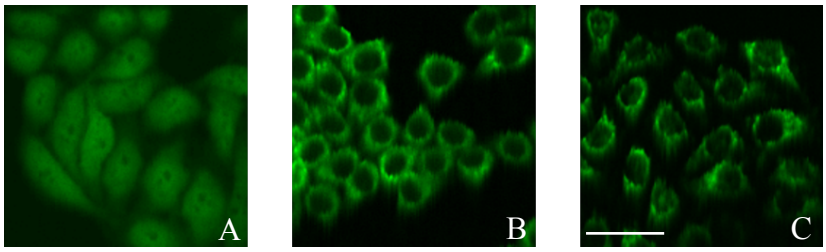

Figure 36: Representative Frames of HyPer probe expressed in different cellular compartments. *Images are acquired using the Ultraview confocal laser scanning microscope equipped with an EC Plan - Neofluar 20X A) HyPerCyto. B) HyPerERLum. C) HyPerMito. Scale bar 50 µm*

5.3 Reagents and Antibodies

All reagents and antibodies used are listed in this section. All will be described in more detail later.

Reagent	Concentration	Cat#	Company	Ref.
Halo ligand R110 direct	2nM	#G322A	Promega	according to manifacturer's instructions
Halo ligand TMR direct	2nM	#G299A	Promega	according to manifacturer's instructions
Halo ligand TMR	2nM	#G8285	Promega	according to manifacturer's instructions
LCS-1	2µM	#567414	EMD millipore	Ting Du et al., Leukemia 2021
S1QEL	33µM	#1-800-364-9897	Cayman Chemical C.	Brand, M.D et al., Cell Metab 2016
S3QEL 2	33µM	#SML1554	Sigma	Orr AL et al., Nat Chem Biol 2015
Tunicamycin	5µM/µl	#IT7765	Sigma	Vitale M. er al., eLife 2019

Table 2: List of Reagents

Antibody	Species	cat#	company	Dilution
Calnexin	Rabbit	#ADI-SPA-860F	Enzo	1:200 in pbs 5% FCS
Calreticulin	Rabbit	#C4606	Sigma	1:200 in pbs 5% FCS
Ero1α	Mouse	clone 2G4	Ronzoni et al., Traffic 2010	1:1000 IN PBS 0,1% Tween 0,5% Milk
Flag Tag M2	Mouse	#F1804	Sigma	1:1000 IN PBS 0,1% Tween 0,5% Milk
GM130	Mouse	#710823	BD Biosciences	1:1000 IN PBS 0,1% Tween 0,5% Milk
GRP94	Rabbit	#ADI-SPA-851	Enzo	1:1000 IN PBS 0,1% Tween 0,5% Milk
Halo Tag	Rabbit	#G9281	Promega	1:1000 IN PBS 0,1% Tween 0,5% Milk
Myc tag	Mouse	clone 9E10	ATCC	1:1000 IN PBS 0,1% Tween 0,5% Milk
Peroxiredoxin 3	Rabbit	#LF-PA0030	Sigma	1:200 in pbs 5% FCS
Sigma Receptor 1	Rabbit	#SAB2701222	Sigma	1:1000 IN PBS 0,1% Tween 0,5% Milk
TOM20	Mouse	#612278	BD Biosciences	1:200 in pbs 5% FCS
Tubulin	Mouse	#T6070	Sigma	1:8000 IN PBS 0,1% Tween 0,5% Milk
Alexa-conjugated 647	Mouse	# A21236	Invitrogen	1:1000 IN PBS 0,1% Tween 0,5% Milk
Alexa-conjugated 546	Rabbit	#A11035	Invitrogen	1:1000 IN PBS 0,1% Tween 0,5% Milk

Table 3: List of the antibodies

5.4 Plasmids, small interfering RNAs, and transfection procedures

Plasmids for expression of *HyPerCyto*, *HyPerMito*, and *HyPerERLum* were gifts of Drs. V. Belousov and M. Geistz (Institute of bioorganic chemistry Moscow) The plasmid for the expression of ER-Catalase (Myc-tagged) was provided by Dr. E. Avezov (University of Cambridge, Department of Clinical Neurosciences). The plasmids to express HaloAQP8, HaloAQP8-Flag, *SyPherERLum,* JcMyc, Halo-RDEL, and HaloGpx8 TM were generated as previously described (Bertolotti *et al*, 2013; Medraño-Fernandez *et al*, 2016; Yoboue *et al*, 2017), while the AQP11mycFlag construct was purchased from Origene (NM_173039) and used to build the proteins HaloAQP11-mycFlag and HaloAQP11. Briefly, the insert containing AQP11 in the original Origene's vector was cloned substituting AQP8 in a HaloAQP8mycFlag-expressing plasmid previously constructed in our lab (Medraño-Fernandez *et al*, 2016), to generate the HaloAQP11-Flag construct. Then, and using the latter as a template, a stop codon was introduced between AQP11 and the C-terminal tags in order to exclude them and generate the appropriate C-terminal tail in order to perform accurate localization studies not influenced by an extended moiety in the vicinity of a putative ER-retention signal (KK motif), with the primers: 5′-AAGGAATAGCGTACGCGGCCGC-3' (forward) and 5′-GCGGCCGCGTACGCTATTCCTT-3' (reverse). Lastly, three consecutive rounds of site-directed mutagenesis were performed on HaloAQP11 to obtain a silencing-resistant version bearing 5 mutations in the region that pairs with the 21 bp target sequence of the AQP11 siRNA (sequence of the siRNA, table 4). The primers used were as follows: first round, 5′-GGAGCTTCG CCTGTAAGAATCCC-3' (forward) and 5′-GGGATTCTTACAGGCGAAGC TCC-3' (reverse); second round 5′-CAGCGAGAGGAGTTTTGCCTGT AAG-3' (forward) and 5′-CTTACAGGCAAAACTCCTCTCGCTG-3' (reverse); and third round 5′-GCCTGTAAAAACCCCATCCGAGTC-3' (forward) and 5′-GACTCGGATGGGGTTTTTACAGGC-3' (reverse). All constructs and mutations were validated by sequencing.

For silencing experiments, 8×10^4 HeLa cells were grown overnight in six-well plates and transfected with 30pmol of each siRNA (see table 4) for 2 days, using RNAiMAX lipofectamine (Invitrogen) according to the manufacturer's instructions.

Name	Target Gene	siRNA ID	Sense Sequence	Brand
AQP11	AQP11	s49052	5′-GAGCUUCGCUUGCAAGAAU-3	Ambion
AQP4	AQP4	ACD0083G	5′-GAUCAGCAUCGCCAAGUCU-3′	Ambion
Ero1α	ERO1A	DPX1396	5'-CUGUUUUAAGCCACAGACA-3'	Merck
Nox4	NOX4	s224161	5'-GCAAGACCUGGUCAGUAUA-3'	Ambion

Table 4: siRNAs description

Silencing was validated by RT-PCR (Table 5).

Primer RT-PCR	Target Gene		Sense Sequence
AQP11	AQP11	Fw	5'-TAGCTTGCAGGAATCCCATC-3'
		Rv	5'-CTCCTGCATAGGCCAAAAAG-3'
AQP4	AQP4	Fw	5'-TGCCAGCATGAATCCCGCCC-3'
		Rv	5'-GCCACCAGCGAGGACAGCTC-3'
ero1α	ERO1A	Fw	5'-GTGTGGCTGCTCAGCTCG-3'
		Rv	5'-TCAATGGTTTCAAACATCACAGG-3'
Nox4	NOX4	Fw	5'-AAGACTCCGAAATTCTGCCC-3'
		Rv	5'-AACCAACGGAAGGACTGGA-3'
GAPDH	GAPDH	Fw	5'-TGAAGGTCGGAGTCAACGGATTT-3'
		Rv	5'-CATGTAAACCATGTAGTTGAGGT-3'

Table 5: RT-PCR primers

To transiently express the engineered recombinant proteins HaloAQP11, HaloAQP11-mycFlag, HaloAQP8, Halo-RDEL, HaloGpx8 TM, Ero1α-Myc or ERp44-HA, $2x10^4$ HeLa cells were transfected using JetPei (Polyplus) and cultured for 48h before immunofluorescence or biochemical analyses. For experiments in which AQP11 expression was reconstituted using the silencing-resistant HaloAQP11 version, cells were first silenced for 24h as described above, and then transfected with the plasmid, and further cultured 24h before imaging experiments.

5.5 Imaging of HyPer oxidation

To perform confocal live imaging assays, 8×10^4 polyclonal HeLa cells stably expressing either *HyPerERLum, HyPerMito, HyPerCyto* were silenced and/or transfected on 13mm glass coverslips following the procedures described in the previous section. When performing *SHyPher*-based imaging, the same numbers of HeLa cells were transfected transiently with the vector. Whenever the experiment required identification of Halo-tagged proteins, 2 nM HaloTag® TMRDirect (Table 2) was added 24h after transfection. After a further 24h, cells on coverslips were equilibrated in Ringer buffer (RB: 140 mM NaCl, 2 mM $CaCl_2$, 1 mM $MgSO_4$, 1.5 mM K_2HPO_4, 10 mM Glucose, pH 7.4) for 10 min at room temperature (RT) before acquisition. Confocal images were collected every 2sec for 5min by dual excitation with a 488-nm argon and 405-nm violet diode lasers. We used an Ultraview confocal laser scanning microscope equipped with either an EC Plan - Neofluar 20X (NA 0.45) Dry (Carl Zeiss) or a 40X oil immersion lens (PerkinElmer).

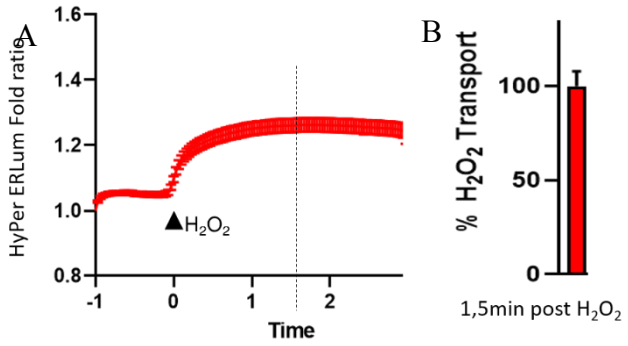

Figure 37: HyPer data representation of the images acquired while analyzing H_2O_2 internalization. *A) HyPer curve obtained by plotting the mean fold change of the 488/405 ratio against time. B) Quantification of HyPer percentual oxidation rate 1,5min after the addition of 50µM exogenous H_2O_2*

The 488/405-nm ratios were calculated by ImageJ software for ≥20 cells, averaged, and showed mean fold change of ratio plotted against time (Fig. 37 Left) ± SEM to show kinetics of uptake of 50uM of exogenous H_2O_2 or as basal ratio of the probe ± SEM to assess the rate of oxidation inside a particular organelle. To facilitate quantification and statistical analyses of some experiments, in the former case we averaged the data obtained at 1.5min after H_2O_2 addition and represented them as the percentage of H_2O_2 transport relative to the corresponding untreated cells (Fig. 37 Right). Following the same lines, the basal ratio of HyPer was also represented as the average of the first 21-60sec acquisition set-points before adding any H_2O_2, the initial 20sec excluded to allow

exposure to laser equilibration, and showed as a ratio or mean fold change of ratio ± SEM. From 2 to 10 experiments were conducted for each condition assayed.

5.6 Interference with mitochondrial redox signals and ER stress induction

Previously to analyze the basal ratio of mitochondria and ER using confocal live imaging experiments, 8×10^4 HeLa cells stably expressing *HyPerERLum/HyPerMito probes or transiently expressing SHyPer* sensors and seeded into coverslips (as described above), were treated of not with 2µM LCS-1, 33µM S1QEL, 33µM S3QEL, 5µM/ml Tunicamycin, depending on the experiment (Table 2).

5.7 Co-localization studies

To evaluate the subcellular localization of AQP11, 10^4 number of the indicated cell lines were plated on 13 mm coverslips, and the HaloAQP11 or the AQP11mycFlag recombinant proteins transfected for 48h. Halo ligands were used to detect appropriately-tagged proteins using the same concentration and timings of HyPer recordings, while AQP11mycFlag proteins were detected using mouse anti-Flag antibodies (Sigma). Rabbit anti-Calnexin to stain the ER was from Enzo Life Sciences, while anti-Peroxiredoxin-3 to label de mitochondria was from Thermo Scientific as described in the antibodies table (Table 3). An in-house generated anti-Myc (9E10) antibody was used to detect the expression of the plasmid coding for the ER-targeted catalase. Briefly, cells were fixed with 4%PFA for 20 min at RT and permeabilized with 0.1% Triton X100 and incubated X time with the indicated antibodies. Suitable anti-mouse or anti-rabbit secondary antibodies Alexa Fluor 488, Alexa Fluor 546, and Alexa Fluor 647 were from Molecular Probes (Table 3).

To stain glycoforms present at the plasma membrane, cells were incubated with Concanavalin A-FITC (Sigma) for 1 h at 4 °C before fixation.

Fluorescent images were acquired either by using a Leica TCS SP8 SMD FLIM microscope equipped with a 63X oil lens (HC PL APO CS 2 63X (NA 1.4)), an Ultraview

confocal laser scanning microscope (PerkinElmer) with a Plan - APOCHROMAT 63X (NA 1.4) Oil lens, or a GE Healthcare DeltaVision™ Ultra microscope and 60x objective lens. Images were processed using either the LASX imaging software from Leica or ImageJ, depending on the microscope used. Pearson Correlation Coefficient was calculated through all the image z-stack by using the ImageJ plugin Coloc2.

5.8 Subcellular fractionation

Confluent 150mm plates of Hela cells were transfected with the construct AQP11-MycFlag and homogenized after 48h. To separate the crude mitochondrial and microsomal fractions were used the classical differential centrifugation method. Subsequently, the crude mitochondrial fraction was resuspended in isolation buffer (250mM mannitol, 5mM Hepes, 0.5mM EGTA, pH 7.4) and further separated on a 30% Percoll gradient to obtain the low-density (denoted as MAM) and the high-density (denoted as pure mitochondria, MP) fractions as described in (Wieckowski *et al*, 2009). Aliquots of the fractions were collected and loaded into an SDS-PAGE. Western blot analyses were done using the antibodies mouse anti-Flag, mouse anti-β−Tubulin and rabbit anti-Sigma R1 from Sigma, mouse anti-myc and rabbit anti-TOM20 from SantaCruz Biotechnology, mouse anti-GM130 from BD, and rabbit antiGRP94 from Enzo Life Sciences (Table 3).

5.9 AQP11 topology analyses

To define the orientation of the end-tails of AQP11, HeLa cells were plated on 13 mm coverslips and transfected with the HaloAQP11mycFlag vector for 48h. A scheme of the protocol followed is depicted in Fig. S3. Briefly, 40 μg/ml Digitonin (Sigma) was used to selectively solubilize the plasma membrane. Then, cells were incubated for 1 h at 4 °C with 2nM of an impermeant fluorescent Halo ligand (Table 2). Subsequently, the Flag tag was decorated with mouse anti-Flag antibodies (Table 3). Cells were then fixed and treated or not with the stronger detergent Triton X100 for selectively permeabilized the

ER membrane. Finally, the ER lumen was stained using an anti-calreticulin antibody (Table 3).

5.10 Deglycosylation assays

HeLa cells transfected with HaloAQP11-Flag vectors were grown to confluency in p100 plates for 48h, then washed once with ice-cold PBS and scraped in modified RIPA buffer (0.1% SDS, 1% NP40, 150 mM NaCl, 50 mM Tris, pH 7.4) with the addition of a cocktail of protease inhibitors (Roche), 10 mM NEM (sigma), 0.4 mM Na3VO4 (sigma), and 10 mM NaF (sigma). Whole HeLa cell lysates were centrifuged at 15,000 rpm, 15 min at 4 °C, and 30µg aliquots of the post-nuclear fractions incubated either with EndoH or PNGase F enzymes from New England Biolabs for 1 h at 37 °C. Resulting deglycosylated protein mixtures were loaded in standard reducing electrophoresis, followed by western blotting using a rabbit anti-Halo antibody (Table 3). Images were acquired using a Typhoon FLA-9000 (GE HealthCare) and processed with ImageJ. The experiments were repeated twice and gave similar results.

5.11 Immunoprecipitations

HeLa cells transiently transfected with AQP11mycFlag and either Halo-RDEL, HaloGpx8 TM, Halo-AQP8, or Halo-AQP11 were grown and lysed as above. For Ero1α immunoprecipitation assays, AQP11mycFlag was transiently transfected and, before the cell lysis plates treated with tunicamycin 5µM/ml for the indicated times.
Postnuclear fractions of each sample were quantified and 1mg of total protein incubated o/n at 4 °C with either a commercial anti-Flag crosslinked beads (Sigma) to pull-down AQP11mycFlag or with anti-Ero1α (Ronzoni *et al*, 2010)(Table 3) bound to protein G/A beads (GE Healtcare) to precipitate endogenous Ero1α. Next, beads were washed three times with a clean-up buffer containing 0.25% NP40 150 mM NaCl 10 mM Tris pH 7.4 and boiled in standard protein sample buffer. Aliquots of both the postnuclear lysates (labeled as inputs) and immunoprecipitated samples were run in a reducing SDS-PAGE,

followed by western blot with rabbit anti-Halo (Promega), mouse anti-Flag (Sigma) and mouse 2G4 anti- Ero1α antibodies as indicated in the correspondent figures. Images were acquired using either a Typhoon FLA-9000 (GE HealthCare) or an ImageQuant 9000 device and processed with ImageJ.

5.12 Sucrose density gradients

P100 plates of confluent HeLa cells were transiently transfected with either HaloAQP11-Flag or HaloAQP8-Flag. After 48h, cells were washed once with ice-cold PBS and scraped in RIPA buffer (0.1% SDS, 1% NP40, 150 mM NaCl, 50 mM Tris, pH 7.4) plus freshly added protease inhibitors, 10 mM NEM, 0.4 mM Na3VO4, and 10 mM NaF. To label both recombinant proteins 30nM HaloTag® TMRDirect (Promega) was added 24h before lysing. Postnuclear lysates were loaded on top of a discontinuous 5–11% sucrose gradient and centrifugated at 32700 rpm 3h at 4 °C in a Beckman Coulter OPTIMA L90K ultracentrifuge equipped with a Beckman Coulter SW55Ti rotor. Aliquots of each phase were precipitated using a 10% solution of trichloroacetic acid (Sigma) and resuspended in a standard reducing protein sample buffer. Samples were run in 3–8% precast gradient gels (NovexTM, Life Technologies) and directly scanned using a Typhoon FLA-9000 (GE HealthCare).

5.13 Transmission Electron Microscopy

Cultured cells were fixed with 2,5 % glutaraldehyde in 0,1 M cacodylate buffer (pH 7,4). After several washes in cacodylate buffer were post-fixed in 1% osmium tetroxide (OsO_4), 1,5% potassium ferricyanide(K_4[Fe(CN)6]) in 0,1M Na Cacodylate buffer for 1 hour on ice, washed with distilled water (dH_2O) and *enbloc* stained with 0.5% uranyl acetate in dH_2O overnight at 4°C in the dark. Finally, samples were rinsed in dH_2O, dehydrated with increasing concentrations of ethanol, embedded in Epon, and cured in an oven at 60°C for 48 h. Ultrathin sections (70 – 90 nm) were obtained using an ultramicrotome (UC7, Leica microsystem), collected, stained with uranyl acetate and

Sato's lead solutions, and observed in a Transmission Electron Microscope Talos L120C (FEI, Thermo Fisher Scientific) operating at 120kV. Images were acquired with a Ceta CCD camera ((FEI, Thermo Fisher Scientific). For MAMs analysis, the perimeters (ROIs) of each mitochondrion were drawn using the freehand selections of ImageJ. All ROIs were extended with the enlarge function by 30nm and the ER fragments were measured using the freehand lines. The distribution of the number of contacts was graphed using the parts of the whole graph of GraphPad Prism software.

5.14 J-chain folding Assay

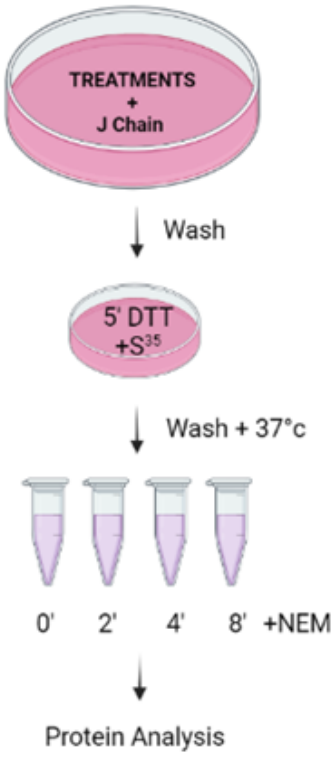

Figure 38: Workflow of J chain Folding Assay. *Built using BioRender*

10^6 HeLa cells were silenced with specific siRNA oligos for AQP11, Ero1α, or a combination of both (AQP11+ Ero1α), as previously described. After 6h, the medium was removed, and cells were transiently transfected with a myc-tagged version of the J chain (JcM). After 48h a radioactive version of the J-Chain Folding assay was performed (Bertoli *et al*, 2004). Briefly, cells were starved in DMEM without methionine and cysteine (Invitrogen) supplemented with 1% dialyzed FBS. After 10 min at 37°C, cells were pulsed for 5 min with 33 µCi of ^{35}S-labeled methionine and cysteine (EasyTag, Perkin Elmer)/10^6 cells plus 5mM DTT at 37°C, then washed twice with cold PBS and chased in DMEM 10% FBS for the indicated times (Fig. 38) before lysis in RIPA Buffer (0.1% SDS, 1% NP40, 150 mM NaCl, 50 mM Tris, pH 7.4) supplemented with freshly added protease inhibitors, 10 mM NEM, 0.4 mM Na3VO4, and 10 mM NaF. Aliquots from the post-nuclear supernatants were incubated with anti-Myc (9E10) crosslinked beads (GE Healtcare). Beads were subjected to different washing steps to get rid of artifactual associated proteins: first with solution composed of 500 mM NaCl, 10 mM Tris-HCl pH 7.5, 0.5% NP40, 0.05% SDS, then with a buffer 150 mM NaCl, 10 mM

Tris-HCl pH7, 0.025% NP-40. Immunoprecipitated material was eluted from the beads by boiling in standard protein sample buffer and resolved by 10%, 1-mm precast polyacrylamide gels (ThermoFischer) under non-reducing conditions. The gel was transferred onto nitrocellulose membranes using the transblot turbo system (BioRad) and then exposed using a LE storage phosphor screen (Amersham). Finally, radioactive signals were acquired using a Typhoon FLA 9000 scanner (GE) and quantified with ImageJ.

5.15 GSH/GSSG analysis

Confluent 6 well plates of HeLa cells were silenced for AQP11, Ero1α, or AQP11+Ero1α using the silencing protocols described before. Six hours after silencing cells were detached, counted, and re-plated in Corning Costar® 3903 p96 plates at a density of $2x10^3$cells/well to perform the assay. After another 42h of culture to finally reach 48h of silencing a luminescence-based assay GSH/GSSG-Glo™ (Promega) was performed according to the manufacturer's instructions. VICTOR3 Multilabel Plate Reader was used for recording and the analysis was executed using the calculation formulas indicated in the commercial protocol.

5.16 Statistical analyses

Statistics were calculated either by using the two-sample t-test for correlated samples or the one-way ANOVA method for multiple samples. When using the latter, Tukey's HSD post hoc test was also applied to find out which groups were significantly different from others. In all cases, statistical significance was defined as $p < 0.05$ (*), $p < 0.01$ (**), or $p < 0.001$ (***).

6 References

Anelli T, Alessio M, Bachi A, Bergamelli L, Bertoli G, Camerini S, Mezghrani A, Ruffato E, Simmen T & Sitia R (2003) Thiol-mediated protein retention in the endoplasmic reticulum: the role of ERp44. *EMBO J* 22: 5015–5022

Anelli T, Bergamelli L, Margittai E, Rimessi A, Fagioli C, Malgaroli A, Pinton P, Ripamonti M, Rizzuto R & Sitia R (2012) Ero1α regulates Ca(2+) fluxes at the endoplasmic reticulum-mitochondria interface (MAM). *Antioxid Redox Signal* 16: 1077–1087

Bae YS, Kang SW, Seo MS, Baines IC, Tekle E, Chock PB & Rhee SG (1997) Epidermal growth factor (EGF)-induced generation of hydrogen peroxide. Role in EGF receptor-mediated tyrosine phosphorylation. *J Biol Chem* 272: 217–221

Bedard K & Krause K-H (2007) The NOX family of ROS-generating NADPH oxidases: physiology and pathophysiology. *Physiol Rev* 87: 245–313

Belousov V V, Fradkov AF, Lukyanov KA, Staroverov DB, Shakhbazov KS, Terskikh A V & Lukyanov S (2006) Genetically encoded fluorescent indicator for intracellular hydrogen peroxide. *Nat Methods* 3: 281–286

Benham AM, van Lith M, Sitia R & Braakman I (2013) Ero1-PDI interactions, the response to redox flux and the implications for disulfide bond formation in the mammalian endoplasmic reticulum. *Philos Trans R Soc London Ser B, Biol Sci* 368: 20110403

Bertoli G, Simmen T, Anelli T, Molteni SN, Fesce R & Sitia R (2004) Two conserved cysteine triads in human Ero1alpha cooperate for efficient disulfide bond formation in the endoplasmic reticulum. *J Biol Chem* 279: 30047–30052

Bertolotti M, Bestetti S, García-Manteiga JM, Medraño-Fernandez I, Dal Mas A, Malosio ML & Sitia R (2013) Tyrosine kinase signal modulation: a matter of H2O2 membrane permeability? *Antioxid Redox Signal* 19: 1447–1451

Bertolotti M, Farinelli G, Galli M, Aiuti A & Sitia R (2016) AQP8 transports NOX2-generated H2O2 across the plasma membrane to promote signaling in B cells. *J Leukoc Biol* 100: 1071–1079

Bestetti S, Galli M, Sorrentino I, Pinton P, Rimessi A, Sitia R & Medraño-Fernandez I (2020) Human aquaporin-11 guarantees efficient transport of H(2)O(2) across the endoplasmic reticulum membrane. *Redox Biol* 28: 101326

Bestetti S, Medraño-Fernandez I, Galli M, Ghitti M, Bienert GP, Musco G, Orsi A, Rubartelli A & Sitia R (2018) A persulfidation-based mechanism controls aquaporin-8 conductance. *Sci Adv* 4: eaar5770

Bienert G, Medraño Fernández I & Sitia R (2017) Regulation of H 2 O 2 Transport across Cell Membranes. In pp 365–385.

Bienert GP, Møller ALB, Kristiansen KA, Schulz A, Møller IM, Schjoerring JK & Jahn TP (2007) Specific aquaporins facilitate the diffusion of hydrogen peroxide across membranes. *J Biol Chem* 282: 1183–1192

Bilan DS & Belousov V V (2018) In Vivo Imaging of Hydrogen Peroxide with HyPer

Probes. *Antioxid Redox Signal* 29: 569–584

Boletta A (2009) Emerging evidence of a link between the polycystins and the mTOR pathways. *Pathogenetics* 2: 6

Booth DM, Enyedi B, Geiszt M, Várnai P & Hajnóczky G (2016) Redox Nanodomains Are Induced by and Control Calcium Signaling at the ER-Mitochondrial Interface. *Mol Cell* 63: 240–248

Brand MD (2010) The sites and topology of mitochondrial superoxide production. *Exp Gerontol* 45: 466–472

Brand MD (2016) Mitochondrial generation of superoxide and hydrogen peroxide as the source of mitochondrial redox signaling. *Free Radic Biol Med* 100: 14–31

Brand MD, Goncalves RLS, Orr AL, Vargas L, Gerencser AA, Borch Jensen M, Wang YT, Melov S, Turk CN, Matzen JT, *et al* (2016) Suppressors of Superoxide-H(2)O(2) Production at Site I(Q) of Mitochondrial Complex I Protect against Stem Cell Hyperplasia and Ischemia-Reperfusion Injury. *Cell Metab* 24: 582–592

Bravo-Sagua R, Rodriguez AE, Kuzmicic J, Gutierrez T, Lopez-Crisosto C, Quiroga C, Díaz-Elizondo J, Chiong M, Gillette TG, Rothermel BA, *et al* (2013) Cell death and survival through the endoplasmic reticulum-mitochondrial axis. *Curr Mol Med* 13: 317–329

Cabibbo A, Pagani M, Fabbri M, Rocchi M, Farmery MR, Bulleid NJ & Sitia R (2000) ERO1-L, a human protein that favors disulfide bond formation in the endoplasmic reticulum. *J Biol Chem* 275: 4827–4833

Cai H (2005) Hydrogen peroxide regulation of endothelial function: origins, mechanisms, and consequences. *Cardiovasc Res* 68: 26–36

Cao SS & Kaufman RJ (2014) Endoplasmic reticulum stress and oxidative stress in cell fate decision and human disease. *Antioxid Redox Signal* 21: 396–413

Chakravarthi S & Bulleid NJ (2004) Glutathione is required to regulate the formation of native disulfide bonds within proteins entering the secretory pathway. *J Biol Chem* 279: 39872–39879

Chiarugi P, Pani G, Giannoni E, Taddei L, Colavitti R, Raugei G, Symons M, Borrello S, Galeotti T & Ramponi G (2003) Reactive oxygen species as essential mediators of cell adhesion: the oxidative inhibition of a FAK tyrosine phosphatase is required for cell adhesion. *J Cell Biol* 161: 933–944

Chin K-T, Kang G, Qu J, Gardner LB, Coetzee WA, Zito E, Fishman GI & Ron D (2011) The sarcoplasmic reticulum luminal thiol oxidase ERO1 regulates cardiomyocyte excitation-coupled calcium release and response to hemodynamic load. *FASEB J Off Publ Fed Am Soc Exp Biol* 25: 2583–2591

Delaunay-Moisan A, Ponsero A & Toledano MB (2017) Reexamining the Function of Glutathione in Oxidative Protein Folding and Secretion. *Antioxid Redox Signal* 27: 1178–1199

Dickinson BC & Chang CJ (2011) Chemistry and biology of reactive oxygen species in signaling or stress responses. *Nat Chem Biol* 7: 504–511

Dixon BM, Heath S-HD, Kim R, Suh JH & Hagen TM (2008) Assessment of endoplasmic

reticulum glutathione redox status is confounded by extensive ex vivo oxidation. *Antioxid Redox Signal* 10: 963–972

Dunn KW, Kamocka MM & McDonald JH (2011) A practical guide to evaluating colocalization in biological microscopy. *Am J Physiol Cell Physiol* 300: C723-42

Eletto D, Chevet E, Argon Y & Appenzeller-Herzog C (2014) Redox controls UPR to control redox. *J Cell Sci* 127: 3649–3658

FIALA S & FIALA AE (1959) On the correlation between metabolic and structural changes during carcinogenesis in rat liver. *Br J Cancer* 13: 136–151

Finkel T (2000) Redox-dependent signal transduction. *FEBS Lett* 476: 52–54

Finn RN & Cerdà J (2011) Aquaporin evolution in fishes. *Front Physiol* 2: 44

Finn RN & Cerdà J (2015) Evolution and functional diversity of aquaporins. *Biol Bull* 229: 6–23

Finn RN, Chauvigné F, Hlidberg JB, Cutler CP & Cerdà J (2014) The lineage-specific evolution of aquaporin gene clusters facilitated tetrapod terrestrial adaptation. *PLoS One* 9: e113686

Foreman J, Demidchik V, Bothwell JHF, Mylona P, Miedema H, Torres MA, Linstead P, Costa S, Brownlee C, Jones JDG, *et al* (2003) Reactive oxygen species produced by NADPH oxidase regulate plant cell growth. *Nature* 422: 442–446

Frand AR, Cuozzo JW & Kaiser CA (2000) Pathways for protein disulphide bond formation. *Trends Cell Biol* 10: 203–210

Frand AR & Kaiser CA (1998) The ERO1 gene of yeast is required for oxidation of protein dithiols in the endoplasmic reticulum. *Mol Cell* 1: 161–170

Fridovich I (1998) Oxygen toxicity: a radical explanation. *J Exp Biol* 201: 1203–1209

Gao C, Cai Y, Wang Y, Kang B-H, Aniento F, Robinson DG & Jiang L (2014) Retention mechanisms for ER and Golgi membrane proteins. *Trends Plant Sci* 19: 508–515

Gao C, Tian Y, Zhang R, Jing J & Zhang X (2017) Endoplasmic Reticulum-Directed Ratiometric Fluorescent Probe for Quantitive Detection of Basal H(2)O(2). *Anal Chem* 89: 12945–12950

Gazzarrini S, Kang M, Epimashko S, Van Etten JL, Dainty J, Thiel G & Moroni A (2006) Chlorella virus MT325 encodes water and potassium channels that interact synergistically. *Proc Natl Acad Sci U S A* 103: 5355–5360

Gechev TS & Hille J (2005) Hydrogen peroxide as a signal controlling plant programmed cell death. *J Cell Biol* 168: 17–20

Geiszt M & Leto TL (2004) The Nox family of NAD(P)H oxidases: host defense and beyond. *J Biol Chem* 279: 51715–51718

Giacomello M & Pellegrini L (2016) The coming of age of the mitochondria–ER contact: a matter of thickness. *Cell Death Differ* 23: 1417–1427

Gilady SY, Bui M, Lynes EM, Benson MD, Watts R, Vance JE & Simmen T (2010) Ero1alpha requires oxidizing and normoxic conditions to localize to the mitochondria-associated membrane (MAM). *Cell Stress Chaperones* 15: 619–629

Gorelick DA, Praetorius J, Tsunenari T, Nielsen S & Agre P (2006) Aquaporin-11: a channel protein lacking apparent transport function expressed in brain. *BMC*

Biochem 7: 14

Han D, Antunes F, Canali R, Rettori D & Cadenas E (2003) Voltage-dependent anion channels control the release of the superoxide anion from mitochondria to cytosol. *J Biol Chem* 278: 5557–5563

Hara-Chikuma M, Chikuma S, Sugiyama Y, Kabashima K, Verkman AS, Inoue S & Miyachi Y (2012) Chemokine-dependent T cell migration requires aquaporin-3-mediated hydrogen peroxide uptake. *J Exp Med* 209: 1743–1752

Hayashi T & Su T-P (2007) Sigma-1 receptor chaperones at the ER-mitochondrion interface regulate Ca(2+) signaling and cell survival. *Cell* 131: 596–610

Henzler T & Steudle E (2000) Transport and metabolic degradation of hydrogen peroxide in Chara corallina: model calculations and measurements with the pressure probe suggest transport of H(2)O(2) across water channels. *J Exp Bot* 51: 2053–2066

Holbrook L-M, Watkins NA, Simmonds AD, Jones CI, Ouwehand WH & Gibbins JM (2010) Platelets release novel thiol isomerase enzymes which are recruited to the cell surface following activation. *Br J Haematol* 148: 627–637

Holmström KM & Finkel T (2014) Cellular mechanisms and physiological consequences of redox-dependent signalling. *Nat Rev Mol Cell Biol* 15: 411–421

Hwang C, Sinskey AJ & Lodish HF (1992) Oxidized redox state of glutathione in the endoplasmic reticulum. *Science* 257: 1496–1502

Ikeda M, Andoo A, Shimono M, Takamatsu N, Taki A, Muta K, Matsushita W, Uechi T, Matsuzaki T, Kenmochi N, *et al* (2011) The NPC motif of aquaporin-11, unlike the NPA motif of known aquaporins, is essential for full expression of molecular function. *J Biol Chem* 286: 3342–3350

Inoue Y, Sohara E, Kobayashi K, Chiga M, Rai T, Ishibashi K, Horie S, Su X, Zhou J, Sasaki S, *et al* (2014) Aberrant glycosylation and localization of polycystin-1 cause polycystic kidney in an AQP11 knockout model. *J Am Soc Nephrol* 25: 2789–2799

Ishibashi K, Tanaka Y & Morishita Y (2014) The role of mammalian superaquaporins inside the cell. *Biochim Biophys Acta* 1840: 1507–1512

James AM & Murphy MP (2002) How mitochondrial damage affects cell function. *J Biomed Sci* 9: 475–487

Kasting JF (1993) Earth's early atmosphere. *Science* 259: 920–926

Konno T, Melo EP, Chambers JE & Avezov E (2021) Intracellular Sources of ROS/H(2)O(2) in Health and Neurodegeneration: Spotlight on Endoplasmic Reticulum. *Cells* 10

Konno T, Pinho Melo E, Lopes C, Mehmeti I, Lenzen S, Ron D & Avezov E (2015) ERO1-independent production of H2O2 within the endoplasmic reticulum fuels Prdx4-mediated oxidative protein folding. *J Cell Biol* 211: 253–259

Koopman WJH, Nijtmans LGJ, Dieteren CEJ, Roestenberg P, Valsecchi F, Smeitink JAM & Willems PHGM (2010) Mammalian mitochondrial complex I: biogenesis, regulation, and reactive oxygen species generation. *Antioxid Redox Signal* 12: 1431–1470

Kühlbrandt W (2015) Structure and function of mitochondrial membrane protein

complexes. *BMC Biol* 13: 89

Kumar V & Maity S (2021) ER Stress-Sensor Proteins and ER-Mitochondrial Crosstalk-Signaling Beyond (ER) Stress Response. *Biomolecules* 11

Laurindo FRM, Araujo TLS & Abrahão TB (2014) Nox NADPH oxidases and the endoplasmic reticulum. *Antioxid Redox Signal* 20: 2755–2775

Lee SR, Kwon KS, Kim SR & Rhee SG (1998) Reversible inactivation of protein-tyrosine phosphatase 1B in A431 cells stimulated with epidermal growth factor. *J Biol Chem* 273: 15366–15372

Leloup C, Tourrel-Cuzin C, Magnan C, Karaca M, Castel J, Carneiro L, Colombani A-L, Ktorza A, Casteilla L & Pénicaud L (2009) Mitochondrial reactive oxygen species are obligatory signals for glucose-induced insulin secretion. *Diabetes* 58: 673–681

Li C & Wang W (2017) Molecular Biology of Aquaporins. *Adv Exp Med Biol* 969: 1–34

Lindström B & Pettersson LJ (2003) A Brief History of Catalysis. *CATTECH* 7: 130–138

Lloyd D, Aon MA & Cortassa S (2001) Why homeodynamics, not homeostasis? *ScientificWorldJournal* 1: 133–145

von Löhneysen K, Noack D, Hayes P, Friedman JS & Knaus UG (2012) Constitutive NADPH oxidase 4 activity resides in the composition of the B-loop and the penultimate C terminus. *J Biol Chem* 287: 8737–8745

Luo J, Liu X, Liu J, Jiang M, Luo M & Zhao J (2016) Activation of TGF-β1 by AQP3-Mediated H(2)O(2) Transport into Fibroblasts of a Bleomycin-Induced Mouse Model of Scleroderma. *J Invest Dermatol* 136: 2372–2379

Lyons TW, Reinhard CT & Planavsky NJ (2014) The rise of oxygen in Earth's early ocean and atmosphere. *Nature* 506: 307–315

Malinouski M, Zhou Y, Belousov V V, Hatfield DL & Gladyshev VN (2011) Hydrogen peroxide probes directed to different cellular compartments. *PLoS One* 6: e14564

Medraño-Fernandez I, Bestetti S, Bertolotti M, Bienert GP, Bottino C, Laforenza U, Rubartelli A & Sitia R (2016) Stress Regulates Aquaporin-8 Permeability to Impact Cell Growth and Survival. *Antioxid Redox Signal* 24: 1031–1044

Medraño-Fernandez I & Sitia R (2020) Chapter 11 - Aquaporins: Gatekeepers in the borders of oxidative stress and redox signaling. In, Sies HBT-OS (ed) pp 167–181. Academic Press

Meng T-C, Fukada T & Tonks NK (2002) Reversible oxidation and inactivation of protein tyrosine phosphatases in vivo. *Mol Cell* 9: 387–399

Miller EW, Dickinson BC & Chang CJ (2010) Aquaporin-3 mediates hydrogen peroxide uptake to regulate downstream intracellular signaling. *Proc Natl Acad Sci U S A* 107: 15681–15686

Molteni SN, Fassio A, Ciriolo MR, Filomeni G, Pasqualetto E, Fagioli C & Sitia R (2004) Glutathione limits Ero1-dependent oxidation in the endoplasmic reticulum. *J Biol Chem* 279: 32667–32673

Morishita Y, Matsuzaki T, Hara-chikuma M, Andoo A, Shimono M, Matsuki A, Kobayashi K, Ikeda M, Yamamoto T, Verkman A, *et al* (2005) Disruption of aquaporin-11 produces polycystic kidneys following vacuolization of the proximal

tubule. *Mol Cell Biol* 25: 7770–7779

Murata K, Mitsuoka K, Hirai T, Walz T, Agre P, Heymann JB, Engel A & Fujiyoshi Y (2000) Structural determinants of water permeation through aquaporin-1. *Nature* 407: 599–605

Nguyen VD, Saaranen MJ, Karala A-R, Lappi A-K, Wang L, Raykhel IB, Alanen HI, Salo KEH, Wang C-C & Ruddock LW (2011) Two endoplasmic reticulum PDI peroxidases increase the efficiency of the use of peroxide during disulfide bond formation. *J Mol Biol* 406: 503–515

Nisimoto Y, Diebold BA, Cosentino-Gomes D & Lambeth JD (2014) Nox4: a hydrogen peroxide-generating oxygen sensor. *Biochemistry* 53: 5111–5120

Nisimoto Y, Jackson HM, Ogawa H, Kawahara T & Lambeth JD (2010) Constitutive NADPH-dependent electron transferase activity of the Nox4 dehydrogenase domain. *Biochemistry* 49: 2433–2442

Nordzieke DE & Medraño-Fernandez I (2018) The Plasma Membrane: A Platform for Intra- and Intercellular Redox Signaling. *Antioxidants (Basel, Switzerland)* 7

Orr AL, Vargas L, Turk CN, Baaten JE, Matzen JT, Dardov VJ, Attle SJ, Li J, Quackenbush DC, Goncalves RLS, *et al* (2015) Suppressors of superoxide production from mitochondrial complex III. *Nat Chem Biol* 11: 834–836

Orrenius S (2007) Reactive oxygen species in mitochondria-mediated cell death. *Drug Metab Rev* 39: 443–455

Orrenius S, Gogvadze V & Zhivotovsky B (2007) Mitochondrial oxidative stress: implications for cell death. *Annu Rev Pharmacol Toxicol* 47: 143–183

Pagani M, Fabbri M, Benedetti C, Fassio A, Pilati S, Bulleid NJ, Cabibbo A & Sitia R (2000) Endoplasmic reticulum oxidoreductin 1-lbeta (ERO1-Lbeta), a human gene induced in the course of the unfolded protein response. *J Biol Chem* 275: 23685–23692

Pagani M, Pilati S, Bertoli G, Valsasina B & Sitia R (2001) The C-terminal domain of yeast Ero1p mediates membrane localization and is essential for function. *FEBS Lett* 508: 117–120

Peskin A V, Low FM, Paton LN, Maghzal GJ, Hampton MB & Winterbourn CC (2007) The high reactivity of peroxiredoxin 2 with H(2)O(2) is not reflected in its reaction with other oxidants and thiol reagents. *J Biol Chem* 282: 11885–11892

Pollard MG, Travers KJ & Weissman JS (1998) Ero1p: a novel and ubiquitous protein with an essential role in oxidative protein folding in the endoplasmic reticulum. *Mol Cell* 1: 171–182

Poole LB (2015) The basics of thiols and cysteines in redox biology and chemistry. *Free Radic Biol Med* 80: 148–157

Preston GM, Carroll TP, Guggino WB & Agre P (1992) Appearance of water channels in Xenopus oocytes expressing red cell CHIP28 protein. *Science* 256: 385–387

Rada B, Hably C, Meczner A, Timár C, Lakatos G, Enyedi P & Ligeti E (2008) Role of Nox2 in elimination of microorganisms. *Semin Immunopathol* 30: 237–253

Ramming T, Hansen HG, Nagata K, Ellgaard L & Appenzeller-Herzog C (2014) GPx8

peroxidase prevents leakage of H2O2 from the endoplasmic reticulum. *Free Radic Biol Med* 70: 106–116

Reth M (2002) Hydrogen peroxide as second messenger in lymphocyte activation. *Nat Immunol* 3: 1129–1134

Ronzoni R, Anelli T, Brunati M, Cortini M, Fagioli C & Sitia R (2010) Pathogenesis of ER storage disorders: modulating Russell body biogenesis by altering proximal and distal quality control. *Traffic* 11: 947–957

Sablina AA, Budanov A V, Ilyinskaya G V, Agapova LS, Kravchenko JE & Chumakov PM (2005) The antioxidant function of the p53 tumor suppressor. *Nat Med* 11: 1306–1313

Sannino S, Anelli T, Cortini M, Masui S, Degano M, Fagioli C, Inaba K & Sitia R (2014) Progressive quality control of secretory proteins in the early secretory compartment by ERp44. *J Cell Sci* 127: 4260–4269

Santos CXC, Hafstad AD, Beretta M, Zhang M, Molenaar C, Kopec J, Fotinou D, Murray T V, Cobb AM, Martin D, *et al* (2016) Targeted redox inhibition of protein phosphatase 1 by Nox4 regulates eIF2α-mediated stress signaling. *EMBO J* 35: 319–334

Satooka H & Hara-Chikuma M (2016) Aquaporin-3 Controls Breast Cancer Cell Migration by Regulating Hydrogen Peroxide Transport and Its Downstream Cell Signaling. *Mol Cell Biol* 36: 1206–1218

Sauer H, Rahimi G, Hescheler J & Wartenberg M (2000) Role of reactive oxygen species and phosphatidylinositol 3-kinase in cardiomyocyte differentiation of embryonic stem cells. *FEBS Lett* 476: 218–223

Sharpe HJ, Stevens TJ & Munro S (2010) A comprehensive comparison of transmembrane domains reveals organelle-specific properties. *Cell* 142: 158–169

Sies H (2018) On the history of oxidative stress: Concept and some aspects of current development. *Curr Opin Toxicol* 7: 122–126

Sies H (2020) Oxidative Stress: Concept and Some Practical Aspects. *Antioxidants (Basel, Switzerland)* 9

SIES H (1985) 1 - Oxidative Stress: Introductory Remarks. In, SIES HBT-OS (ed) pp 1–8. London: Academic Press

Sies H, Berndt C & Jones DP (2017) Oxidative Stress. *Annu Rev Biochem* 86: 715–748

Sies H & Jones D (2007) Oxidative Stress*. In, Fink GBT-E of S (Second E (ed) pp 45–48. New York: Academic Press

Sies H & Jones DP (2020) Reactive oxygen species (ROS) as pleiotropic physiological signalling agents. *Nat Rev Mol Cell Biol* 21: 363–383

Simmen T, Lynes EM, Gesson K & Thomas G (2010) Oxidative protein folding in the endoplasmic reticulum: tight links to the mitochondria-associated membrane (MAM). *Biochim Biophys Acta* 1798: 1465–1473

Somwar R, Erdjument-Bromage H, Larsson E, Shum D, Lockwood WW, Yang G, Sander C, Ouerfelli O, Tempst PJ, Djaballah H, *et al* (2011) Superoxide dismutase 1 (SOD1) is a target for a small molecule identified in a screen for inhibitors of the growth of

lung adenocarcinoma cell lines. *Proc Natl Acad Sci U S A* 108: 16375–16380

Soti C & Csermely P (2003) Aging and molecular chaperones. *Exp Gerontol* 38: 1037–1040

St-Pierre J, Buckingham JA, Roebuck SJ & Brand MD (2002) Topology of superoxide production from different sites in the mitochondrial electron transport chain. *J Biol Chem* 277: 44784–44790

Sundaresan M, Yu ZX, Ferrans VJ, Irani K & Finkel T (1995) Requirement for generation of H2O2 for platelet-derived growth factor signal transduction. *Science* 270: 296–299

Surani MA (1979) Glycoprotein synthesis and inhibition of glycosylation by tunicamycin in preimplantation mouse embryos: compaction and trophoblast adhesion. *Cell* 18: 217–227

Tavender TJ & Bulleid NJ (2010) Molecular mechanisms regulating oxidative activity of the Ero1 family in the endoplasmic reticulum. *Antioxid Redox Signal* 13: 1177–1187

Thenard L (1818) Observations sur l'Influence de l'Eau dans la Formation des Acides Oxigénés. *Ann Chim* 9: 314–317

Thénard LJ (1818) Observations sur des nouvelles combinaisons entre l'oxigène et divers acides. *Ann Chim Phys* 8: 306–312

Tien A-C, Rajan A, Schulze KL, Ryoo HD, Acar M, Steller H & Bellen HJ (2008) Ero1L, a thiol oxidase, is required for Notch signaling through cysteine bridge formation of the Lin12-Notch repeats in Drosophila melanogaster. *J Cell Biol* 182: 1113–1125

Törnroth-Horsefield S, Hedfalk K, Fischer G, Lindkvist-Petersson K & Neutze R (2010) Structural insights into eukaryotic aquaporin regulation. *FEBS Lett* 584: 2580–2588

Tu BP, Ho-Schleyer SC, Travers KJ & Weissman JS (2000) Biochemical basis of oxidative protein folding in the endoplasmic reticulum. *Science* 290: 1571–1574

Tu BP & Weissman JS (2004) Oxidative protein folding in eukaryotes: mechanisms and consequences. *J Cell Biol* 164: 341–346

Ushio-Fukai M (2006) Localizing NADPH oxidase-derived ROS. *Sci STKE* 2006: re8

Verkman AS (2011) Aquaporins at a glance. *J Cell Sci* 124: 2107–2112

van Vliet AR, Verfaillie T & Agostinis P (2014) New functions of mitochondria associated membranes in cellular signaling. *Biochim Biophys Acta* 1843: 2253–2262

Wall SB, Oh J-Y, Diers AR & Landar A (2012) Oxidative modification of proteins: an emerging mechanism of cell signaling. *Front Physiol* 3: 369

Watanabe S, Moniaga CS, Nielsen S & Hara-Chikuma M (2016) Aquaporin-9 facilitates membrane transport of hydrogen peroxide in mammalian cells. *Biochem Biophys Res Commun* 471: 191–197

Wieckowski MR, Giorgi C, Lebiedzinska M, Duszynski J & Pinton P (2009) Isolation of mitochondria-associated membranes and mitochondria from animal tissues and cells. *Nat Protoc* 4: 1582–1590

Winterbourn CC (2013) The biological chemistry of hydrogen peroxide. *Methods Enzymol* 528: 3–25

Winterbourn CC (2018) Biological Production, Detection, and Fate of Hydrogen Peroxide. *Antioxid Redox Signal* 29: 541–551

Winterbourn CC & Hampton MB (2008) Thiol chemistry and specificity in redox signaling. *Free Radic Biol Med* 45: 549–561

Winterbourn CC & Metodiewa D (1999) Reactivity of biologically important thiol compounds with superoxide and hydrogen peroxide. *Free Radic Biol Med* 27: 322–328

Yang B, Zhao D & Verkman AS (2006) Evidence against functionally significant aquaporin expression in mitochondria. *J Biol Chem* 281: 16202–16206

Yoboue ED, Rimessi A, Anelli T, Pinton P & Sitia R (2017) Regulation of Calcium Fluxes by GPX8, a Type-II Transmembrane Peroxidase Enriched at the Mitochondria-Associated Endoplasmic Reticulum Membrane. *Antioxid Redox Signal* 27: 583–595

Yoboue ED, Sitia R & Simmen T (2018) Redox crosstalk at endoplasmic reticulum (ER) membrane contact sites (MCS) uses toxic waste to deliver messages. *Cell Death Dis* 9: 331

Zhang J, Zhu Q, Wang X, Yu J, Chen X, Wang J, Wang X, Xiao J, Wang C-C & Wang L (2018) Secretory kinase Fam20C tunes endoplasmic reticulum redox state via phosphorylation of Ero1α. *EMBO J* 37

Zito E, Chin K-T, Blais J, Harding HP & Ron D (2010a) ERO1-beta, a pancreas-specific disulfide oxidase, promotes insulin biogenesis and glucose homeostasis. *J Cell Biol* 188: 821–832

Zito E, Melo EP, Yang Y, Wahlander Å, Neubert TA & Ron D (2010b) Oxidative protein folding by an endoplasmic reticulum-localized peroxiredoxin. *Mol Cell* 40: 787–797

7 Appendix

Appendix A

Supplementary data of Results showed in 3.1 section and already published in Bestetti S. et al., Redox Biology, 2020.

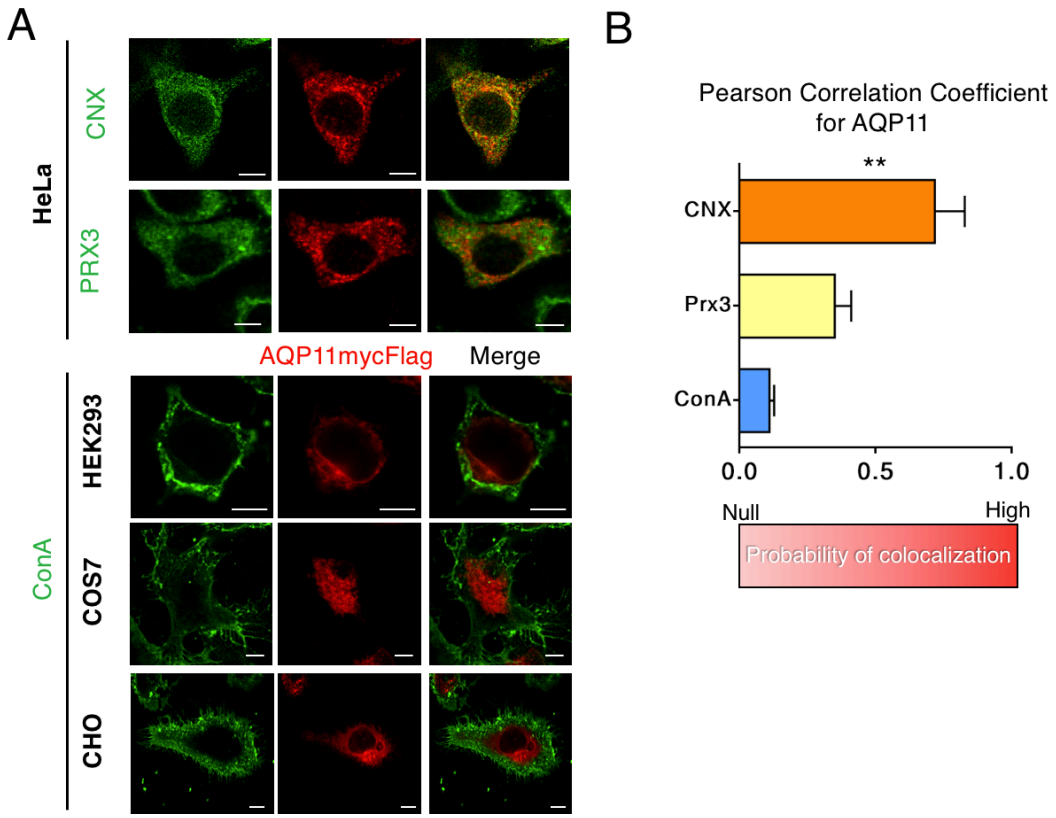

Figure S1: AQP11 does not reach the plasma membrane and localizes mainly in the ER of different cell lines.

A) HeLa, HEK293, COS7, and CHO cells were transfected with AQP11mycFlag and immunofluorescence analyses were performed using markers of different intracellular organelles, as described in Fig. 22. Scale bars in all images = 10µm.

B) To assess the probability of co-distribution of AQP11 Pearson Correlation Coefficient was performed. Images of overexpressed AQP11 were compared with different organelle markers through the entire cell volume. Average on ≥3 experiments ± SEM.

(Bestetti et al, 2020)

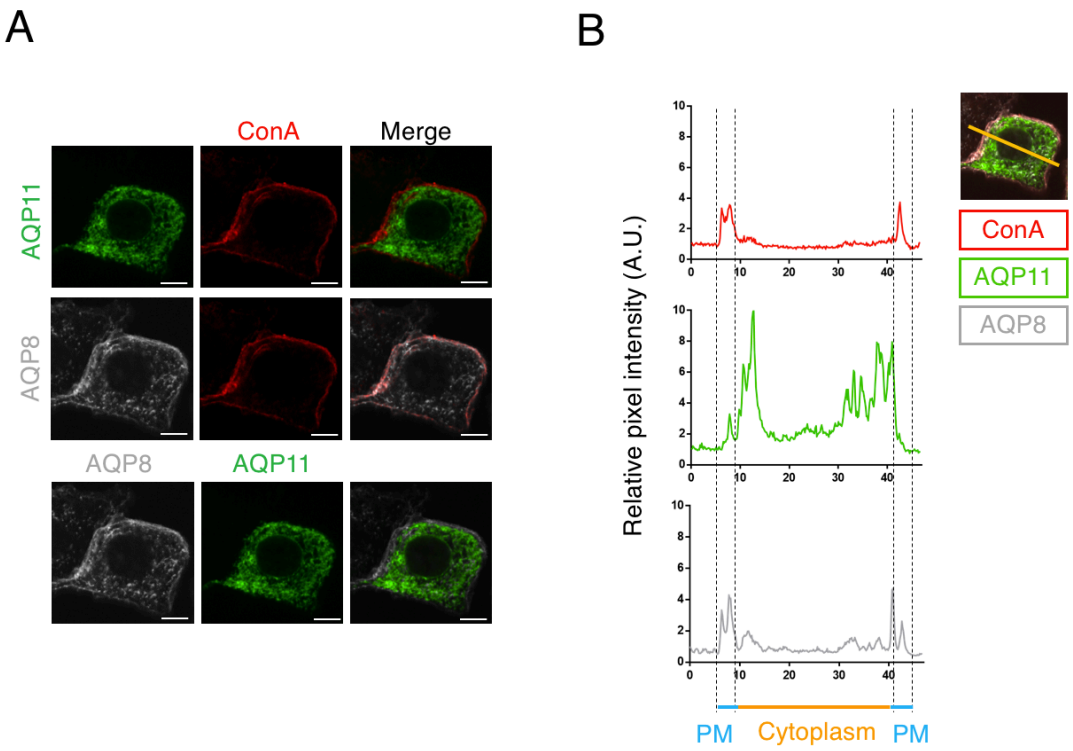

Figure S2: AQP11 and AQP8 have distinct subcellular localization

A) HeLa cells were co-transfected with AQP8 and AQP11 that have different tags (N-terminal Halo for AQP8 and C-terminal Flag for AQP11). Cells were stained with ConA-FITC before permeabilization and then decorated with tag-specific antibodies. Note that the signals of ConA and AQP8 colocalize while ConA does not overlap with AQP11. Scale bar = 10µm.

B) Pixel intensity profiles of a 47µm line sectioning the image in A. Dashed lines denote plasma membrane areas (PM, in blue), and at the same time delimit the cytoplasm extent (Cytoplasm, in orange). Other 3 different cell cross-sections profiles give similar results.

(Bestetti et al, 2020)

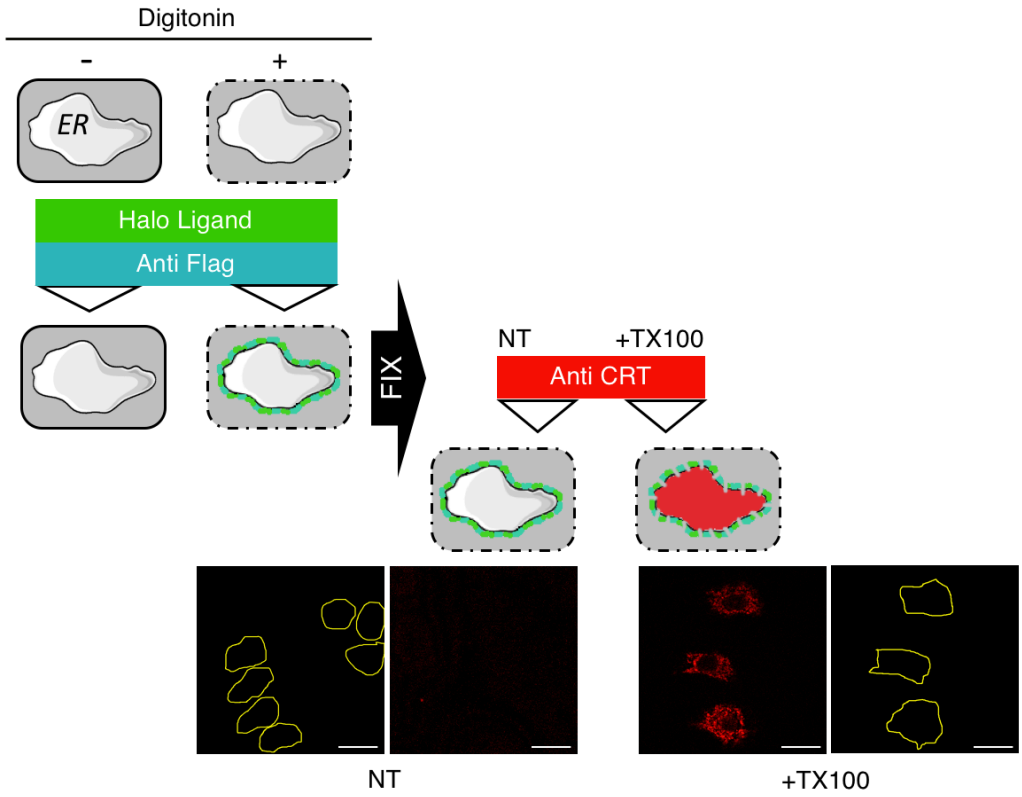

Figure S3: Strategy followed to determine AQP11 topology. *Schematic representation of the workflow for the data shown in Fig. 23A. Concisely, the cholesterol-rich plasma membrane was selectively permeabilized with digitonin, permitting the impermeant Halo ligands and Flag specific antibodies to bind their respective epitopes in AQP11 termini if protruding into the cytosol. To confirm that the ER membrane was not damaged, the coverslips were stained also with anti-calreticulin antibodies. Only after permeabilization of the ER membrane with Triton X100, they can reach the ER lumen. The yellow lines in the bottom panels indicate the perimeter of cells as determined by phase-contrast microscopy. Scale bar = 50µm.*
(Bestetti et al, 2020)

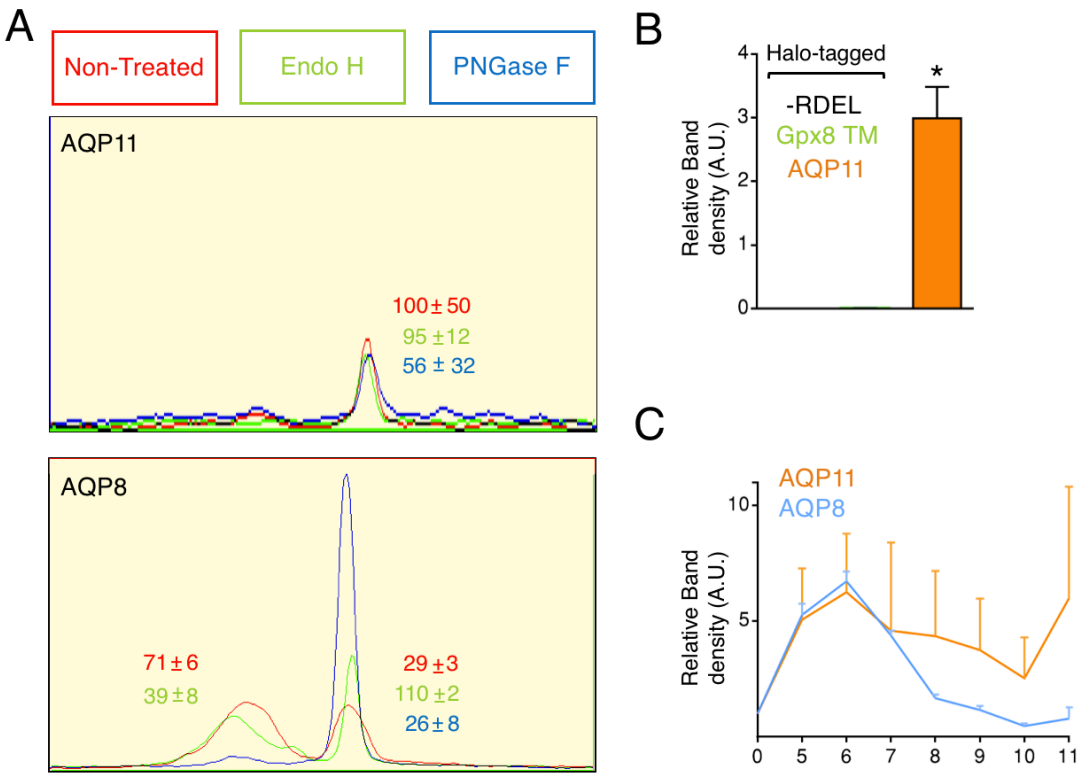

Figure S4: Quantification of AQP11 characterization assays

A) Densitometric analyses of gels like the one shown in Fig.23B prove that -differently from AQP8 (low panel)- AQP11 (top panel) is not N-glycosylated and hence it does not change after Endo-H or PNGase F treatments. Numbers on each graph correspond to the average of 2 experiments ± SEM.

B) Densitometric quantifications of gels like the one shown in Fig.24A confirm that HaloAQP11, but neither Halo-RDEL nor HaloGpx8 TM associates with AQP11mycFlag in the ER of HeLa co-transfectants. The average on 3 experiments ± SEM.

C) Distribution profile of HaloAQP11-Flag and HaloAQP8-Flag recombinant proteins through a discontinuous 5-11% sucrose gradient. The average on 2 experiments ± SEM.

(Bestetti et al, 2020)

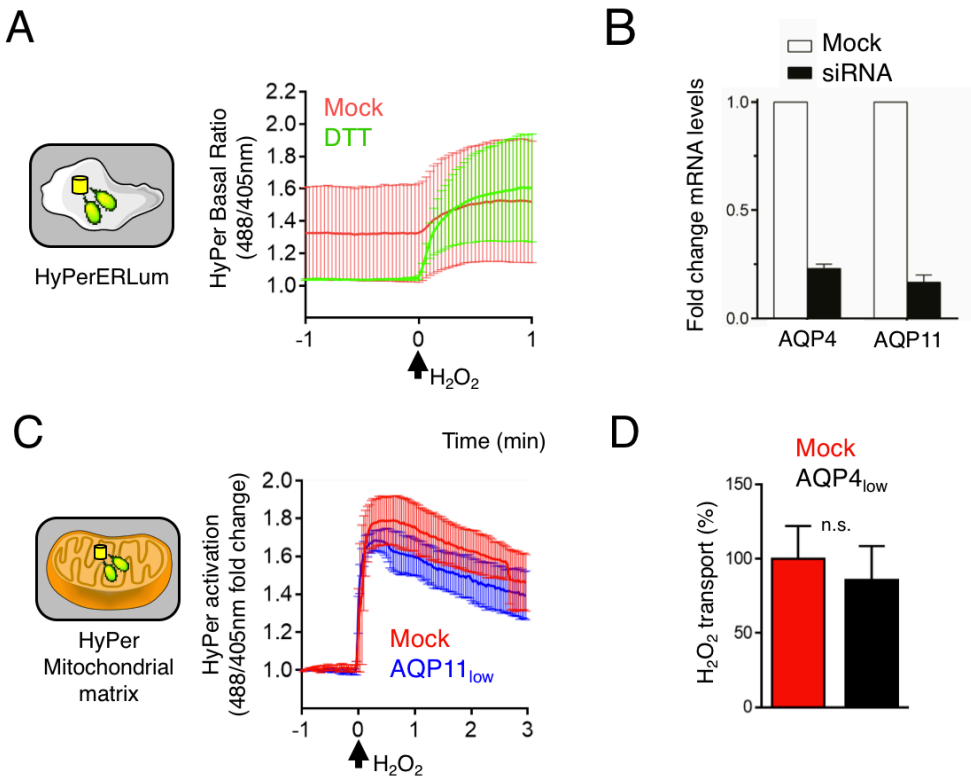

Figure S5: Specificity of AQP11 localization and activity.

A) Control of HyPerERLum probe ability to record the exogenous addition of ≥50µM H_2O_2 even if it is already partially activated at a steady state. Cells pretreated with 5mM DTT - that reduces the HyPerERLum probe- start from a lower oxidation level but reach the same degree of activation after sensing H_2O_2. The graph corresponds to the time-course analyses of the 488/405nm average ratio of 3 experiments ± SEM.

B) As determined by RT-PCR, at least 80% of AQP11-specific transcripts were absent after 72 hours of silencing. Since cells have similar phenotypes, we expected that partial silencing was sufficient to efficiently block the transport in the majority of cells. Similar levels of AQP4 mRNA transcripts were present after AQP4-specific siRNA.

C) The kinetics of activation of polyclonal HeLa cells stably expressing HyPer in the mitochondrial matrix (HyPerMito) after the exposure to 50µM of exogenous H_2O_2 did not change significantly in cells expressing normal (mock) or reduced levels of AQP11 ($AQP11_{low}$). Average of 2 experiments ± SEM is shown.

D) AQP4 silencing does not avoid the activation of HyPerERLum. Results are represented as the percentage of H_2O_2 transported in each condition 1,5 min after H_2O_2 addition. The average on 3 experiments ± SEM.

(Bestetti et al, 2020)

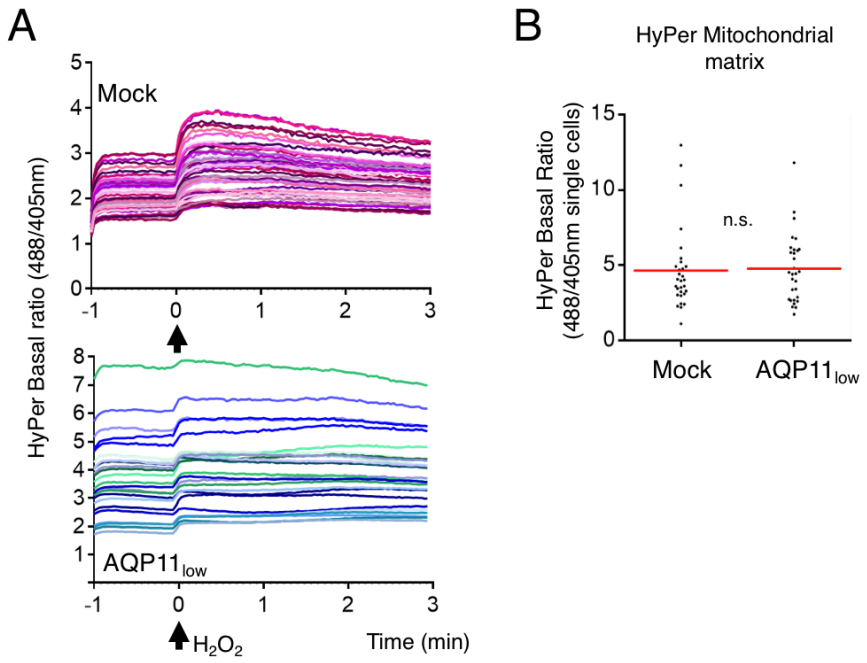

Figure S6: The basal oxidation state of the HyPer ER luminal probe but not of HyPerMito is increased after AQP11 silencing

A) The profiles of HyPerERLum oxidation in individual cells confirm that AQP11$_{low}$ cells have a higher basal oxidation level. The graph shows the time-course analysis of one of the experiments that have been averaged in Fig. 25A.

B) No significant differences were measured between the basal oxidative state of the HyPerMito probe before or after AQP11 silencing. Each dot represents a single cell distributed in the graph according to its 488/405nm ratio.

(Bestetti et al, 2020)

Appendix B

Supplementary data of Results showed in 3.2 section Sorrentino I. et al., manuscript in preparation

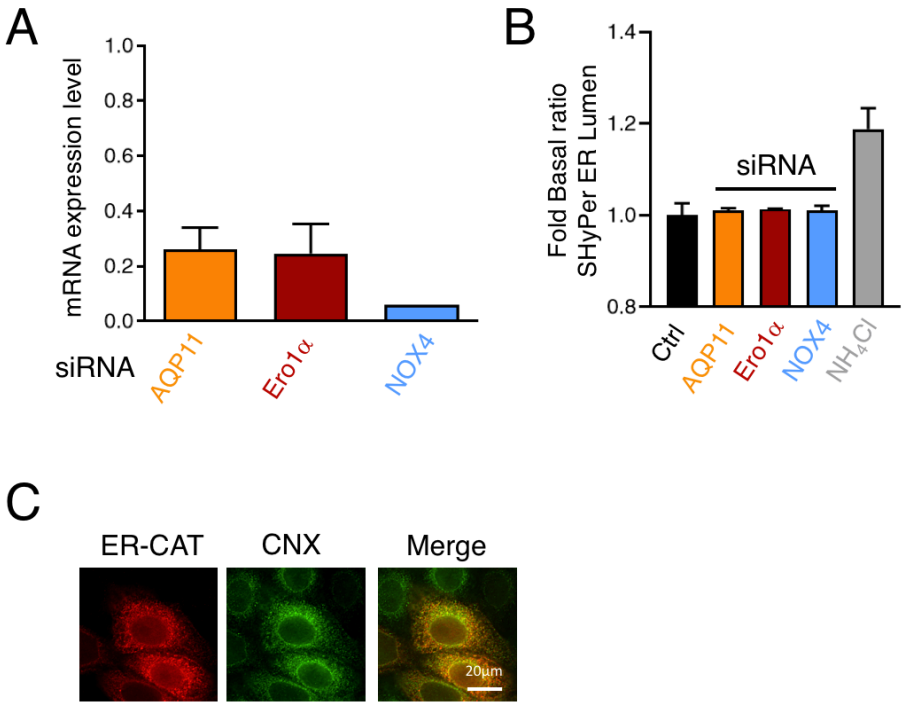

Figure S7: H_2O_2 increases inside the ER upon Ero1α silencing.

A) The mRNA expression level of AQP11, Ero1α, and NOX4 after 48h of silencing.

B) Fold change of the basal ratio of the same samples of fig. 27A. Cells were silenced and after 6h transiently transfected with SHyPer-ERLum probe and acquired after a further 42h for a total transient transfection time of 48h. All the silencing conditions did not show differences. NH_4Cl was used as a positive control to monitor that the probe indeed sensed changes in pH. The graph is the ratio of the 488/405nm analyses expressed in the fold change of SHyPer-ERLum. The average ratio of 3 experiments ± SEM.

C) Immunofluorescences of HeLa cells overexpressing a myc-tagged ER-Catalase co-stained with an anti-Calnexin (ER marker) antibody to confirm its ER localization. Scales Bar= 20μm.

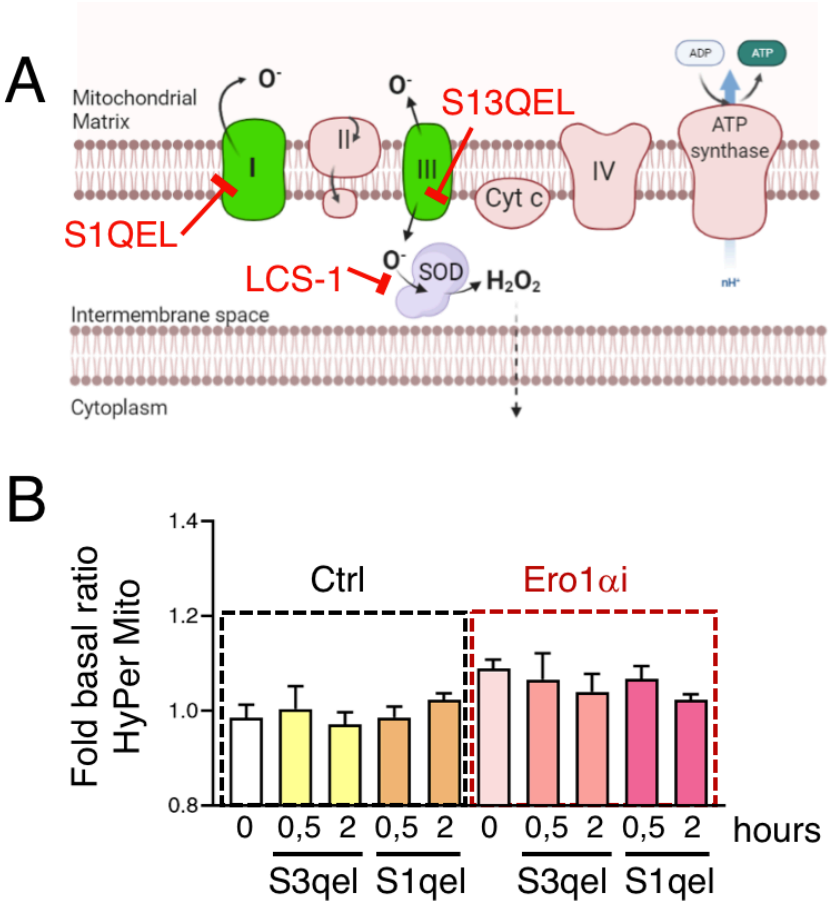

Figure S8: ETC Complex III is the producer of the influx of H_2O_2 sensed in the ER when Ero1α is absent.

A) Schematic representation of ETC complex. In green are highlighted Complex I and Complex III, the producers of superoxide in ETC, and the direction (arrow) in which they pump redox equivalents. SOD1is present in the IMS and rapidly converts superoxide into H_2O_2. In red is shown where the drugs used to inhibit these specific proteins.

B) Analyses of the fold change of the basal ratio (488/405) of HyPer stably expressed in the MM. Average of at least 3 experiments ± SEM.

A

	Number of mitochondria	Number of contacts	%
Ctrl	268 ± 30	127 ± 30	37 ± 2
Ero1αi	250 ± 14	217,50 ± 44,50	58,90 ± 6,90
Ero1αi + AQP11i	352	333	59,375

B

	Number of contacts (%)					
	0	1	2	3	4	5
Ctrl	62,55 ± 2,15	29,77 ± 0,91	6,25 ± 2,47	1,26 ± 0,42	0,17 ± 0,17	0,0±0
Ero1αi	40,61 ± 7,27	37,75 ± 2,58	16,65 ± 3,51	4,58 ± 1,19	0,62 ± 0,20	0,0±0
Ero1αi + AQP11i	40,62	32,95	19,31	5,68	1,13	0,28

Figure S9: MAMs are reshaped after the silencing of Ero1α.

A) The table shows the raw data collected during the analyses of TEM images. The first column displays the total number of mitochondria that were counted. The second illustrates the total number of contacts. The third is the percentage of contacts.

B) The table shows the distribution of the contacts (mitochondria with 0, 1, 2, 3,4, or 5 contacts). Mean of two independent experiments

Appendix C

The data presented in this section are preliminary.

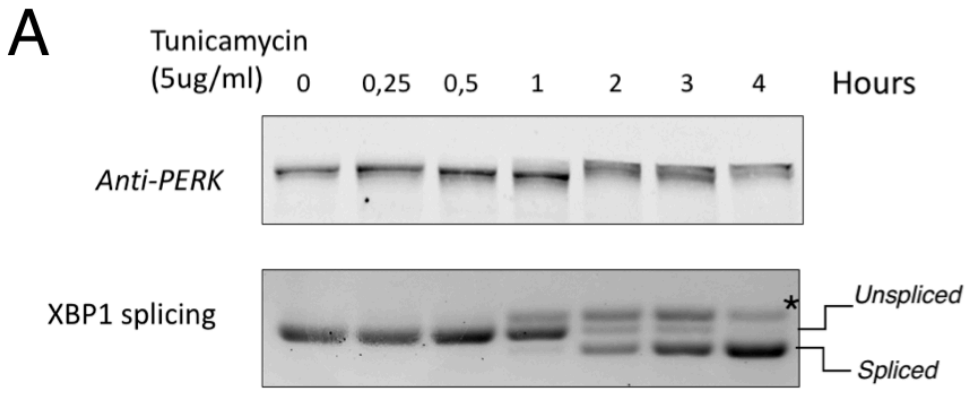

Figure S10: Tunicamycin treatment activates two of the branches of the UPR at the same time-point.

A) Hela cells were treated with tunicamycin for different time points to visualize the activation of the UPR sensors PERK and Ire1. The upper panel Western blot is decorated with anti-Perk antibody, the shift corresponding to phosphorylated bands (activation) appears at 1h. Lower panel 3% agarose gel to monitor XBP1 splicing reveals that activation of this branch is also observed after 1h. At least three independent experiments for each condition were performed.